

BIOGENESIS OF FIBROBLAST GROWTH FACTOR 8-
BINDING HEPARAN SULFATE MOTIFS

by

Thao Kim Nu Nguyen

A dissertation submitted to the faculty of
The University of Utah
in partial fulfillment of the requirements for the degree of

Doctor of Philosophy

Department of Bioengineering

The University of Utah

December 2012

Copyright © Thao Kim Nu Nguyen 2012

All Rights Reserved

The University of Utah Graduate School

STATEMENT OF DISSERTATION APPROVAL

The dissertation of Thao Kim Nu Nguyen
has been approved by the following supervisory committee members:

<u>Kuberan Balagurunathan</u>	, Chair	<u>08-May-2012</u> Date Approved
<u>Joshua Bonkowsky</u>	, Member	<u>29-April-2012</u> Date Approved
<u>Richard I. Dorsky</u>	, Member	<u>24-April-2012</u> Date Approved
<u>Vladimir Hlady</u>	, Member	<u>24-April-2012</u> Date Approved
<u>Patrick A. Tresco</u>	, Member	<u>24-April-2012</u> Date Approved

and by Vladimir Hlady, Chair of
the Department of Bioengineering

and by Charles A. Wight, Dean of The Graduate School.

ABSTRACT

Heparan sulfate (HS) chains play roles in numerous biological processes as they bind to various signaling molecules including fibroblast growth factors (FGFs). This graduate research aims at investigating the structural requirements and the biogenesis pathways of FGF8-binding HS motifs.

In the first part, the importance of HS multivalency in regulating FGF8 and FGF receptor (FGFR) interactions *in vivo* was examined. A library of mono-, bis- or tris-xylosides was injected into zebrafish embryos to stimulate the production of monomeric, dimeric or trimeric glycosaminoglycan (GAG) chains that are connected covalently, and thereby mimic naturally occurring proteoglycans. Upon their injection, bis- and tris-xylosides caused an elongation phenotype whereas mono-xylosides did not. *In situ* hybridization and other experiments showed that FGF8/FGFR signaling was specifically hyperactivated in elongated embryos. Based on our findings, we propose a molecular model in which two covalently linked GAG chains interact with two FGF8 molecules and their cognate FGFRs and induce FGFR dimerization that leads to the elongation phenotype. This proposed molecular model was reaffirmed by the results of experiments testing syndecan-1 constructs containing zero, one, two or three HS side chains, in which multivalency again demonstrated its essential role in activating FGF8 signaling.

In the second part, a library of HS oligosaccharides with defined sizes and structures was enzymatically synthesized to study the assembly of FGF8-binding HS motifs. Firstly, HS backbones, *N*-acetylheparosan, were produced in *E.coli* K5. The HS backbones were then fragmented to obtain size-defined oligosaccharides. Secondly, HS biosynthetic enzymes including *N*-deacetylase *N*-sulfotransferase, C5-epimerase, 2-*O*-sulfotransferase, 6-*O*-sulfotransferases and 3-*O*-sulfotransferases were expressed and purified. The actions of these isoforms were then studied to provide guidance to assemble the HS oligosaccharide library. Finally, this library was tested on zebrafish embryos for their effect on FGF8 signaling. With these results, we were able to reveal the minimum size, the specific structures and the biogenesis pathway of HS structural motifs that can activate FGF8 signaling *in vivo*.

In summary, the results provide new insights into how FGF8-binding HS motifs are synthesized *in vivo* and give rise to synthetic tools that facilitate the establishment of HS structure-function relationships in a comprehensive manner.

TABLE OF CONTENTS

ABSTRACT	iii
LIST OF TABLES	vii
LIST OF ABBREVIATIONS	viii
ACKNOWLEDGEMENTS	x
Chapter	
1 INTRODUCTION	1
1.1 Overview of proteoglycans	2
1.2 Research objectives	20
1.3 References	24
2 DIMERIZED GLYCOSAMINOGLYCAN CHAINS INCREASE FGF SIGNALING DURING ZEBRAFISH DEVELOPMENT.....	30
2.1 Introduction	31
2.2 Experimental procedures	32
2.3 Results	39
2.4 Discussion	56
2.5 Supplemental data	61
2.6 References	70
3 ENZYMATIC SYNTHESIS OF FGF8- BINDING HS MOTIFS.....	74
3.1 Overview.....	75
3.2 Characterization of uniformly and atom-specifically ¹³ C-labeled heparin and heparan sulfate polysaccharide precursors using ¹³ C NMR spectroscopy and ESI mass spectrometry.....	78
3.3 A synthetic heparan sulfate oligosaccharide library reveals the novel enzymatic action of D-glucosaminyl 3-O-sulfotransferase-3a.....	84
3.4 Investigating the mechanism of the assembly of FGF1-binding heparan sulfate motifs.....	95

3.5 <i>In vitro</i> synthesis of HS library and screening for FGF8 binding HS motifs in zebrafish embryos.....	101
3.6 References	123
4 CONCLUSIONS	125
4.1 Conclusions.....	126
4.2 References.....	132

LIST OF TABLES

2.1	Structures of the xylosides studied in zebrafish embryos.....	40
2.S.1	Structures of additional mono-xylosides tested in zebrafish embryos.....	61
2.S.2	Effect of bis-xylosides and mono-xylosides on the elongation phenotype at 12 hpf and on <i>mkp3</i> expression at 8 hpf.....	63
3.1	¹ H and ¹³ C chemical shifts of HS precursors in D ₂ O at 25°C.....	83
3.2	Structures of oligosaccharides examined as potential substrates for 3-OST3a and 3-OST1.....	86
3.3	Potential 3-O-sulfated disaccharides resulted from 3-OST3a modified oligosaccharides with their expected mass	87
3.4	Assembly of HS polysaccharide structures.....	106
3.5	NS oligosaccharides utilized in the study.....	109
3.6	MS profiles of NS oligosaccharides before and after epimerization by C5-epimerase.....	111
3.7	MS profiles of NSEpi2S oligosaccharides	116
3.8	MS profiles of NS6S oligosaccharides.....	119

LIST OF ABBREVIATIONS

ATIII	antithrombin III
C5-Epi	C5-epimerase
CS	chondroitin sulfate
Dp	degree of polymerization
DS	dermatan sulfate
ECM	extracellular matrix
EXT	exostoses
FGF	fibroblast growth factor
FGFR	fibroblast growth factor receptor
GAG	glycosaminoglycan
Gal	galactose
GalNAc	<i>N</i> -acetyl galactosamine
GlcA	glucuronic acid
GlcNAc	<i>N</i> -acetyl glucosamine
GPI	glycosylphosphatidylinositol
Hpf	hours post fertilization
HS	Heparan sulfate
HSV	herpes simplex virus

IdoA	iduronic acid
KS	keratan sulfate
LC	liquid chromatography
MS	mass spectrometry
NA	<i>N</i> -acetyl
NS	<i>N</i> -sulfo
NS6S	<i>N</i> -sulfated, 6- <i>O</i> -sulfated
NSEpi	<i>N</i> -sulfated, epimerized
NSEpi2S	<i>N</i> -sulfated, epimerized, 2- <i>O</i> -sulfated
NDST	<i>N</i> -deacetylase <i>N</i> -sulfotranferase
OST	<i>O</i> -sulfotransferase
PAPS	3'-phosphoadenosine-5'-phosphosulfate
PG	proteoglycans
S-AF350	Streptavidin-Alexa Fluor 350
SPR	surface plasmon resonance
SULF	sulfatase

ACKNOWLEDGEMENTS

First and foremost, I would like to express my sincere gratitude to my mentor, Prof. Kuberan Balagurunathan, for his support, guidance and motivation throughout my PhD study. I thank him for always being resourceful, positive and supportive of me.

I would like to thank Prof. Chi-Bin Chien and Prof. Richard I. Dorsky for their support and guidance for my research, especially for my zebrafish experiments. Without them, I could not have had such a successful collaboration. I would like to thank Prof. Vladimir Hlady, Prof. Patrick A. Tresco and Prof. Joshua Bonkowsky for their helpful comments and encouragement.

I sincerely thank my labmates, Dr. Xylophone Victor, Vy Tran, Karthik Raman, Spencer Brown, Dr. Manivannan Ethirajan, Dr. Sorna Venkataswamy, Dr. Sailaja Arungundram, Dr. Babu Ponnusamy, Vimal Swarup and Caitlin Mencio, for their help, insightful discussion for my research and support for my life in Utah. I also thank Chien lab members for their support.

I would like to thank my parents, my brother and my sister-in-law for their continuous support.

Last but not least, I thank Hai Pham, my beloved husband, for his unconditional support and love.

CHAPTER 1

INTRODUCTION

1.1 Overview of proteoglycans

1.1.1 Structures of proteoglycans

Proteoglycans (PGs) are basic components of the extracellular matrix. Each PG molecule consists of a core protein and multiple glycosaminoglycan (GAG) side chains. The following four types of GAG chains are found to be attached to PG core proteins: heparan sulfate (HS), chondroitin sulfate (CS), dermatan sulfate (DS) and keratan sulfate (KS). Proteoglycans, such as syndecan, glypican, aggrecan, perlecan, decorin and biglycan can be categorized based on their core protein sequence, and the number and the type of their GAG side chains. A structural overview of PG family members is depicted in Figure 1.1.

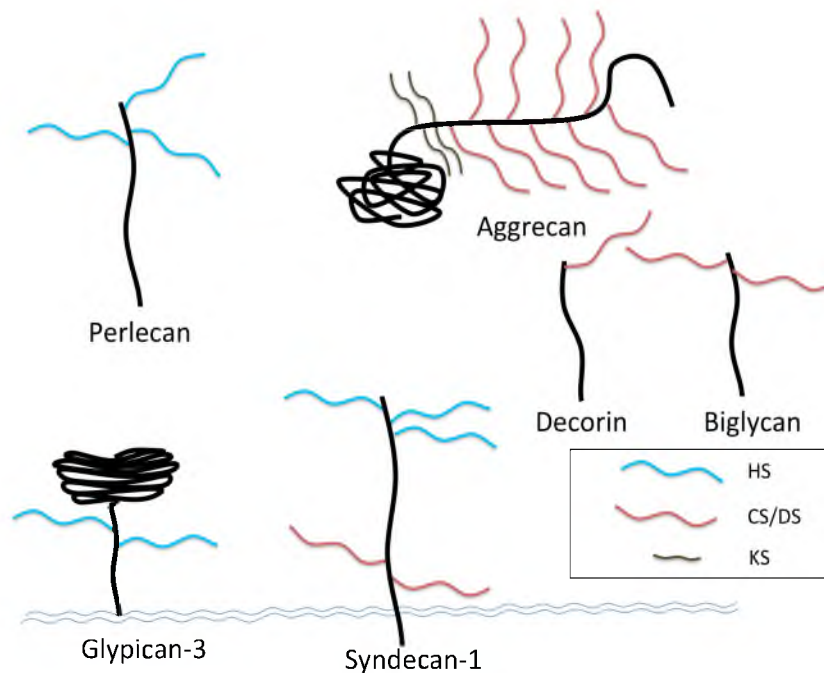


Figure 1.1 Structural representation of a few proteoglycans (adapted from (1)). Glypicans are GPI-linked cell surface PGs; syndecans are transmembrane cell surface PGs; perlecan, aggrecan, decorin and biglycan are secreted proteins found in the ECM. Most PGs contain two or more GAG side chains.

Syndecan is a group of transmembrane proteins with 3-5 HS and CS attachment sites on each core protein, whereas glypican is a group of glycosylphosphatidylinositol (GPI) anchored proteins with 2-3 HS attachment sites on each core protein. Aggrecan, the major component of cartilage, is another protein group with each molecule containing two globular structural domains at the N-terminal, a globular C-terminal, a CS region having several hundreds CS chains and a KS region. Perlecan is a group of secreted proteins with each molecule containing 3 attachment sites for HS or CS. Decorin and biglycan are small core proteins with leucine-rich repeats and each of their molecules contains single or 2 CS/DS attachment sites, respectively (2).

The GAG side chains are linear, sulfated polysaccharides containing repeating disaccharide units of hexosamine (glucosamine/galactosamine) and hexuronic acid (glucuronic/iduronic). GAG chains differ by the type of repeating units, glycosidic linkage and positions of sulfate groups. Particularly, HS contains glucuronic acid (GlcA) or iduronic acid (IdoA) and *N*-acetyl glucosamine (GlcNAc), CS contains GlcA and *N*-acetyl galactosamine (GalNAc), DS contains GlcA or IdoA and GalNAc, and KS contains galactose (Gal) and GlcNAc. Disaccharide building blocks of each type of GAG are illustrated in Figure 1.2.

1.1.2 Biosynthesis of proteoglycans

The biosynthesis of PGs requires many enzymes and their isoforms as well as various sugar activators and transporters. Differential expression of these enzymes and transporters creates diverse fine structures in a tissue-specific manner. An overview of the biosynthetic process of a PG is depicted in Figure 1.3. The first step in this process is

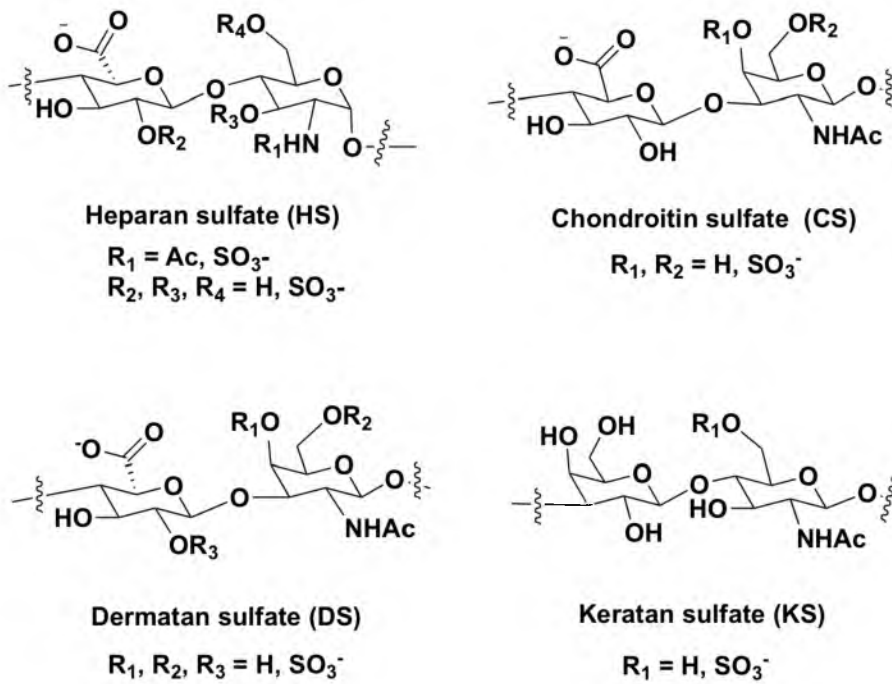


Figure 1.2 Structures of repeating disaccharide units that are found in heparan sulfate, chondroitin sulfate, dermatan sulfate and keratan sulfate.

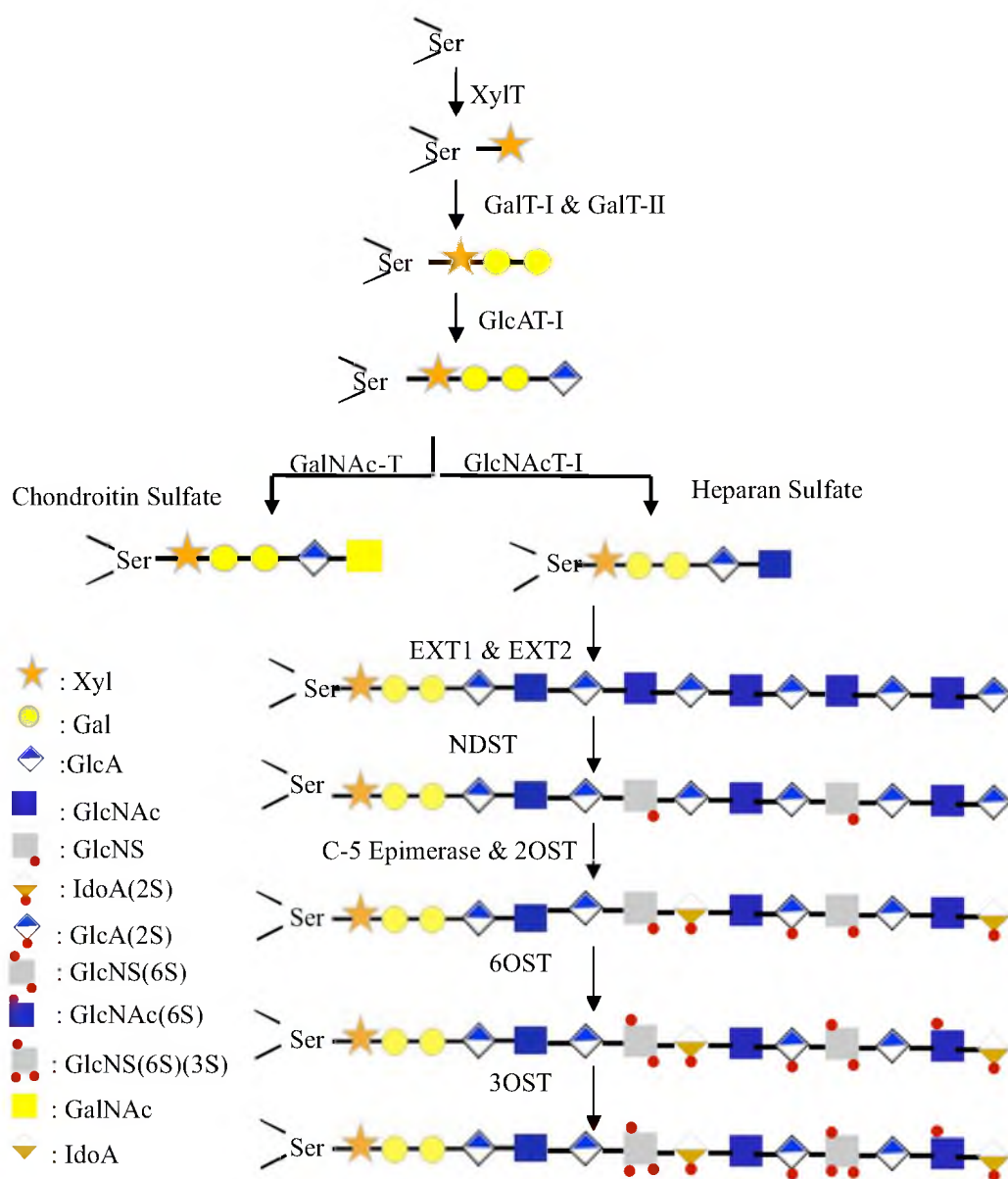


Figure 1.3 Overview of proteoglycan biosynthesis (3). See the text for the detailed description.

the assembly of a tetrasaccharide linkage on specific serine residues within the core protein. A xylose residue is first transferred from UDP-xylose to a specific serine residue by xylosyltransferase. Three other enzymes subsequently transfer two Gal residues and finally one GlcA residue to complete the assembly of the linkage. This tetrasaccharide linkage region can be modified by phosphorylation and sulfation that may likely play a decisive role in the later assembly processes. The second step is the polymerization of the GAG chain. If a α 1,4-linked GlcNAc is added as a fifth residue to the linker tetrasaccharide, HS chain will be assembled, whereas if a β 1,4-linked GalNAc is added to the tetrasaccharide, CS chain assembly will occur. The factors that control the addition of the fifth residue, which dictates the fate of GAG type assembly, are largely unknown.

For HS chains, repeating disaccharide units containing GlcA and GlcNAc are added to the nascent chain by exostoses (EXT1 and EXT2) followed by a series of modifications. These modifications take place in specific compartments containing specific enzymes in the Golgi apparatus called GAGOSOMES. The first modification normally is *N*-deacylation and *N*-sulfation of GlcNAc residues, a gateway modification for subsequent modifications. GlcA can be epimerized to IdoA by C5-epimerase immediately following *N*-sulfation but prior to other *O*-sulfations. A variety of *O*-sulfotransferase (OST) enzymes add sulfate groups to C6 (6-OST) and C3 (3-OST) of glucosamine residues and C2 (2-OST) of IdoA predominantly and GlcA rarely. These enzymes transfer the sulfate group from 3'-Phosphoadenosine-5'-phosphosulfate (PAPS) to the HS chain at a specific position. It has been reported that the concentration of the sulfate donor PAPS partly controls the extent of sulfation. Moreover, four NDST isoforms, one C5-epimerase, one 2-OST, seven 3-OST isoforms and three 6-OST

isoforms have been found in humans and other organisms. These isoforms are expressed in a spatio-temporal manner and have distinct substrate specificity, giving rise to a vast structural diversity of HS chains. Substrate specificity of different enzyme isoforms is largely unknown with the exception of several enzymes. To further augment HS structural diversity, HS has a domain-like architecture composed of highly sulfated domains (NS domains), nonsulfated domains (NA domains), and partially sulfated domains (NA/NS domains). It is believed that the presence of GAGOSOMES containing specific composition and location of HS biosynthetic enzymes gives rise to these different domains. In addition, 6-*O*-sulfate groups can be later removed outside of the cell by sulfatase (SULF). All of the factors mentioned above create a large structural diversity of HS chains, which are believed to regulate the precise functions of PGs (4). Understanding the HS structure-function relationships is probably the most intriguing topic in the field, even though only very few cases are well-understood up to now.

For CS chains, GlcA and GalNAc units are added alternatively to the growing chain by chondroitin sulfate synthase. Sulfation by specific sulfotransferases may occur at C4 and C6 of GalNAc. The differences in the sulfation sites categorize CSs into four classes, including CS A, C, D and E. For DS chains, GlcA/IdoA and GalNAc are the repeating disaccharide units. The sulfation of DS occurs at C4, C6 of GalNAc and C2 of IdoA.

1.1.3 Biological functions of heparan sulfate

The diverse functions of HS are determined by its interactions with various protein partners such as growth factors, chemokines, cytokines, morphogens, receptors

and enzymes (5). Therefore, HS is involved in regulating cell proliferation, adhesion, migration and differentiation. It has been shown that HS plays important functional roles in angiogenesis, axonal growth, anticoagulation, cell signaling and embryonic development, among others (6). HS is also associated with various pathological phenomena such as tumor growth, inflammation and microbial pathogenesis.

The first and most well-known function of HS is its anticoagulation activity (Figure 1.4A). This function was first discovered with heparin, the highly sulfated form of HS that is produced mostly in connective tissue mast cells. Heparin/HS promotes anticoagulation through the binding of a specific pentasaccharide sequence (GlcNAc6S-GlcA-GlcNS3S6S-IdoA2S-GlcNS6S) to antithrombin III (ATIII), leading to a conformational change of ATIII and thus enhancing ATIII binding to its target proteases including thrombin and factor Xa (7-9).

HS binds to numerous viruses and bacteria, facilitating their entry and thereby assisting their infections (Figure 1.4B). It has been shown that HS is involved in the infections of over 16 viruses including herpes simplex virus (HSV), HIV and hepatitis C virus (10). The interactions of HS with viruses have been extensively studied in the last two decades, suggesting the function of HS as specific receptors in viral infection. A well-studied example is 3-*O*-sulfated *N*-unsubstituted GlcN3S, which has been shown to be required for HS binding to herpes simplex gD protein and promoting HSV infection (11).

It has been shown that HS can bind to a variety of cytokines such as chemokines and interferon γ , transport them across cells and present them at the cell surface (Figure

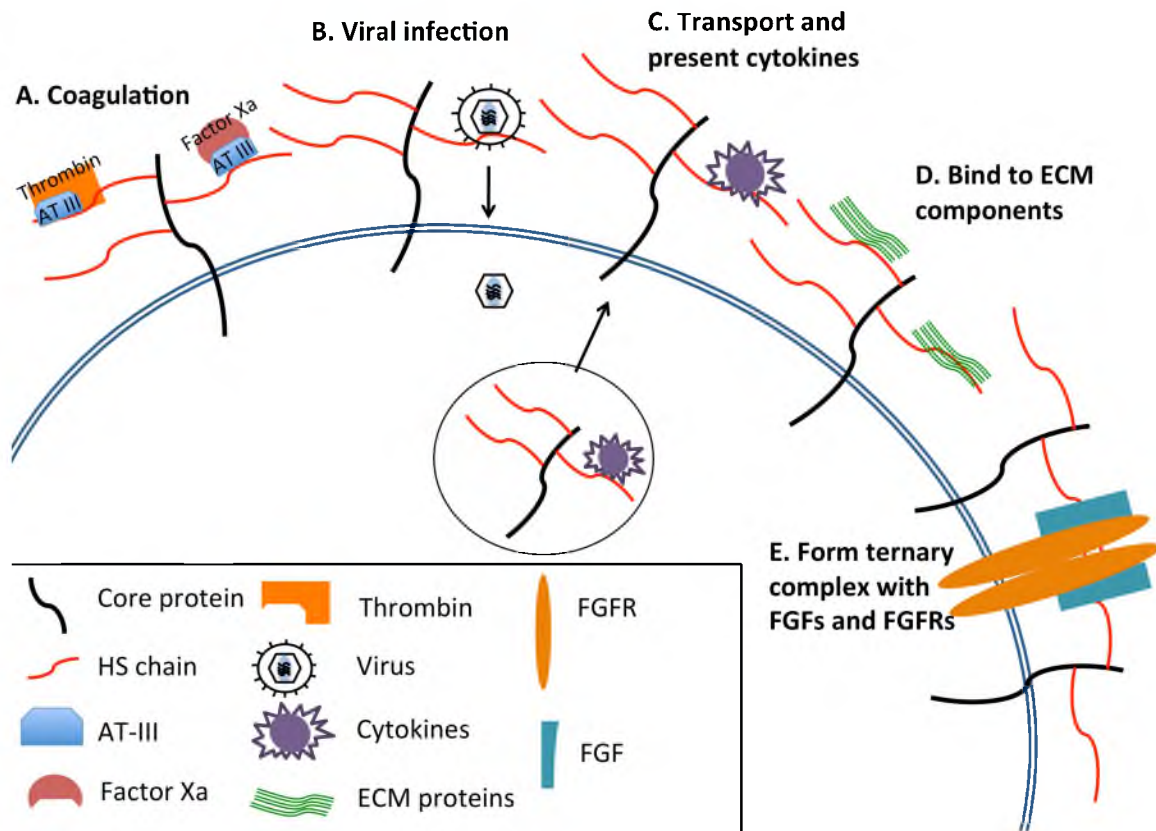


Figure 1.4 The many roles of HS (adapted from (12)). **A:** HS binds to ATIII and has coagulant activity. **B:** HS binds to various viruses and assists their infection. **C:** HS transports and presents a number of cytokines to the cellular surface. **D:** HS binds to a variety of ECM proteins, promoting cell adhesion and forming ECM. **E:** HS binds to various growth factors and their cognate receptors.

1.4C). This explains a number of HS functions in anti-angiogenesis, procoagulations, leukocyte activation, neutrophil adhesion and migration (12, 13).

HS binds to a number of extracellular matrix components including fibronectin and collagens (Figure 1.4D), and regulates the formation of extracellular matrix, cell adhesion and cell motility processes. HS also plays important roles in modulating a variety of growth factor signaling pathways including fibroblast growth factors (FGFs), which are crucial in embryonic development, homeostasis and regenerative processes (Figure 1.4E) (14, 15). It has been shown that HS functions as co-receptor for growth factors and their tyrosine kinase receptors. HS can also sequester the growth factors, release or present them at the cell surface (12). A large number of *in vitro* studies claimed the importance of HS in regulating FGF/FGFR signaling pathways but mainly focused on two proteins, FGF1 and FGF2, of the FGF family. Many groups have been attempting to deduce the absolute required sequence of HS in FGF signaling as in the case with ATIII (14, 15). However, more and more evidence has been found to prove that several HS structures can activate the same FGF signaling. These characterized structural requirements of HS in FGF signaling are discussed in details in Section 1.1.5. This is also the central matter of this thesis, in which structural requirements of HS in FGF8 signaling are studied and the absence of single HS sequence for activating FGF8 signaling is shown.

A number of genetic studies have been carried out using invertebrates and vertebrates to understand how specific modifications of HS affect its interactions with proteins and hence their functions. Mutations in HS biosynthetic enzymes in *D. melanogaster* and *C. elegans* revealed that HS is important for many crucial biological

pathways such as wingless, Hedgehog, Notch and FGF signaling (16-22). Nevertheless, a significant disadvantage of genetic approaches is that mutations in the genes encoding HS biosynthetic enzymes, e.g., 2-OST, NDST1 in mice, normally cause neonatal lethality or have no effect due to compensation by other isoforms (23-25).

The importance of biological functions of HS is also understood through a variety of disorders in humans due to mutations in the genes involved in GAG biosynthetic pathways. Chromosomal mutation in glypican-3 is linked to Simpson-Golabi-Behmel overgrowth syndrome (26). Mutations in EXT, HS biosynthetic polymerase, are responsible for hereditary multiple exostosis, a bone disorder (27). Deficiencies of any one of 11 different enzymes, required for the degradation of GAGs, cause seven heritable lysosomal storage disorders, collectively known as mucopolysaccharidosis, which can lead to severe physical/facial deformation and mental retardation (28).

One of the major questions in the glycobiology field is to understand the critical structural parameters of HS chains that are essential for their interactions with a wide array of protein partners. Many attempts to further our understanding on these matters have been made in the past two decades using various biochemical, structural biology and molecular modeling approaches (6). The interactions of HS with proteins are regulated by strong ionic interactions, van der Waals forces, hydrophobic and hydrophilic interactions, and hydrogen bonding. There have been a number of studies on HS-protein interactions using X-ray crystallography but they have not been able to identify HS functional groups required for binding to proteins. Moreover, there is a lack of *in vivo* studies of these important interactions and their functional consequences.

The functions of PGs are regulated not only by the GAG fine structure but also by the position and the number of their side chains. For example, the importance of multiple HS chains for syndecan-1 function has been investigated by expressing syndecan-1 having a variable number of HS chains (zero, one, two, or three) in a cellular system (29). The presence of two HS chains instead of three chains resulted in a slight to moderate decrease in cell adhesion. Loss of two chains resulted in a significant decrease in cell adhesion, whereas elimination of all three chains led to total loss of adhesion. These findings clearly point out that the clustering of HS chains on adjacent amino acids within the core protein is essential for optimal cellular behavior.

1.1.4 FGFs and their biological functions

FGF are polypeptide growth factors of 150-250 amino acid residues, sharing a conserved β -trefoil core containing 100-120 residues and variable N- and C-terminal regions (30). There are 22 FGF members and 4 FGFR genes that have been described in humans. In zebrafish, there are 27 FGF members due to additional genome duplication (30). FGF signaling pathways have been found to be involved in many developmental processes including cell proliferation, migration and differentiation as well as in numerous physiological processes.

FGF gene families, together with their evolution and their functions in development, metabolism and disease, have been well studied in humans, mice and zebrafish. The majority of FGF functions have been studied by using FGF knockout mice, FGF knockout and knockdown zebrafish, and human hereditary diseases. In zebrafish development, it has been reported that FGFs play a key role in many

morphogenesis processes including dorsal-ventral patterning of the gastrula and midbrain-hindbrain boundary formation (FGF8) (31, 32), optic placode and vesicle formation (FGF3, FGF8) (33), lens and retina development (FGF19) (34), fin formation (FGF10a, FGF16, FGF24) (35-37), fin regeneration (FGF20a) (38), forebrain development (FGF19) (39), primordium formation (FGF3, FGF10) (40) and hematopoiesis (FGF21) (41). In adult zebrafish, FGFs regulate a vast number of biological processes including homeostasis, wound healing, regeneration, cholesterol metabolism and serum phosphate regulation. Failure in FGF signaling leads to a variety of pathological conditions including skeletal, retinal, olfactory, metabolic disorders and cancer. FGFs have been also shown to be involved in many human diseases such as Michel aplasia (FGF3) (42), Borjeson-Forssman-Lehmann syndrome (FGF13) (43), Parkinson disease (FGF20) (44), Kallmann syndrome (FGF8) (45) and LADD syndrome (FGF10) (46).

1.1.5 FGF signaling and HS

FGF signaling is activated through the formation of two HS/FGF/FGFR ternary complexes leading to the dimerization and tyrosine autophosphorylation of the FGFRs. A large number of *in vitro* studies reported the importance of HS in regulating FGF/FGFR signaling pathways (14, 15). FGFs and their cognate receptors need to interact with HS chains to form a stable and fully functional ternary complex. HS is also believed to ensure FGF stability and availability at appropriate concentrations as well as the level and the duration of FGFR occupancy (47). Many studies have examined the nature of interactions among FGFs, FGFRs and HS or heparin, a closely related form of

HS produced by mast cells. In fact, heparin has a higher percentage of iduronic acid and sulfation density and does not contain domain structures like HS. In addition, most studies focus on FGF1 and FGF2, the first two FGFs isolated. Biophysical studies have revealed the crystal structure of the 2:2:2 complex of FGF2, FGFR1 and heparin decasaccharide and the 2:2:1 complex of FGF1, FGFR2 and heparin decasaccharide, as shown in Figure 1.5 (48, 49).

Understanding the structural requirements of HS in its interactions with FGF and FGFR is a topic of great interest in the glycobiology field. There are a few studies indicating that these interactions can be regulated by the type of sulfation, the chain length as well as the sulfation density of HS chains (50-53).

Various studies have shown that particular types of sulfation are required for HS interactions with particular FGFs and FGFRs. For instance, 2-*O*-sulfation is essential for FGF2 binding, 6-*O*-sulfation is important for FGF10 binding, while both 2-*O* and 6-*O* sulfation are critical for FGF1, 4, 7 and 8 binding (50-52). On the other hand, both 2-*O* and 6-*O* sulfations are required for the activation of FGF2-FGFR mediated signaling pathway (52). However, there has been no evidence of the contribution of specific sequences or sulfation patterns on interactions.

The HS backbone typically contains 50-150 monosaccharide units, thus it is possible that multiple FGFs and FGFRs can bind to one HS chain (54). Moreover, the analysis of HS polymer can be very challenging. Therefore, the minimum size of HS oligosaccharides for binding to FGFs has been investigated. FGF1 binds tetrasaccharide (Dp4), FGF2 binds pentasaccharide (Dp5) and FGF8b binds 5-7 mer oligosaccharides

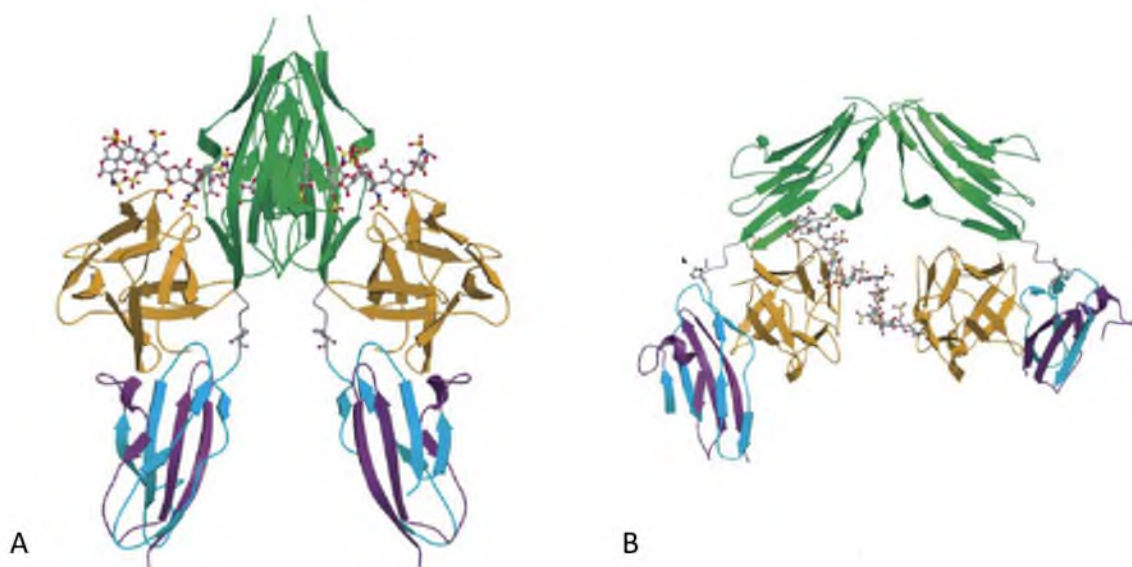


Figure 1.5 Two different crystal structures of FGF/FGFR/heparin ternary complex (55). A: Ribbon diagram of the 2:2:2 FGF2/FGFR1c/heparin crystal structure. B: Ribbon diagram of the 2:2:1 FGF2/FGFR2c/heparin crystal structure. FGF ligand is colored in orange. FGFR is colored in green, blue and purple. Heparin is drawn with colored atom, gray for carbon, blue for nitrogen, red for oxygen and yellow for sulfur.

(53, 56, 57). However, the minimum size of oligosaccharides that can promote FGF activity is actually longer, 6-8 mer for FGF1 and 12-14 mer for FGF8b (56).

Beside the evidence stated above on the contribution of HS structural specificity on the interactions with FGFs, several studies have suggested that highly sulfated HS can mask the importance of specific sulfation (47, 58). Therefore, the total number of sulfate groups/sulfation density is also critical for HS/FGF/FGFR interactions. In a study using HS deca-saccharide (Dp10), at least 4 *O*-sulfate groups are required to promote the ternary complex formation with FGF1/2 and FGFR. However, oligosaccharides with at least 6 *O*-sulfate groups can generate much more stable complexes (47). In another study using HS octa-saccharide (Dp8), 7-8 sulfate groups are required for the complex formation with FGF7 and FGFR2(IIIb) (58).

Due to the lack of a homogenous and structurally defined HS source, only the importance of *N*-sulfation, 2-*O* and 6-*O* sulfation in HS/FGF/FGFR interactions has been studied. There has been no report on the role of 3-*O*-sulfation, the rare modification, in the interactions of HS with FGF and FGFR. Moreover, as mentioned earlier, the previous studies mostly focused on FGF1 and FGF2. Meanwhile, FGF8 is one of the FGFs that is expressed earliest during development and plays crucial roles in limb, central nervous system and cardiac outflow tract development (30). Our understanding of how HS orchestrates dynamic interactions with FGF8/FGFR *in vivo* remains obscure. Therefore, studying the structural requirements of HS in its interactions with FGF8/FGFR can provide a molecular basis of these crucial interactions and help expand our knowledge of FGF/FGFR-mediated signaling pathways.

There are only a few techniques available to determine the structural requirements of HS for FGF/FGFR interactions. To analyze the ability of binary and ternary complex formation, gel mobility shift assay, filter trap assay, protein bound oligosaccharide analysis and surface plasmon resonance (SPR) have been developed (57, 59). However, these methods require specially modified HS such as radioactive labeling or functional group conjugation. Furthermore, these assays are performed *in vitro*, which may not necessarily recapitulate interactions that occur *in vivo*. The only available assay for FGF activity is the mitogenic activation assay on BaF3 cell systems, transfected with specific FGFR or on xylosyltransferase mutated CHO cells, which do not produce any GAG. In this assay, HS is tested in terms of stimulating FGF activity or inhibiting FGF activity through competing with endogenous HS or added heparin. It is important to note that beside this proliferation assay, there is no other assay to determine the direct roles of HS

in two other major FGF-modulated cellular processes, which are cell differentiation and cell migration.

1.1.6 Major sources of HS used for HS-FGF interaction studies

Due to the important roles of HS-protein interactions in various biological processes, designed HS has been synthesized (52, 57, 60). These exogenous HS molecules activate or inactivate targeted signaling pathways by competing with endogenous HS or inhibiting HS biosynthesis. Many small molecules that mimic the protein-binding structures of HS have been designed (61, 62). However, due to our limited understanding of the HS fine structures, applications of these molecules have not advanced our knowledge on HS structure-function relationships. The central difficulty is to discover the structures that can bind to proteins with nanomolar binding affinity and specificity.

The most common source of HS/heparin is from animals, this HS/heparin is purified, fractionated and modified through many different procedures. However, purification from natural sources remains a challenge. For instance, heparin, a world-wide used anticoagulant purified from animal sources, has been reported to be tainted with over sulfated chondroitin sulfate chains that are linked to adverse clinical reactions (63). Substrates used in most HS/FGF/FGFR interaction studies are chemically modified from natural HS/heparin. Usually in these molecules, particular sulfate groups, i.e., *N*-sulfate, *O*-sulfate, 2-*O*-sulfate or 6-*O*-sulfate groups can be selectively removed or re-sulfated (52, 53, 64). However, due to the nonspecific nature of chemical reactions, absolute conclusions could not be drawn in some cases.

The organic synthesis of HS is impractical due to structural complexity and difficulties in introducing labile functional groups in a regioselective manner. This process involves numerous steps and results in very low yield especially with oligosaccharides of higher sizes (65). A pentasaccharide-based anticoagulant that functions as well as heparin has been successfully synthesized but this is a result of three decades of extensive studies of heparin interactions with antithrombin III by Rosenberg and Lindahl groups (7, 8).

A recently developed and widely used approach is chemo-enzymatical synthesis of HS. In this approach, specific modifications are done on *N*-acetylheparosan, which is the HS backbone produced in *E.coli* K5 or chemically modified heparins (57, 60, 66). The modifications are achieved by a combination of HS biosynthetic recombinant enzymes, mimicking the reactions that happen in the Golgi apparatus. This approach can result in the assembly of bioactive HS molecules in a much shorter time with higher yield than the chemical process (60).

In addition, oligosaccharides are also obtained from these different HS sources by enzymatic and chemical cleavage. The advantages of utilizing synthetic oligosaccharides in structure-function relationship studies are that these substrates can be homogenous in size and structure. The chemo-enzymatic approach to synthesize size-defined oligosaccharides is very useful to study HS structure-function relationships. However, this approach requires the availability of all HS biosynthetic enzymes and careful characterization of each structure by high sensitive mass spectrometry. Therefore, only a few groups can utilize this approach. This thesis exploits this approach to deduce the structural requirements of HS in its interactions with FGF8 and FGFR.

The only approach to produce HS *in vivo* is utilizing a group of small molecules, designated as xylosides, to induce the biogenesis of HS inside the cells. Each xyloside molecule contains a xylose residue and a hydrophobic moiety that can prime HS, CS and/or DS in the absence of core proteins. Aglycone moiety of xylosides influences the priming activity and the nature of the primed GAG chains (67, 68). The xyloside-primed GAG chains are secreted to the extracellular matrix and regulate various biological processes. Mono-xylosides have been used in studies for over three decades (69-71). Treatment of β -mono-xylosides eliminates left-right asymmetry in the *Xenopus laevis* cardiac loop through competitively inhibiting proteoglycan biosynthesis (71). HS primed on β -D-xylosides behaves like endogenous HS in term of its ability to function as co-receptor for FGF2 (71). Mono-xylosides can only initiate the formation of monomeric GAG chains. However, most proteoglycans contain more than one GAG side chain. Therefore, multimeric GAG chains primed by cluster xylosides might be better mimics for PGs. These cluster xylosides contain more than one xylose residue per scaffold; thus, they can prime covalently bonded multimeric GAG chains. However, there have been no studies on cluster xylosides *in vivo*. The GAG-priming process of a bis-xyloside, a cluster xyloside containing two xylose residues, is presented in Figure 1.6.

In summary, it is necessary to produce HS with specific structural parameters both *in vivo* and *in vitro* so that we can further our knowledge on the structural requirement of HS in its interactions with proteins including FGF/FGFR. Understanding the fine structural requirements of HS for its biological interactions with protein ligands is very crucial to the development of novel therapeutic agents.

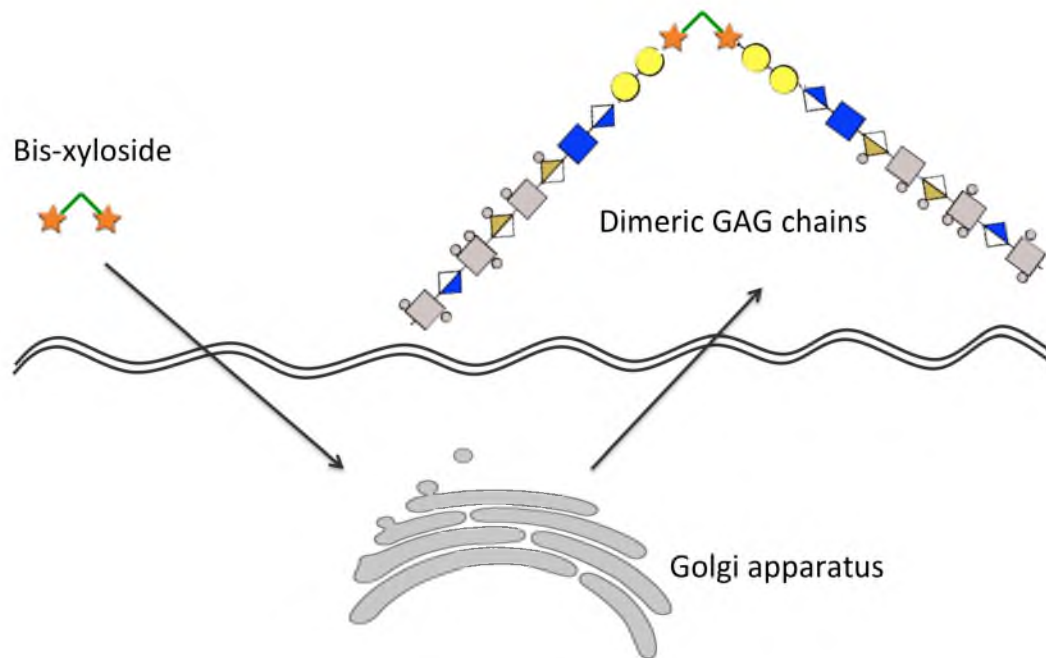


Figure 1.6 GAG-priming process by a bis-xyloside. A bis-xyloside containing two xylose residues (stars) diffuses into the Golgi apparatus and makes a PG mimetic containing two GAG chains. The primed molecule is subsequently secreted to the ECM.

1.2 Research objectives

HS acts as co-receptor for FGF and FGFR to form a ternary complex, inducing receptor dimerization and signal transduction. Numerous models have been proposed to explain FGFR dimerization at the molecular level (48, 49). All of these models attempted to elucidate the nature of HS/FGF/FGFR interactions based on various *in vitro* or *ex vivo* biochemical and biophysical studies. However, the structural basis for the role of HSPGs in assisting FGF/FGFR signaling *in vivo* requires careful re-evaluation because most models employed single or two covalently disconnected, highly sulfated heparin oligosaccharides whereas naturally occurring PGs carry two or more GAG chains, suggesting the importance of GAG chain valency.

Our goal is to study the biogenesis pathway and structural requirements of HS including multivalency, sizes and specific sulfation compositions in the interactions and activation of FGF8/FGFR in a biological system. Our major questions are: What is the function of the multimeric form of HS in its interactions with FGF8 and FGFR? What are structural attributes, in terms of molecular size and specific functional groups of HS, required for assembling and activating the HS/FGF8/FGFR ternary complexes? Finally, how are these FGF8 binding HS motifs generated *in vivo*? To answer these fundamental questions, we used two approaches. The first approach involves the utilization of a library of xylosides, synthetic small molecules that can initiate the formation of single or multiple HS chains, to study the effect of HS multivalency on FGF8 signaling in zebrafish embryos during development. The second approach involves the utilization of enzymatic strategy to prepare a library of defined oligosaccharide structures to study the biogenesis of FGF8-binding HS motifs.

1.2.1 Specific Aim I

Utilizing a library of mono- and cluster-xylosides in zebrafish embryos to reveal the importance of GAG multivalency in FGF8 signaling during early development.

Endogenous PGs often possess multiple HS chains arranged in a clustered fashion. Thus, the contribution of clustered HS chains of PGs to FGFR dimerization and *in vivo* signaling through their co-operative interactions has not yet been shown in any animal model. We presume that one of the possible reasons for the inconsistency among published data stems from neglecting the significance of clustered HS chains, which

naturally occurs in all PG structures. Therefore, in this study, a library of xylosides was screened in zebrafish embryos for their effect on FGF signaling throughout early development. This library included mono-, bis- and tris-xylosides, which can initiate the formation of monomeric, dimeric and trimeric GAG chains, respectively. By introducing these xylosides into zebrafish embryos, we were able to evaluate the importance of GAG multivalency in developing zebrafish embryos through modulating FGF signaling pathways.

1.2.2 Specific Aim II

***In vitro* enzymatic synthesis of HS oligosaccharides to elucidate the structural requirements of HS in activating FGF8/FGFR signaling *in vivo*.**

The HS backbone is highly modified by about 20 different enzymes and their isoforms to make specific sulfation patterns, which are believed to be responsible for a wide array of HS functions. There have been no studies that attempted to elucidate the sulfation patterns critical for *in vivo* HS/FGF/FGFR interactions and how biogenesis of such sulfation patterns occurs. Therefore, by employing enzymatic synthesis to produce a library of HS oligosaccharides with different sizes for testing their effect on FGF8 signaling during zebrafish development, we were able to reveal the importance of specific modifications of HS in FGF8 signaling *in vivo*.

The results from this study provide new insights into both HS assembly and HS-FGF interactions. As mentioned earlier, in order to develop bioactive HS, knowledge of the fine structures of HS that are crucial for HS-proteins interactions is required, but thus far these have not been well understood except for ATIII-binding HS motifs. By looking

closely at the structures of HS and particularly at specific structural features required for FGF8 signaling, we could uncover their fine structures, their biogenetic pathways and their functional roles. The results also provide the basis for studies on the interactions of HS with other proteins, which play crucial roles in many developmental processes. This could be a foundation for the development of *in vivo* glycoengineering approaches to rescue developmental defects caused by impaired HS signaling pathways.

1.3 References

1. Perrimon, N.; Bernfield, M., Specificities of Heparan Sulphate Proteoglycans in Developmental Processes. *Nature* **2000**, *404* (6779), 725-8.
2. Varki, A., Cummings, R., Esko, J., Freeze, H., Hart, G., Marth, J., *Essentials of Glycobiology*. Cold Spring Harbor Laboratory Press: La Jolla, 1999.
3. Raman, K., Kuberan, B., Chemical Tumor Biology of Heparan Sulfate Proteoglycans. *Current Chemical Biology* **2009**, *4* (1), 20-31.
4. Esko, J. D.; Lindahl, U., Molecular Diversity of Heparan Sulfate. *J Clin Invest* **2001**, *108* (2), 169-73.
5. Bernfield, M.; Gotte, M.; Park, P. W.; Reizes, O.; Fitzgerald, M. L.; Lincecum, J.; Zako, M., Functions of Cell Surface Heparan Sulfate Proteoglycans. *Annu Rev Biochem* **1999**, *68*, 729-77.
6. Gandhi, N. S.; Mancera, R. L., The Structure of Glycosaminoglycans and Their Interactions with Proteins. *Chemical Biology & Drug Design* **2008**, *72* (6), 455-82.
7. Bourin, M.; Lindahl, U., Glycosaminoglycans and the Regulation of Blood Coagulation. *Biochemical Journal* **1993**, *289* (Pt 2), 313-30.
8. Atha, D. H.; Stephens, A. W.; Rosenberg, R. D., Evaluation of Critical Groups Required for the Binding of Heparin to Antithrombin. *Proc Natl Acad Sci U S A* **1984**, *81* (4), 1030-4.
9. Lindahl, U.; Backstrom, G.; Thunberg, L.; Leder, I. G., Evidence for a 3-O-Sulfated D-Glucosamine Residue in the Antithrombin-Binding Sequence of Heparin. *Proc Natl Acad Sci U S A* **1980**, *77* (11), 6551-5.
10. Liu, J.; Thorp, S. C., Cell Surface Heparan Sulfate and Its Roles in Assisting Viral Infections. *Med Res Rev* **2002**, *22* (1), 1-25.
11. Shukla, D.; Liu, J.; Blaiklock, P.; Shworak, N. W.; Bai, X.; Esko, J. D.; Cohen, G. H.; Eisenberg, R. J.; Rosenberg, R. D.; Spear, P. G., A Novel Role for 3-O-Sulfated Heparan Sulfate in Herpes Simplex Virus 1 Entry. *Cell* **1999**, *99* (1), 13-22.
12. Bishop, J. R.; Schuksz, M.; Esko, J. D., Heparan Sulphate Proteoglycans Fine-Tune Mammalian Physiology. *Nature* **2007**, *446* (7139), 1030-7.
13. Stringer, S. E.; Gallagher, J. T., Heparan Sulphate. *Int J Biochem Cell Biol* **1997**, *29* (5), 709-14.

14. Rapraeger, A. C.; Krufka, A.; Olwin, B. B., Requirement of Heparan Sulfate for Bfgf-Mediated Fibroblast Growth and Myoblast Differentiation. *Science* **1991**, *252* (5013), 1705-8.
15. Gallagher, J. T.; Turnbull, J. E., Heparan Sulphate in the Binding and Activation of Basic Fibroblast Growth Factor. *Glycobiology* **1992**, *2* (6), 523-8.
16. Bulik, D. A.; Wei, G.; Toyoda, H.; Kinoshita-Toyoda, A.; Waldrip, W. R.; Esko, J. D.; Robbins, P. W.; Selleck, S. B., Sqv-3, -7, and -8, a Set of Genes Affecting Morphogenesis in *Caenorhabditis Elegans*, Encode Enzymes Required for Glycosaminoglycan Biosynthesis. *Proc Natl Acad Sci U S A* **2000**, *97* (20), 10838-43.
17. Herman, T.; Horvitz, H. R., Three Proteins Involved in *Caenorhabditis Elegans* Vulval Invagination Are Similar to Components of a Glycosylation Pathway. *Proc Natl Acad Sci U S A* **1999**, *96* (3), 974-9.
18. Hacker, U.; Lin, X.; Perrimon, N., The *Drosophila* Sugarless Gene Modulates Wingless Signaling and Encodes an Enzyme Involved in Polysaccharide Biosynthesis. *Development* **1997**, *124* (18), 3565-73.
19. Binari, R. C.; Staveley, B. E.; Johnson, W. A.; Godavarti, R.; Sasisekharan, R.; Manoukian, A. S., Genetic Evidence That Heparin-Like Glycosaminoglycans Are Involved in Wingless Signaling. *Development* **1997**, *124* (13), 2623-32.
20. Lin, X.; Buff, E. M.; Perrimon, N.; Michelson, A. M., Heparan Sulfate Proteoglycans Are Essential for Fgf Receptor Signaling During *Drosophila* Embryonic Development. *Development* **1999**, *126* (17), 3715-23.
21. Bellaiche, Y.; The, I.; Perrimon, N., Tout-Velu Is a *Drosophila* Homologue of the Putative Tumour Suppressor Ext-1 and Is Needed for Hh Diffusion. *Nature* **1998**, *394* (6688), 85-8.
22. Kamimura, K.; Rhodes, J. M.; Ueda, R.; McNeely, M.; Shukla, D.; Kimata, K.; Spear, P. G.; Shworak, N. W.; Nakato, H., Regulation of Notch Signaling by *Drosophila* Heparan Sulfate 3-O Sulfotransferase. *J Cell Biol* **2004**, *166* (7), 1069-79.
23. Bullock, S. L.; Fletcher, J. M.; Beddington, R. S.; Wilson, V. A., Renal Agenesis in Mice Homozygous for a Gene Trap Mutation in the Gene Encoding Heparan Sulfate 2-Sulfotransferase. *Genes Dev* **1998**, *12* (12), 1894-906.
24. Fan, G.; Xiao, L.; Cheng, L.; Wang, X.; Sun, B.; Hu, G., Targeted Disruption of Ndst-1 Gene Leads to Pulmonary Hypoplasia and Neonatal Respiratory Distress in Mice. *FEBS Lett* **2000**, *467* (1), 7-11.
25. Ringvall, M.; Ledin, J.; Holmborn, K.; van Kuppevelt, T.; Ellin, F.; Eriksson, I.; Olofsson, A. M.; Kjellen, L.; Forsberg, E., Defective Heparan Sulfate

- Biosynthesis and Neonatal Lethality in Mice Lacking N-Deacetylase/N-Sulfotransferase-1. *J Biol Chem* **2000**, 275 (34), 25926-30.
26. Filmus, J.; Selleck, S., Glypicans: Proteoglycans with a Surprise. *Journal of Clinical Investigation* **2001**, 108 (4), 497-501.
 27. Duncan, G.; McCormick, C.; Tufaro, F., The Link between Heparan Sulfate and Hereditary Bone Disease: Finding a Function for the Ext Family of Putative Tumor Suppressor Proteins. *J Clin Invest* **2001**, 108 (4), 511-6.
 28. Yogalingam, G.; Hopwood, J., Molecular Genetics of Mucopolysaccharidosis Type Iiia and Iiib: Diagnostic, Clinical, and Biological Implications. *Human Mutation* **2001**, 18 (4), 264-81.
 29. Langford; Stanley, M.; Cao, D.; Sanderson, R., Multiple Heparan Sulfate Chains Are Required for Optimal Syndecan-1 Function. *Journal of Biological Chemistry* **1998**, 273 (45), 29965-71.
 30. Itoh, N., The Fgf Families in Humans, Mice, and Zebrafish: Their Evolutional Processes and Roles in Development, Metabolism, and Disease. *Biol Pharm Bull* **2007**, 30 (10), 1819-25.
 31. Furthauer, M.; Van Celst, J.; Thisse, C.; Thisse, B., Fgf Signalling Controls the Dorsoventral Patterning of the Zebrafish Embryo. *Development* **2004**, 131 (12), 2853-64.
 32. Picker, A.; Brennan, C.; Reifers, F.; Clarke, J. D.; Holder, N.; Brand, M., Requirement for the Zebrafish Mid-Hindbrain Boundary in Midbrain Polarisation, Mapping and Confinement of the Retinotectal Projection. *Development* **1999**, 126 (13), 2967-78.
 33. Walshe, J.; Maroon, H.; McGonnell, I. M.; Dickson, C.; Mason, I., Establishment of Hindbrain Segmental Identity Requires Signaling by Fgf3 and Fgf8. *Curr Biol* **2002**, 12 (13), 1117-23.
 34. Nakayama, Y.; Miyake, A.; Nakagawa, Y.; Mido, T.; Yoshikawa, M.; Konishi, M.; Itoh, N., Fgf19 Is Required for Zebrafish Lens and Retina Development. *Dev Biol* **2008**, 313 (2), 752-66.
 35. Norton, W. H.; Ledin, J.; Grandel, H.; Neumann, C. J., Hspg Synthesis by Zebrafish Ext2 and Extl3 Is Required for Fgf10 Signalling During Limb Development. *Development* **2005**, 132 (22), 4963-73.
 36. Nomura, R.; Kamei, E.; Hotta, Y.; Konishi, M.; Miyake, A.; Itoh, N., Fgf16 Is Essential for Pectoral Fin Bud Formation in Zebrafish. *Biochem Biophys Res Commun* **2006**, 347 (1), 340-6.

37. Fischer, S.; Draper, B. W.; Neumann, C. J., The Zebrafish Fgf24 Mutant Identifies an Additional Level of Fgf Signaling Involved in Vertebrate Forelimb Initiation. *Development* **2003**, *130* (15), 3515-24.
38. Whitehead, G. G.; Makino, S.; Lien, C. L.; Keating, M. T., Fgf20 Is Essential for Initiating Zebrafish Fin Regeneration. *Science* **2005**, *310* (5756), 1957-60.
39. Miyake, A.; Nakayama, Y.; Konishi, M.; Itoh, N., Fgf19 Regulated by Hh Signaling Is Required for Zebrafish Forebrain Development. *Dev Biol* **2005**, *288* (1), 259-75.
40. Nechiporuk, A.; Raible, D. W., Fgf-Dependent Mechanosensory Organ Patterning in Zebrafish. *Science* **2008**, *320* (5884), 1774-7.
41. Yamauchi, H.; Hotta, Y.; Konishi, M.; Miyake, A.; Kawahara, A.; Itoh, N., Fgf21 Is Essential for Haematopoiesis in Zebrafish. *EMBO Rep* **2006**, *7* (6), 649-54.
42. Tekin, M.; Hismi, B. O.; Fitoz, S.; Ozdag, H.; Cengiz, F. B.; Sirmaci, A.; Aslan, I.; Inceoglu, B.; Yuksel-Konuk, E. B.; Yilmaz, S. T.; Yasun, O.; Akar, N., Homozygous Mutations in Fibroblast Growth Factor 3 Are Associated with a New Form of Syndromic Deafness Characterized by Inner Ear Agenesis, Microtia, and Microdontia. *Am J Hum Genet* **2007**, *80* (2), 338-44.
43. Gecz, J.; Baker, E.; Donnelly, A.; Ming, J. E.; McDonald-McGinn, D. M.; Spinner, N. B.; Zackai, E. H.; Sutherland, G. R.; Mulley, J. C., Fibroblast Growth Factor Homologous Factor 2 (Fhf2): Gene Structure, Expression and Mapping to the Borjeson-Forssman-Lehmann Syndrome Region in Xq26 Delineated by a Duplication Breakpoint in a Bfls-Like Patient. *Hum Genet* **1999**, *104* (1), 56-63.
44. van der Walt, J. M.; Noureddine, M. A.; Kittappa, R.; Hauser, M. A.; Scott, W. K.; McKay, R.; Zhang, F.; Stajich, J. M.; Fujiwara, K.; Scott, B. L.; Pericak-Vance, M. A.; Vance, J. M.; Martin, E. R., Fibroblast Growth Factor 20 Polymorphisms and Haplotypes Strongly Influence Risk of Parkinson Disease. *Am J Hum Genet* **2004**, *74* (6), 1121-7.
45. Falardeau, J.; Chung, W. C.; Beenken, A.; Raivio, T.; Plummer, L.; Sidis, Y.; Jacobson-Dickman, E. E.; Eliseenkova, A. V.; Ma, J.; Dwyer, A.; Quinton, R.; Na, S.; Hall, J. E.; Huot, C.; Alois, N.; Pearce, S. H.; Cole, L. W.; Hughes, V.; Mohammadi, M.; Tsai, P.; Pitteloud, N., Decreased Fgf8 Signaling Causes Deficiency of Gonadotropin-Releasing Hormone in Humans and Mice. *J Clin Invest* **2008**, *118* (8), 2822-31.
46. Milunsky, J. M.; Zhao, G.; Maher, T. A.; Colby, R.; Everman, D. B., Ladd Syndrome Is Caused by Fgf10 Mutations. *Clin Genet* **2006**, *69* (4), 349-54.
47. Jastrebova, N.; Vanwildemeersch, M.; Lindahl, U.; Spillmann, D., Heparan Sulfate Domain Organization and Sulfation Modulate Fgf-Induced Cell Signaling. *J Biol Chem* **2010**, *285* (35), 26842-51.

48. Pellegrini, L.; Burke, D.; von Delft, F.; Mulloy, B., Crystal Structure of Fibroblast Growth Factor Receptor Ectodomain Bound to Ligand and Heparin. *Nature* **2000**, *407*, 1029-34.
49. Schlessinger, J.; Plotnikov, A. N.; Ibrahimi, O. A.; Eliseenkova, A. V.; Yeh, B. K.; Yayon, A.; Linhardt, R. J.; Mohammadi, M., Crystal Structure of a Ternary Fgf-Fgfr-Heparin Complex Reveals a Dual Role for Heparin in Fgfr Binding and Dimerization. *Mol Cell* **2000**, *6* (3), 743-50.
50. Ashikari-Hada, S.; Habuchi, H.; Kariya, Y.; Itoh, N.; Reddi, A. H.; Kimata, K., Characterization of Growth Factor-Binding Structures in Heparin/Heparan Sulfate Using an Octasaccharide Library. *J Biol Chem* **2004**, *279* (13), 12346-54.
51. Ashikari-Hada, S.; Habuchi, H.; Sugaya, N.; Kobayashi, T.; Kimata, K., Specific Inhibition of Fgf-2 Signaling with 2-O-Sulfated Octasaccharides of Heparan Sulfate. *Glycobiology* **2009**, *19* (6), 644-54.
52. Guimond, S.; Maccarana, M.; Olwin, B. B.; Lindahl, U.; Rapraeger, A. C., Activating and Inhibitory Heparin Sequences for Fgf-2 (Basic Fgf). Distinct Requirements for Fgf-1, Fgf-2, and Fgf-4. *J Biol Chem* **1993**, *268* (32), 23906-14.
53. Maccarana, M.; Casu, B.; Lindahl, U., Minimal Sequence in Heparin/Heparan Sulfate Required for Binding of Basic Fibroblast Growth Factor. *J Biol Chem* **1993**, *268* (32), 23898-905.
54. Kreuger, J.; Spillmann, D.; Li, J. P.; Lindahl, U., Interactions between Heparan Sulfate and Proteins: The Concept of Specificity. *J Cell Biol* **2006**, *174* (3), 323-7.
55. Mohammadi, M.; Olsen, S. K.; Ibrahimi, O. A., Structural Basis for Fibroblast Growth Factor Receptor Activation. *Cytokine Growth Factor Rev* **2005**, *16* (2), 107-37.
56. Loo, B. M.; Salmivirta, M., Heparin/Heparan Sulfate Domains in Binding and Signaling of Fibroblast Growth Factor 8b. *J Biol Chem* **2002**, *277* (36), 32616-23.
57. Wu, Z. L.; Zhang, L.; Yabe, T.; Kuberan, B.; Beeler, D. L.; Love, A.; Rosenberg, R. D., The Involvement of Heparan Sulfate (Hs) in Fgf1/Hs/Fgfr1 Signaling Complex. *J Biol Chem* **2003**, *278* (19), 17121-9.
58. Luo, Y.; Ye, S.; Kan, M.; McKeehan, W. L., Structural Specificity in a Fgf7-Affinity Purified Heparin Octasaccharide Required for Formation of a Complex with Fgf7 and Fgfr2iib. *J Cell Biochem* **2006**, *97* (6), 1241-58.
59. Zhang, F.; Zhang, Z.; Lin, X.; Beenken, A.; Eliseenkova, A. V.; Mohammadi, M.; Linhardt, R. J., Compositional Analysis of Heparin/Heparan Sulfate Interacting with Fibroblast Growth Factor.Fibroblast Growth Factor Receptor Complexes. *Biochemistry* **2009**, *48* (35), 8379-86.

60. Kuberan, B.; Lech, M. Z.; Beeler, D. L.; Wu, Z. L.; Rosenberg, R. D., Enzymatic Synthesis of Antithrombin Iii-Binding Heparan Sulfate Pentasaccharide. *Nat Biotechnol* **2003**, *21* (11), 1343-6.
61. Casu, B.; Naggi, A.; Torri, G., Heparin-Derived Heparan Sulfate Mimics to Modulate Heparan Sulfate-Protein Interaction in Inflammation and Cancer. *Matrix Biol* **2010**, *29* (6), 442-52.
62. Hassan, H. H., Chemistry and Biology of Heparin Mimetics That Bind to Fibroblast Growth Factors. *Mini Rev Med Chem* **2007**, *7* (12), 1206-35.
63. Viskov, C.; Bouley, E.; Hubert, P.; Martinez, C.; Herman, F.; Jeske, W.; Hoppensteadt, D.; Walenga, J. M.; Fareed, J., Isolation and Characterization of Contaminants in Recalled Unfractionated Heparin and Low-Molecular-Weight Heparin. *Clin Appl Thromb Hemost* **2009**, *15* (4), 395-401.
64. Powell, A. K.; Yates, E. A.; Fernig, D. G.; Turnbull, J. E., Interactions of Heparin/Heparan Sulfate with Proteins: Appraisal of Structural Factors and Experimental Approaches. *Glycobiology* **2004**, *14* (4), 17R-30R.
65. Petitou, M.; Herault, J. P.; Bernat, A.; Driguez, P. A.; Duchaussoy, P.; Lormeau, J. C.; Herbert, J. M., Synthesis of Thrombin-Inhibiting Heparin Mimetics without Side Effects. *Nature* **1999**, *398* (6726), 417-22.
66. Kuberan, B.; Beeler, D. L.; Lech, M.; Wu, Z. L.; Rosenberg, R. D., Chemoenzymatic Synthesis of Classical and Non-Classical Anticoagulant Heparan Sulfate Polysaccharides. *J Biol Chem* **2003**, *278* (52), 52613-21.
67. Fritz, T. A.; Lagemwa, F. N.; Sarkar, A. K.; Esko, J. D., Biosynthesis of Heparan Sulfate on Beta-D-Xylosides Depends on Aglycone Structure. *J Biol Chem* **1994**, *269* (1), 300-7.
68. Victor, X. V.; Nguyen, T. K.; Ethirajan, M.; Tran, V. M.; Nguyen, K. V.; Kuberan, B., Investigating the Elusive Mechanism of Glycosaminoglycan Biosynthesis. *J Biol Chem* **2009**, *284* (38), 25842-53.
69. Gibson, K. D.; Segen, B. J.; Audhya, T. K., The Effect of Beta-D-Xylosides on Chondroitin Sulphate Biosynthesis in Embryonic Chicken Cartilage in the Absence of Protein Synthesis Inhibitors. *Biochem J* **1977**, *162* (2), 217-33.
70. Platt, J. L.; Brown, D. M.; Granlund, K.; Oegema, T. R.; Klein, D. J., Proteoglycan Metabolism Associated with Mouse Metanephric Development: Morphologic and Biochemical Effects of Beta-D-Xyloside. *Dev Biol* **1987**, *123* (2), 293-306.
71. Yost, H. J., Inhibition of Proteoglycan Synthesis Eliminates Left-Right Asymmetry in *Xenopus Laevis* Cardiac Looping. *Development* **1990**, *110* (3), 865-74.

CHAPTER 2

DIMERIZED GLYCOSAMINOGLYCAN CHAINS INCREASE FGF SIGNALING DURING ZEBRAFISH DEVELOPMENT

2.1 Introduction

The regulation of cell-cell and cell-matrix interactions is critical for various developmental processes including left-right axis induction, organ development, neuronal wiring and formation of blood vessels. Secreted molecules such as FGFs, Wnts and BMPs provide necessary informational cues through binding to their cognate cell surface receptors and subsequent activation of intracellular signaling pathways. It has been shown that proteoglycans (PGs) are essential to facilitate these interactions (1-4).

PGs consist of a core protein to which multiple glycosaminoglycan (GAG) chains are attached at specific amino acids (5, 6). Several types of GAGs exist, including heparan sulfate (HS), chondroitin sulfate (CS) and dermatan sulfate (DS; previously known as chondroitin sulfate B). Some PGs such as syndecans carry more than one type of GAG chain. Mutations altering GAG attachment sites on core proteins or disrupting GAG biosynthetic enzymes affect signaling and lead to a variety of disorders in human (7, 8). It is important to note that all naturally occurring PGs except decorin possess two or more GAG side chains. This suggests that multiple GAG chains are imperative for biological functions *in vivo*. However, only a few studies have examined the importance of GAG multivalency using cellular systems (9-11).

A large body of *in vitro* data indicates that PGs are essential for FGF/FGFR signaling (12, 13). HS chains facilitate FGF-mediated dimerization of FGFRs and subsequently regulate intracellular signal transduction pathways during development (14). Recently, there has also been more evidence suggesting the roles of CS in FGF signaling (15, 16). Numerous models have been proposed to explain FGFR dimerization at the molecular level based on biochemical and biophysical studies (17-19). However,

these models have not taken into consideration the effects of GAG multivalency, since the contribution of multiple GAG chains of PGs to FGFR dimerization has not previously been elucidated *in vivo*.

We hypothesized that the presence of dimeric GAG chains on endogenous PGs is essential for biological functions *in vivo*. In this study, we investigated whether GAG multivalency, as found in endogenous PGs, can regulate FGF/FGFR-mediated signaling pathways during development. It has been shown that mono-xylosides, which prime GAG chains free of core proteins, modulate development in various systems (20, 21). Our laboratory has recently utilized click chemistry to generate mono-xylosides and their fluorinated analogs that respectively stimulate or inhibit GAG biosynthesis in a cellular system (22, 23). In our companion studies, we have utilized a similar chemical approach to synthesize a library of bis- and tris-xylosides, and have probed the mechanism of their priming activity and GAG biosynthesis in a cellular system. Here, we use the embryonic zebrafish as an *in vivo* system to examine whether these bis- and tris-xylosides induce proteoglycan mimetics *in vivo*, and then further define their roles in modulating FGF/FGFR-mediated signaling pathway. Based on our findings, we propose that GAG multivalency plays a major role in the regulation of FGF-mediated signal transduction pathways during development.

2.2 Experimental procedures

2.2.1 Animals and materials

Zebrafish were raised and bred according to standard procedures (24). Strains used were Tübingen wildtypes and *Tg(TOP:dGFP)^{w25}* (25). Zebrafish experiments were

approved by the University of Utah Institutional Animal Care and Use Committee. Xylosides were synthesized using click chemistry as described in our companion paper and in earlier studies (22). Xylosides were dissolved in distilled water to a final concentration of 100 mM for injection into embryos. *lefty1* probe, SU5402, *sprouty4* and syndecan constructs were generously provided by Drs. H.J. Yost, T. Piotrowski, L. Maves and R.D. Sanderson, respectively. Commercial sources: RNA polymerase-based labeling kit and BM Purple, Roche Applied Science; Rabbit anti-phospho ERK1/2, Cy-3 anti-rabbit secondary antibody and *Streptomyces griseus* protease type XIV, disaccharide standards, Sigma-Aldrich; SU5402, Pfizer; mMessage mMachine transcription kit, Ambion; DEAE-sepharose and sephacel gel, NAP-10, Amersham Biosciences; Streptavidin-Alexa Fluor 350 conjugate (S-AF350), Invitrogen; G3000SWxl columns (7.8 mm x 30 cm, 5 μ m particle size), Tosoh Bioscience LLC; Sep-Pak Plus column, Waters.

2.2.2 Screening of xylosides in zebrafish embryos

Embryos were obtained by natural mating and raised at 28.5 °C in E3 buffer (5 mM NaCl, 0.17 mM KCl, 0.33 mM CaCl₂, 0.33 mM MgSO₄). Xylosides were diluted with 1 % phenol red and each xyloside (33 pmoles) was microinjected in a 1 nl bolus into the blastomere of one-cell stage embryos. Embryos were staged and their phenotypes were compared to those of wild type (WT) embryos (24).

2.2.3 RNA *in situ* hybridization

Antisense digoxigenin-labeled probes were generated from cDNA clones using a SP6 or T7 RNA polymerase-based labeling kit. The following probes were used: *mkp3* (26), *gsc* (27), *gfp* (25), *bmp2b* (28), *bambi* (29) and *lefty1* (30). Embryos were fixed overnight in 4% PFA, and then washed with PBST (0.1% Tween-20 phosphate buffer saline). Whole mount *in situ* hybridization experiments were performed as previously described (31). Embryos were then stained with BM Purple for imaging.

2.2.4 Whole mount antibody staining

Embryos were fixed with 4% PFA for 2.5 h at room temperature, washed with PBST, blocked with NCST (10% heat-inactivated newborn calf serum, 0.1% Tween-20, 1% DMSO, in PBS) overnight at 4°C, incubated with rabbit anti-phospho ERK1/2 antibody at 1:300 for 12 h at 4°C, washed with PBST, incubated with Cy-3 conjugated anti-rabbit secondary antibody at 1:300 overnight at 4°C, washed with PBST, mounted and finally imaged on an Olympus confocal microscope.

2.2.5 FGFR tyrosine kinase inhibitor SU5402 treatment

Twenty-five pmoles of xyloside **II** was injected per embryo at the one-cell stage and the embryos were subsequently dechorionated. Two-thirds of the embryos were placed in 3 ml of E2 buffer (15 mM NaCl, 0.5 mM KCl, 1 mM CaCl₂, 1 mM MgSO₄, 0.15 mM KH₂PO₄, 0.042 mM Na₂HPO₄) with 25 μM SU5402, and the remaining one-third were placed in 3 ml of E2 buffer as controls. SU5402 treated embryos were then compared to untreated embryos at 12 hpf.

2.2.6 mRNA and morpholino injection

Sprouty4 mRNA was synthesized using a SP6 mMessage mMachine transcription kit. An antisense morpholino against *fgf8* (32) was obtained from Gene Tools (5'-GAGTCTCATGTTTATAGCCTCAGTA-3'; start codon is underlined). To insure uniform xyloside dosing, we used a double-injection protocol. First, xyloside **II** (25 pmoles/embryo) was injected into all embryos at the one-cell stage. Then, two-thirds of xyloside-treated embryos were injected with 70 pg of *sprouty4* mRNA or 6 ng of *fgf8* morpholino. These embryos were then compared at 12 hpf with the remaining one-third embryos.

2.2.7 Purification of GAGs

One hundred embryos were injected with biotinylated xyloside **XIII** or **XVII** at the one-cell stage, lyophilized at 12 hpf and treated with 0.016% *Streptomyces griseus* protease type XIV (pronase) at 37°C overnight. After centrifugation at 16,000 x g for 5 min, supernatant was diluted with one volume of 0.016% Triton X-100 and loaded onto a 0.2 ml DEAE-sepharose mini column that had been pre-equilibrated with 2 ml of wash buffer (20 mM NaOAc, 0.1 M NaCl and 0.01 % Triton X-100, pH 6.0). After washing with 6 ml of wash buffer, the bound GAGs were eluted with 1.2 ml of elution buffer (20 mM NaOAc, 1 M NaCl, pH 6.0), desalted and concentrated with 3000 MWCO Amicon columns. S-AF350 (0.2 µg) was added, and the resulting mixture was incubated at room temperature in the dark overnight to capture the primed GAGs.

2.2.8 Structural and compositional analysis of primed GAGs

GAG-streptavidin complexes were analyzed using a high-pressure size exclusion column coupled to a fluorescent detector with excitation and emission wavelength set at 346 nm and 442 nm. The GAG-streptavidin conjugate was loaded onto two tandem G3000SWx1 columns and was then eluted with phosphate buffer (100 mM KH_2PO_4 , 150 mM NaCl, pH 6.0) over 60 min at 0.5ml/min flow rate. GAGs from untreated embryos were also treated with S-AF350 and used as controls. The GAG-streptavidin conjugate was then digested with heparitinases I, II and III (in 3.3 mM $\text{Ca}(\text{OAc})_2$ and 40 mM NH_4OAc , pH 7.0) or chondroitinase ABC (in 33 mM Tris, 33 mM NaOAc and 0.1 mg/ml BSA, pH 8.0) overnight at 37°C. The digested samples were subsequently loaded onto the size exclusion column (G3000SWx1) to determine HS/CS composition.

2.2.9 Disaccharide analysis of HS and CS/DS purified from zebrafish embryos

WT, bis-xyloside **VI** injected and mono-xyloside **XVI** injected embryos (100 embryos per sample) were collected and freeze-dried at 12 hpf. Each sample was digested with 0.4 mg pronase at 55°C for 20 h, terminating the reaction by heating for 5 min at 96°C, then adding MgCl_2 to a final concentration of 2 mM. Each sample was then treated with 12.5 units of benzonase and incubated for additional 2 h at 37°C. The reaction was terminated by heating for 2 min at 96°C. Samples were loaded onto a Sep-Pak Plus column that had been primed in methanol and washed in water, then with equilibration buffer (50 mM Tris, 0.1 M NaCl, pH 8.0). The loaded cartridge was washed twice with the same buffer. Flowthrough and wash fractions were pooled and

loaded onto a column of 200 μ l DEAE-sephacel, equilibrated with 50 mM Tris, 0.1 M NaCl, 0.1 % Triton X-100, pH 8.0. The flowthrough was loaded once again and the column was washed with six bed volumes each of a) 50 mM Tris, 0.1 M NaCl, 0.1 % Triton X-100, pH 8.0, b) 50 mM NaOAc, 0.1 M NaCl, 0.1% Triton X-100, pH 4.0, c) 50 mM Tris, 0.1 M NaCl, pH 8.0. GAGs were eluted with 600 μ l of 50 mM Tris, 1.5 M NaCl, pH 8.0 and desalted on a NAP10 column. The isolated polysaccharides were incubated with 50 mU chondroitinase at 37°C for 3.5 h. After removal of 10 μ l for CS analysis by RPIP-HPLC, HS was recovered using a second round of DEAE-sephacel chromatography as described above for total GAG isolation. Each sample was lyophilized, then digested at 37°C overnight with 0.4 mU each of heparitinase I, II and III, terminated by heat inactivation at 96°C for 2 min. The resulting HS disaccharides were separated by RPIP-HPLC analysis followed by post-column derivatization with cyanoacetamide and in-line detection using a fluorescence detector. Disaccharide standards were used to determine each disaccharide peak.

2.2.10 Injection of purified GAGs into zebrafish embryos

GAGs were isolated as above from approximately 1,000 embryos (12 hpf) that were injected with xyloside **XIII**. The isolated GAG chains were then digested with heparitinases I, II and III or chondroitinase ABC overnight at 37°C. The undigested CS/DS or HS, respectively, was then purified and concentrated to a final volume of 20 μ l using 3000 MWCO Amicon columns. One nl of each sample was injected into the animal pole of dome-stage embryos at 4 hpf. The phenotypes of these embryos were compared to those of WT embryos that had been injected with 1% phenol red.

2.2.11 Injection of purified GAGs into zebrafish embryos

GAGs were isolated as above from approximately 1,000 embryos (12 hpf) that were injected with xyloside **XIII**. The isolated GAG chains were then digested with heparitinases I, II and III or chondroitinase ABC overnight at 37°C. The undigested CS/DS or HS, respectively, was then purified and concentrated to a final volume of 20 µl using 3000 MWCO Amicon columns. One nl of each sample was injected into the animal pole of dome-stage embryos at 4 hpf. The phenotypes of these embryos were compared to those of WT embryos that had been injected with 1% phenol red.

2.2.12 Injection of mutated syndecan-1 mRNAs into zebrafish embryos

Seven mutagenic constructs of syndecan-1, in which serine residues at positions 37, 45 and 47 were replaced by alanine residues in all possible combinations, were generously provided by Dr. R.D. Sanderson (University of Alabama at Birmingham). The DNA fragments encoding the first 200 amino acids of each of the seven mutagenic constructs were subcloned into pCS2+ at BamHI and XhoI sites using forward primer 5'-GATCATGGATCCATGAGACGCGCGGCGCT -3' and reverse primer 5'-CATCTCGAGTTAGTGATGGTGATGGTGATGTTTCCTTCCTGTCCAAAA -3'. A similar experiment was done with the wild type. mRNAs of these DNA fragments carrying zero, one, two or three HS initiation sites were synthesized using a SP6 mMessage mMachine transcription kit. Each mRNA was injected into the blastomere of one-cell stage embryos at the concentration of 45 pg per embryo. These embryos were then compared at 12 hpf with WT.

2.3 Results

2.3.1 Bis- and tris-xylosides affect the early development of

zebrafish embryos

Mono-xylosides have been used in various systems to define the role of GAG chains (13, 20, 21). We have also previously reported the synthesis of *click*-xylosides and their ability to prime distinct GAG chains in the absence of a core protein in a cellular system (22, 33). However, mono-xylosides can only prime a single GAG chain per xyloside. On the other hand, bis- and tris-xylosides can prime multiple GAG chains that are covalently attached on the same scaffold, better mimicking naturally-occurring PGs (34). Various xylosides were synthesized using click chemistry in such a way that some scaffolds carry single xylose units and others carry two or three xylose units, allowing us to determine the importance of GAG multivalency as found in endogenous PGs (Table 2.1). Furthermore, a number of bis-xylosides were prepared with variable distances between two xylose residues. All of these xylosides were tested by injection into the blastomere of one-cell stage zebrafish embryos at a series of concentrations. Such injections provide convenient access to the cytoplasmic compartment without the need for plasma membrane permeability; as embryonic cells divide, injected material is partitioned into daughter cells. Bis- and tris-xylosides (xylosides **I-XIII**) at dosages of 33 pmoles/embryo effectively caused elongation at 12 hpf (Figure 2.1A, C) whereas mono-xylosides (xylosides **XIV-XVII**) failed to cause any elongation at 33 pmol/embryo (Figure 2.1A, D), or even at higher dosages (up to 160 pmoles/embryo; see supplemental data). Xylosides **I-VI**, in which two xylose residues are linked by an aromatic ring, all effectively induced elongation in a majority of embryos, with the exception of xyloside **I**,

Table 2.1 Structures of the xylosides studied in zebrafish embryos.

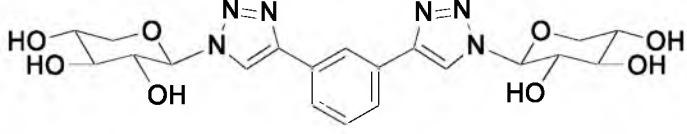
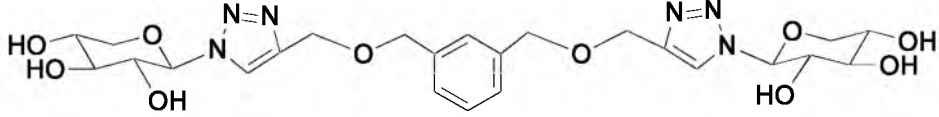
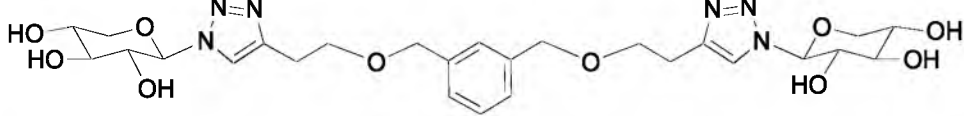
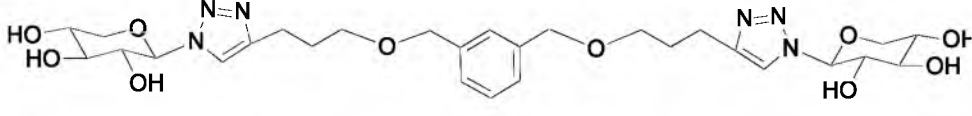
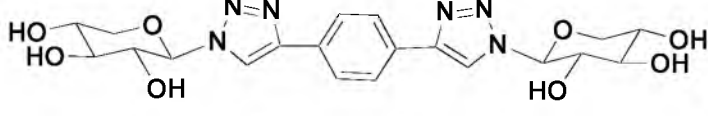
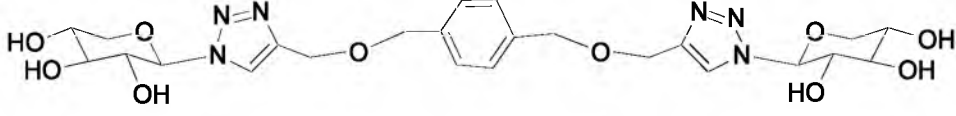
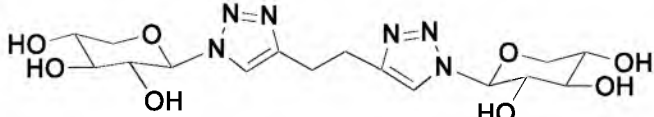
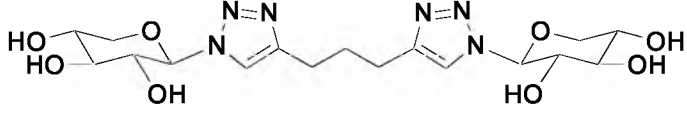
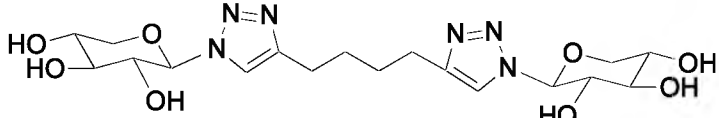
Number	Structure
I	
II	
III	
IV	
V	
VI	
VII	
VIII	
IX	

Table 2.1 continued

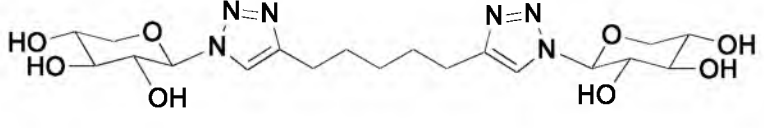
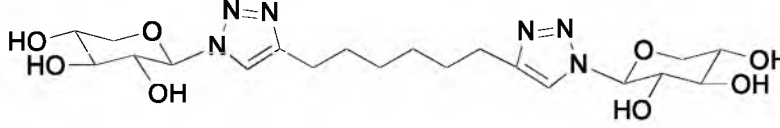
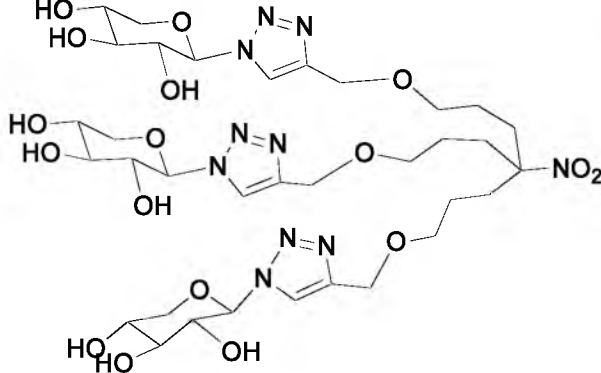
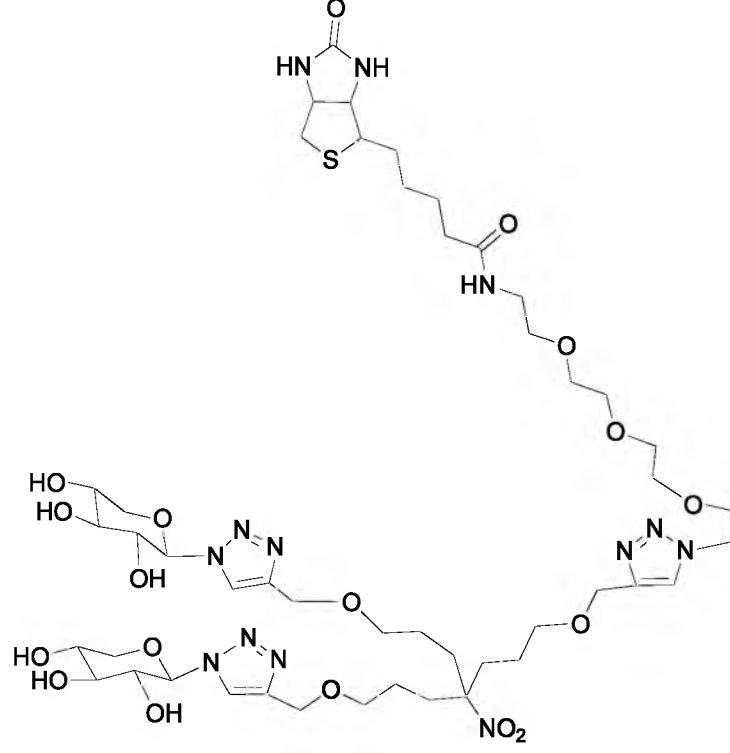
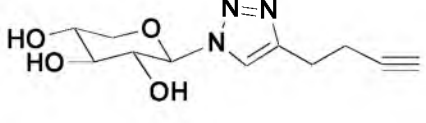
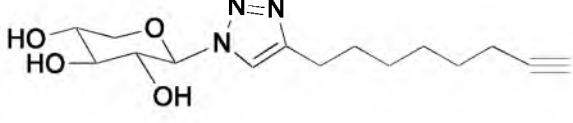
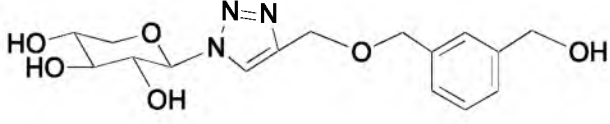
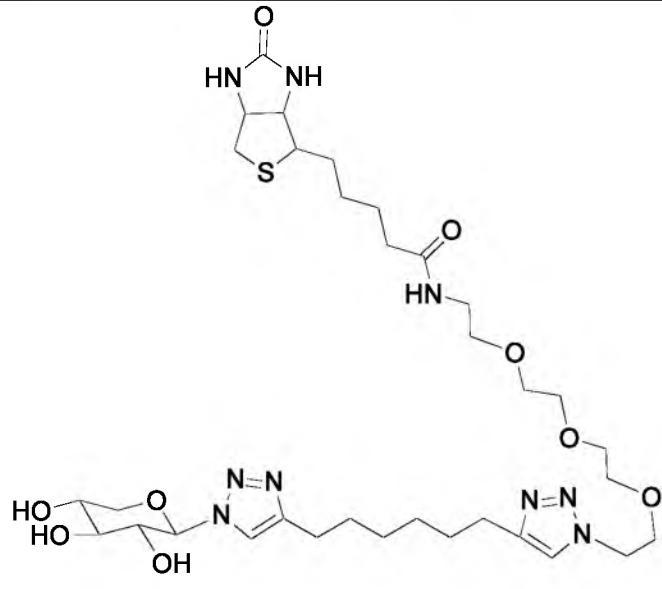
Number	Structure
X	
XI	
XII	
XIII	

Table 2.1 continued

Number	Structure
XIV	
XV	
XVI	
XVII	

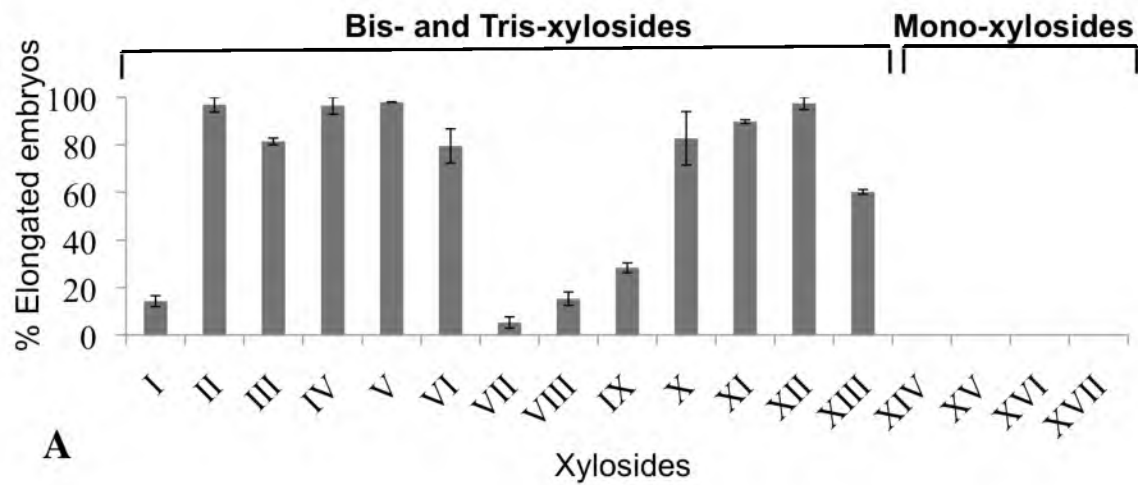


Figure 2.1 Xylosides cause elongation of developing zebrafish embryos at 12 hpf. A: Treatment with bis- and tris-xylosides causes elongation. Mean \pm SEM from 3 experiments ($n = 145-246$ embryos) are presented. B: Control embryo (WT). C: Elongated embryo treated with bis-xyloside **II**. D: Nonelongated embryo treated with mono-xyloside **XIV**. Lateral views, dorsal right, anterior up. Xyloside structures are shown in Table 2.1. Xylosides (33 pmoles) were injected into the blastomere of one-cell stage embryos.

which induced elongation in only 14.3% of treated embryos (n =152). It is interesting to note that xyloside **I** has the shortest distance between the two xylose residues. In the case of xylosides **VII-XI**, in which two xylose residues are linked by a linear alkyl chain, a longer spacer between the two xylose residues induced elongation in a higher percentage of embryos (Figure 2.1A). These results suggest that both the multimeric nature and the conformational flexibility of the newly primed multivalent GAG chains are critical to have an effect on signal transduction during developmental processes.

2.3.2 Elongated embryos show specific increases in FGF signaling

Elongation of an embryo can result from activation of WNT, FGF or Nodal signaling or from inhibition of BMP signaling (35-38). To distinguish between these possibilities, we analyzed patterns of early gene expression in embryos treated with bis-xylosides and control embryos using *in situ* hybridization and immunostaining. When embryos were treated with bis-xyloside **II**, the expression of the FGF pathway target gene *mkp3* at 8 hpf (26) was expanded (Figure 2.2A). The *mkp3* pattern, a broadened ring around the margin, is just what would be expected from enhanced FGF signaling, given the expression of Fgfs at this stage in a marginal ring (26). A similar effect on *mkp3* was seen at 6 hpf. When treating with bis-xylosides **VII-XI**, the percentage of embryos with expanded *mkp3* expression varied with linker length in concordance with the percentage of elongated embryos (see supplemental data). On the other hand, the expression of *mkp3* remained normal in embryos treated with mono-xylosides (see supplemental data). By contrast, the expression of the dorsal marker *gsc* (27) was unaffected by the injection of bis-xylosides (Figure 2.2B and see supplemental data). Thus at 8 hpf, bis-xylosides

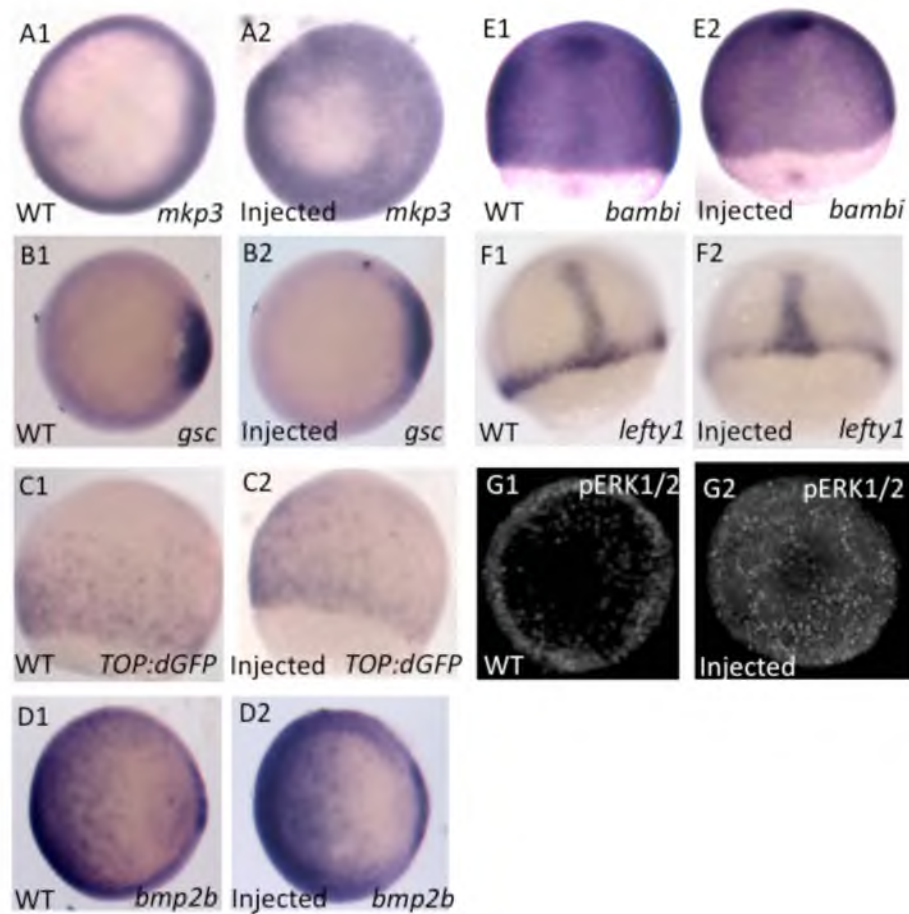


Figure 2.2 Analysis of developmental patterning in WT and bis-xyloside II-treated embryos. A – F: *in situ* hybridization of control (A1-F1) and bis-xyloside II-treated (A2-F2) embryos at 8 hpf with probes for the FGF signaling target gene *mcp3*, dorsal marker *gsc*, WNT signaling reporter *TOP:dGFP*, BMP signaling ligand *bmp2b*, BMP signaling target gene *nma/bambi* and Nodal signaling target gene *lefty1*, respectively. A, B, D: animal pole view, dorsal right; C: lateral view, dorsal right; E, F: dorsal view. Only the expression of *mcp3* was expanded, suggesting that FGF signaling is predominantly affected at 8hpf. G: Immunostaining with phospho-Erk 1/2 antibody in control (G1) and bis-xyloside II-treated (G2) embryos at 6 hpf. Animal pole view, dorsal right. Phospho-Erk 1/2 was expanded towards the animal pole in bis-xyloside II-treated embryos compared to control.

enhanced FGF signaling without a detectable effect on dorsoventral patterning.

To investigate whether the Wnt, BMP or Nodal signaling pathways were also affected, the expression of corresponding pathway readouts was examined at 8 hpf. The expression of the transgenic Wnt reporter *TOP:dGFP* (25), which carries 4 TCF/LEF binding sites driving destabilized GFP, appeared unchanged following bis-xyloside **II** injection (Figure 2.2C). Similar observations were made for the BMP ligand *bmp2b* (28), the BMP pathway target *nma/bambi* (39) and the Nodal pathway target *lefty1* (30) (Figure 2.2D, E, F). The expression of these genes was also unchanged following mono-xyloside injections (see supplemental data). Furthermore, immunostaining revealed that bis-xyloside-treated embryos have higher phospho-Erk 1/2 expression than controls, again with the greatest effect near the margin, indicating increased FGF activity through the FGFR/Ras/Mapk signaling pathway (Figure 2.2G). These results suggest that the FGF pathway is the only, or at least the primary, signaling pathway affected by bis-xyloside at 8 hpf. Once FGF signaling is affected, we would expect secondary effects on other pathways. For example, Furthauer *et al.* have shown that FGF signaling inhibits BMP signaling during early development (36). Hence, expression patterns of the FGF target *mkp3* and BMP target *nma/bambi* were analyzed at 12 hpf. The expression of *mkp3* expanded in the ventral ectoderm while the expression of *bambi* decreased in bis-xyloside **II** injected embryos compared to WT (see supplemental data). These results indicate that the primary effect of dimeric GAG chains primed by bis-xylosides is increased FGF signaling, with decreased BMP signaling as a later, secondary consequence.

2.3.3 Inhibition of FGFR-mediated signaling rescues the elongation phenotype

If bis-xylosides primarily activate the FGF/FGFR-mediated intracellular signaling pathway, we predicted that its inhibition would prevent the elongation phenotype. We used a well-known FGFR tyrosine kinase inhibitor, SU5402 (40), and applied a concentration (25 μ M) at which the kinase inhibitor has no significant effect on the normal morphology of the embryos through 12 hpf. After injection with bis-xyloside **II**, the embryos were immediately treated with SU5402. After continuous treatment through 12 hpf, there was a complete rescue: no elongation was observed (n = 111; Figure 2.3D). When embryos were treated with SU5402 starting at 8 hpf instead of immediately after injection with bis-xyloside **II**, only 24 % (n = 115) of embryos developed normally, suggesting that bis-xyloside **II** exerts its activity by augmenting FGF signaling before or during gastrulation. We also tested whether expression of *sprouty4*, an FGF signaling antagonist, could rescue the phenotype. When injected with bis-xyloside **II** and 70 pg of *sprouty4* mRNA, 18.7 % (n = 149) of the embryos were elongated at 12 hpf. In comparison, 85% of the embryos (n = 119) were elongated when injected with bis-xyloside **II** only (Figure 2.3C, E). These results confirm the activation of FGF/FGFR-mediated signaling pathways upon treatment with bis-xylosides.

2.3.4 Suppression of FGF8 rescues the elongation phenotype

Which FGF is involved? FGF signaling is essential for many developmental processes (41), and FGF 3, 8, 17b and 24 are the main FGFs expressed during zebrafish gastrulation (42). Among these, FGF8 is thought to have the greatest role in early

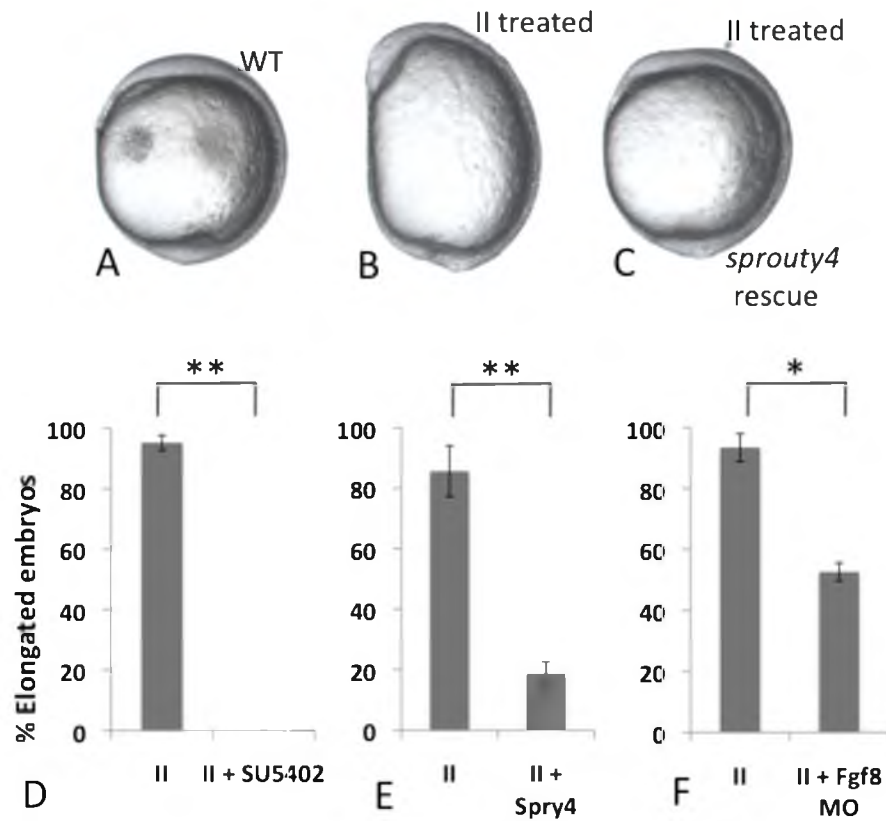


Figure 2.3 Rescue of elongation phenotype by inhibition of FGF signaling. A-C: Examples of control, elongated and rescued embryos at 12 hpf. Lateral views, dorsal right, anterior up. A: Control embryo. B: Embryo treated with bis-xyloside II. C: Embryo treated with bis-xyloside II and rescued by sprouty4 mRNA injection. D-F: Percentage of elongated embryos following treatment with bis-xyloside II alone, or with bis-xyloside II as well as 25 μ M SU5402 (D, n = 111), 70 pg of sprouty4 mRNA (E, n = 149) or 6 ng of fgf8 morpholino (F, n = 98). All three treatments show significant rescue. *, $p < .05$; **, $p < .01$ using Student's t-test.

developmental events. Therefore, we investigated whether FGF8 is involved in causing elongation of embryos when treated with bis-xylosides. Bis-xyloside **II** and *fgf8* translation blocking morpholino were sequentially injected into one-cell embryos. After 12 hpf, 52.6 % of these embryos were elongated (n = 98), whereas 93% of those that were injected with bis-xyloside **II** only were elongated (n = 125; Figure 2.3F). These results suggest that bis-xylosides activate FGFR signaling pathways at least partially via FGF8, and furthermore show that the effect of bis-xyloside **II** is FGF8-dependent.

2.3.5 Structural analysis of primed GAG chains

What type of GAG chains are primed by xylosides? Biotin conjugated bis-xyloside (xyloside **XIII**) and mono-xyloside (xyloside **XVII**) were therefore synthesized to identify primed GAG chains and to distinguish them from endogenous GAGs. Thirty-three pmoles of biotinylated xylosides **XIII** and **XVII** were injected into embryos at the one-cell stage. The GAG chains primed by these biotinylated xylosides were purified and captured with fluorescent-tagged streptavidin, S-AF350, as described in Experimental Procedures. Size exclusion chromatography (SEC) analysis confirmed the priming activity of these two xylosides: in both cases, the unbound S-AF350 peak was reduced or absent, and replaced by a GAG-streptavidin peak (Figure 2.4A). This result indicates that both mono- and bis-xylosides prime GAG chains in zebrafish embryos (Figure 2.4A). In the case of mono-xyloside, a small fraction of the unbound S-AF350 peak still remained at 37 min. This result suggests that mono-xyloside **XVII** may not be as good a primer as bis-xyloside **XIII**. This is contrary to our findings, reported in our companion paper, that mono-xylosides are a better primer than bis-xylosides. To

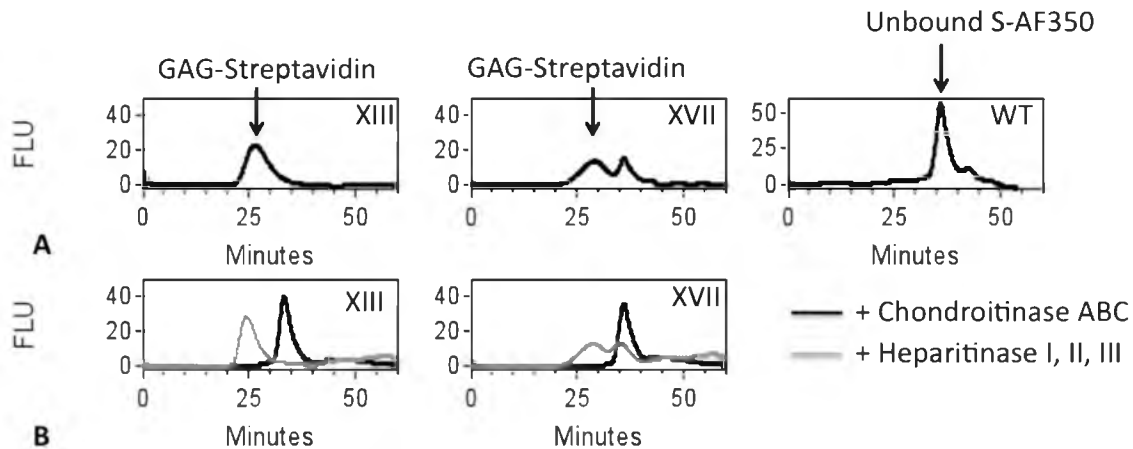


Figure 2.4 Structural analysis of GAG chains primed by xylosides. A: Fluorescent detection of GAG chains primed in embryos by biotinylated bis-xyloside **XIII** or biotinylated mono-xyloside **XVII**, or untreated embryos, after purification, complexing with streptavidin-Alexa Fluor 350, and elution from an HPLC-size exclusion column. B: Fluorescent detection of GAG chains primed by biotinylated xylosides (**XIII** and **XVII**) after treatment with chondroitinase ABC or heparitinases I, II and III to determine the relative proportion of HS and CS/DS, respectively.

exclude the possibility that differential priming activity may account for the elongation phenotype, we screened a number of additional mono-xylosides, which were found to be better primers than bis-xylosides (see supplemental data). None of these additional mono-xylosides caused elongation phenotype. In order to further demonstrate that the GAG chain valency plays a central role in causing the elongation phenotype, bis-xyloside XIII was injected at a lower concentration (15 pmoles per embryo). At this concentration, bis-xyloside XIII was found to have a similar priming activity as mono-xyloside XVII (see supplemental data) but still caused the elongation phenotype in 33 % total embryos ($n = 240$). Thus, these experimental outcomes suggest that the dimerized GAG chains are essential in causing the elongation phenotype. Since streptavidin is a globular multivalent protein, we could not determine the exact molecular weights of the

GAG chains. We estimated the HS/CS/DS composition of primed GAG chains by determining the extent to which GAG-Streptavidin conjugates were susceptible to heparitinase I, II and III or chondroitinase ABC treatment (Figure 2.4B). The results indicated that both bis-xyloside **XIII** and mono-xyloside **XVII** primed mostly CS/DS (> 95 %) and very little HS (< 5 %) Similar results were obtained with GAG chains from 6 hpf embryos (see supplemental data).

2.3.6 Kinetics of *in vivo* xyloside priming

To characterize the kinetics of priming, GAG chains primed by bis-xyloside **XIII** at different time points (2, 4, 6, 8, 10 and 12 hpf) were isolated and their size exclusion profiles compared (see supplemental data). Primed GAGs were detectable at 2 hpf; nearly all xyloside appeared to have primed by 4 hpf. The results suggest that the amount of primed GAGs increased throughout early development, and furthermore that the structure of primed GAGs continued to change, as reflected in differential SEC elution times (see supplemental data). The sulfation density of bis-xyloside primed GAG chains at 10 hpf was compared with the sulfation density of heparin using anion-exchange chromatography. The bis-xyloside primed GAG chains eluted at 33 min while heparin eluted at 55 min (see supplemental data), suggesting that the extent of sulfation of GAG chains synthesized during early development was much lower than that of heparin. Finally, disaccharide profiles of HS and CS/DS in WT embryos, bis-xyloside **VI** injected embryos and mono-xyloside **XVI** injected embryos were analyzed using HPLC coupled to a post-column reactor (Figure 2.5). The disaccharide composition of HS and CS chains were largely identical for WT, mono- and bis-xyloside injected embryos,

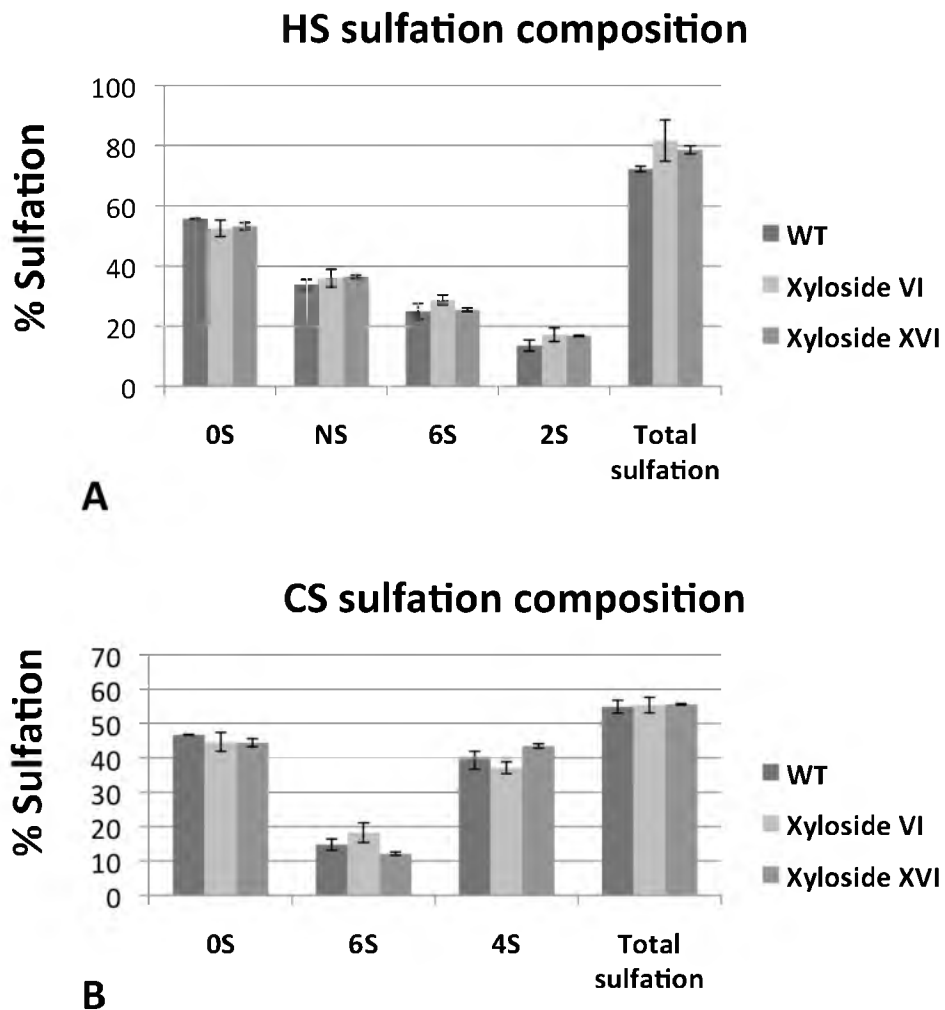


Figure 2.5 Specific sulfation of GAG chains isolated from bis-xyloside **VI**-treated, mono-xyloside **XVI**-treated and WT embryos. Disaccharide compositions were obtained as described in Experimental Procedures. Results show that treatment with either bis- or mono-xyloside does not affect overall sulfation of GAG chains, yielding specific sulfation types identical to those of endogenous GAGs. **A**: Percentage of different modifications of endogenous and xyloside-primed HS. **B**: Percentage of different modifications of endogenous and xyloside-primed CS/DS.

suggesting that these synthetic scaffolds do not overwhelm or disturb the GAG synthetic machinery *in vivo*, and that xyloside-primed GAGs have relatively normal sulfation.

2.3.7 Determination of GAG chain type responsible for the elongation phenotype

Our data showed that both mono- and bis-xylosides primed mostly CS/DS and a small amount of HS (Figure 2.4B). Therefore, we investigated which GAG type, HS or CS/DS, could cause the elongation of zebrafish embryos when assembled on bis-xylosides. GAG chains were purified from 12 hpf xyloside **II**-treated embryos as described in the “Methods” section. The GAG chains were then subjected to heparitinase I, II and III or chondroitinase ABC treatment to obtain CS/DS or HS, respectively. Both samples were injected into zebrafish embryos at 4 hpf. At 12 hpf, 22% of embryos (n = 102) were elongated after injection with HS and 16% of embryos (n = 100) were elongated after injection with CS/DS. These results imply that both dimeric HS and CS/DS primed by xylosides can cause the elongation phenotype. In order to further study the roles of these different GAG types, we injected commercially available monomeric GAG chains including heparin, CS-A, CS-C and DS (1ng/embryo) into zebrafish embryos. We found that injection into the animal pole at the dome stage (4 hpf) caused more frequent elongation than at other time points (0, 2 and 6 hpf). Injection of heparin, DS, CS-A and CS-C, respectively, caused 95%, 90%, 5% and 17% (n > 300) elongation phenotype at 12 hpf. Most notably, heparin caused 90% of the embryos to exhibit an elongation phenotype even at a lower dose (0.2 ng/embryo), whereas other GAG types

failed to cause the effect at this dose. Expression of the FGF target *mkp3* was analyzed after injection with heparin, DS, CS-A and CS-C. Seventy-seven percent (n = 35) of embryos injected with heparin and 72.5% (n = 40) of embryos injected with DS overexpressed *mkp3*, compared to CS-A (11 %, n = 45) and CS-C (16.3 %, n = 43) injected embryos (see supplemental data). The findings that elongation is seen after injecting either *in vivo*-primed GAGs or exogenous GAGs back into the cell mass of 4 hpf embryos (which is unlike one-cell stage injections, which deliver xyloside intracytoplasmically), show that these GAGs can in fact act extracellularly, suggesting that *in vivo*-primed GAGs are likely secreted and act outside the cell. It is important to note that GAG chains primed by xylosides *in vivo* have a lower sulfation density than commercial GAG chains (see supplemental data). Thus, we speculate that the high sulfation of heparin and commercial DS allows them to undergo somewhat artificial interactions, while under *in vivo* conditions, primed GAG chains must be multimeric to facilitate ternary complex formation with FGF and FGFR and subsequently lead to FGFR dimerization and signal transduction.

2.3.8 Syndecan-1 carrying two and three HS chains causes

elongation in significant number of treated embryos

One of the limitations of xyloside treatment in zebrafish embryos is our inability to ascertain the *in vivo* priming activity of each xyloside except in the case of biotinylated xylosides. Therefore, in order to confirm that GAG valency, rather than xyloside priming activity, is important in causing the elongation phenotype, syndecan-1 mutated mRNAs carrying zero, one, two or three HS initiation sites were injected (Figure 2.6). Injection

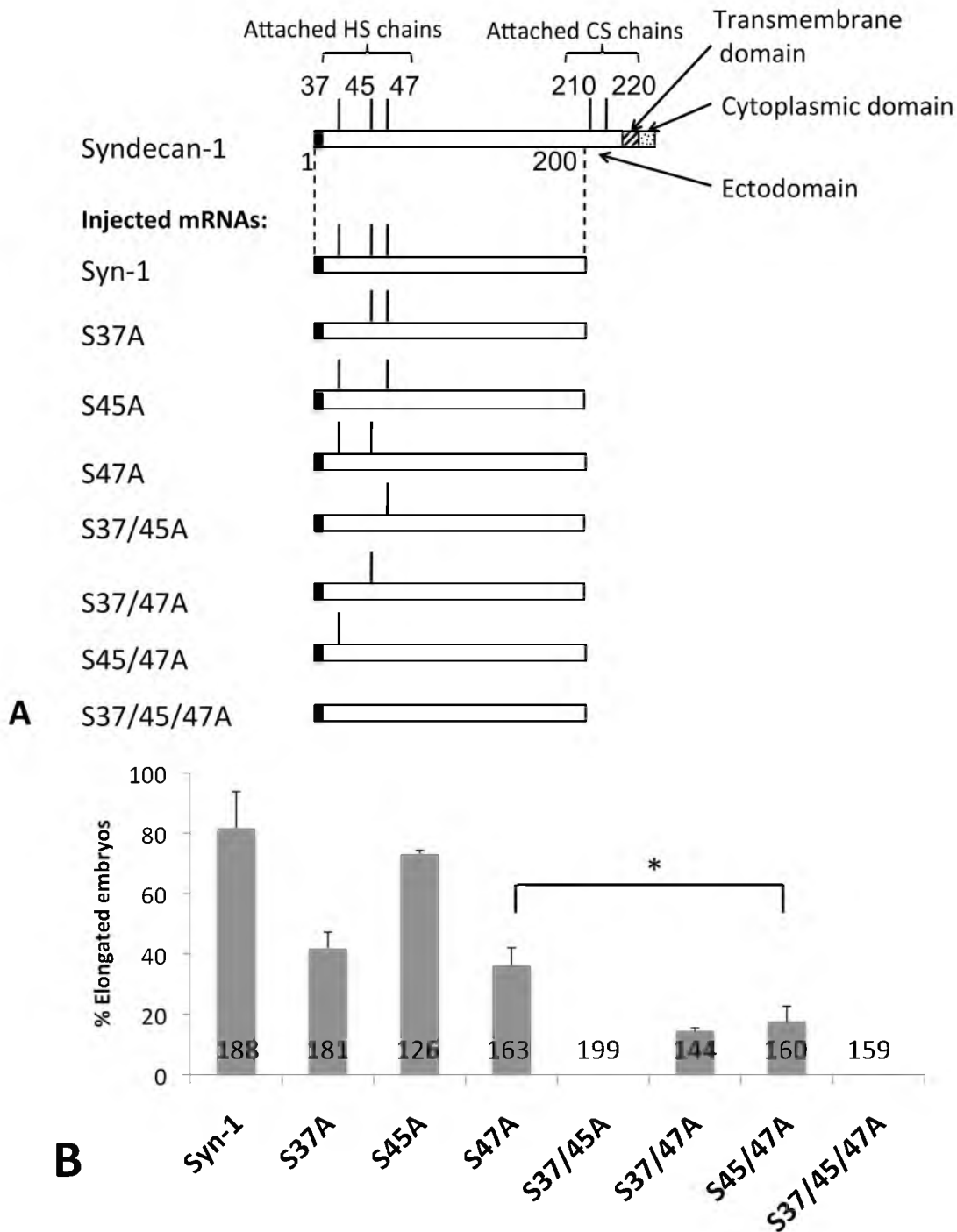


Figure 2.6 Injection of mRNAs encoding mutated syndecan-1 carrying two and three HS chains significantly caused the elongation phenotype. A: Structures of syndecan-1 and mutated syndecan-1 with zero, one, two or three HS initiation sites. B: Percentage of elongated embryos after the treatment with 45 pg of each mRNA at one-cell stage. Total numbers of embryos injected with Syn-1, S37A, S45A, S47A, S37/45A, S37/47A and S45/47A are 188, 181, 126, 163, 199, 144, 160 and 159, respectively. *, p < .05 using Student's t-test.

of mRNA carrying all three HS initiation sites caused the elongation phenotype at 12 hpf in 81.5 % of treated embryos (n = 188). Injection of mRNAs carrying two HS initiation sites at positions 45, 47; 37, 47; or 37, 45 caused the elongation phenotype at 12 hpf in 41.5 %, 72.9 % or 35.9 % of treated embryos, respectively. Injection of mRNAs carrying one HS initiation site at position 47, 45 or 37 caused the elongation phenotype in 0 %, 14.2 % or 17.4% of the treated embryos at 12 hpf. On the other hand, injection of mRNA carrying no HS initiation site did not cause any elongation phenotype at 12 hpf (n = 159). This result unequivocally indicates that proteoglycans with two or three HS side chains are more effective than proteoglycans with one or no HS side chain in hyperactivating FGF signaling in zebrafish embryos.

2.4 Discussion

All PGs, except decorin, have multiple GAG side chains, suggesting that multimeric GAG chains are essential for optimal biological activity (43). Surprisingly, only a few studies examined the importance of multiple HS chains of syndecan-1 and syndecan-4 in cellular systems and HS chain valency was shown to affect cell adhesion (10, 11). We surmise that the multivalency of GAG chains has a significant role in regulating complex spatiotemporal interactions with proteins, including FGF and FGFR, during the development.

A large body of *in vitro* data indicates that PGs are essential for FGF/FGFR signaling (12, 13, 44). FGFs activate their cognate receptor tyrosine kinases by inducing receptor dimerization. Numerous models have been proposed to explain FGFR dimerization at the molecular level (17-19). All of these models, based on biochemical

and biophysical studies, attempted to elucidate the nature of interactions. However, the structural basis for the role of PGs in assisting FGF/FGFR signaling *in vivo* requires careful re-evaluation because the synergistic or individual contribution of multiple GAG chains of PGs to FGFR dimerization and the subsequent *in vivo* signaling have not yet been elucidated in any animal model. Our results presented here are the first ones to show the induction of PG mimetic *in vivo* with two or three GAG chains connected covalently and to study a plausible synergistic role of GAG chain valency in regulating FGF and FGFR interactions.

Mono-xylosides have been used in various organisms over three decades to define the role of GAG chains (20, 21, 45). However, these mono-xylosides can only make a single GAG chain per xyloside. On the other hand, bis- and tris-xylosides can prime two and three GAG chains that are covalently attached on the same scaffold. Therefore, GAG chains primed by bis- and tris-xylosides are able to better mimic naturally occurring PGs displaying multiple GAG chains. Our results indicate that treatment of embryos with any bis- or tris-xylosides, but none of mono-xylosides, caused elongation (Figure 2.1). Our *in situ* hybridization and whole-mount antibody staining experiments as well as rescue experiments with tyrosine kinase inhibitor SU5402, mRNA for FGF antagonist *sprouty4* and FGF8 morpholino indicated that FGF signaling is the direct target for bis-xyloside primed GAG chains (Figures 2.2 and 2.3).

It is important to note that in earlier studies, mono-xylosides have been shown to compete with endogenous core proteins for GAG priming and function as “decoys” by preventing HS from being attached to its acceptor sites on endogenous core proteins (20, 21). In this case, we proved that the elongation phenotype is not caused by decoy activity

by several measures. Firstly, the similarity in the types of sulfation of GAG chains obtained from WT and xyloside-injected embryos suggests that xyloside primers do not disturb the endogenous GAG biosynthesis (Figure 2.5). Secondly, bis-xyloside-primed GAG chains purified from zebrafish embryos can activate FGF signaling when injected back into embryos. It is important to note that injection of primed-dimeric GAGs, irrespective of whether they are heparin lyase or chondroitinase ABC susceptible, can cause the FGFR hyperactivation/ elongation phenotype under conditions where endogenous GAGs are largely unaffected. Lastly, injection of bis-fluoroxylosides (xyloside **XVIII** - **XX**, Figure 2.7A) did not cause elongation phenotype. These bis-fluoroxylosides are bis-xyloside analogs, in each of which the hydroxyl group at C4 position is replaced by a fluorine group, therefore they can not prime GAG chains.

This result confirms that bis-xylosides do not act as “decoys” but act through their primed GAG chains (Figure 2.7B). Therefore, the elongation phenotype is best explained by a *gain of function* mechanism in which xyloside-primed multivalent GAG chains transit through the secretory pathway to the cell surface/ECM, recruit FGFs, facilitate GAG/FGF/FGFR signaling complex formation and eventually lead to FGFR hyperactivation (Figure 2.7B). This explanation is further corroborated by the fact that up to 160 pmoles of mono-xyloside, 5 times the injected dose for bis-xylosides, did not cause any elongation phenotype. Thus, primed GAG chains need to be at least dimeric to affect FGF signaling. However, except in the case of biotinylated xylosides, the *in vivo* priming activity of xylosides was difficult to be determined. Therefore, mRNAs encoding mutated syndecan-1 carrying zero, one, two or three HS initiation sites were injected. Injection of mRNAs carrying three or two HS chains caused a significantly higher

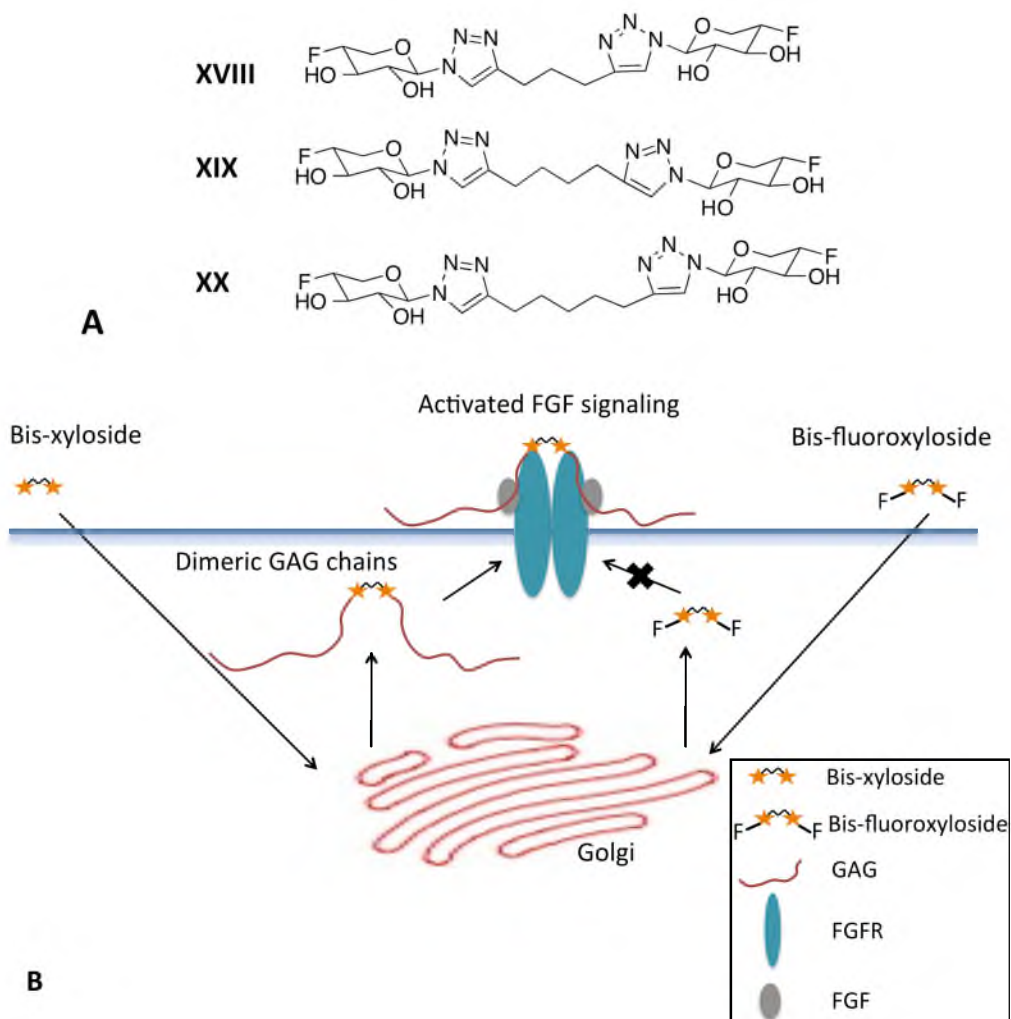


Figure 2.7 Structures of screened bis-fluoroxylsides and their actions in zebrafish embryos compared to bis-xylosides. **A:** Structures of bis-fluoroxylsides (**XVIII-XX**) injected into zebrafish embryos. These compounds are analogs of bis-xylosides (**VIII-X**), in each of which the hydroxyl group at C4 position is replaced by a fluorine group. **B:** Mechanistic roles of bis-xylosides and bis-fluoroxylsides in the activation of FGF signaling in zebrafish embryos. Bis-xyloside enters the Golgi apparatus and primes dimeric GAG chains. The dimeric GAG chains are secreted to the extracellular matrix, form the ternary complexes with FGFs and FGFRs. Two complexes are then brought closer for active FGFR dimerization. On the other hand, bis-fluoroxylsides enters the Golgi but can not prime GAG chains. Therefore, bis-fluoroxylsides can not activate FGF signaling in zebrafish embryos.

percentage of elongated embryos as compared to mRNAs carrying one or zero HS chain. This result confirms the importance of GAG valency in hyperactivating FGF signaling in zebrafish embryos. Based on our current *in vivo* study, we propose a molecular model in which two covalently linked GAG chains interact with two FGF8 molecules and their cognate FGFRs, inducing FGFR dimerization that leads to the elongation phenotype. This model is also strengthened by the fact that all naturally occurring PGs bear multiple GAG chains.

One may alternatively argue that FGF8 could be sequestered in specific regions under normal conditions through its interaction with endogenous proteoglycans. When bis- or tris-xylosides are injected into embryos, the primed GAG chains, as long as these chains are at least dimeric, may effectively compete with endogenous PGs and increase FGF8-mediated FGFR dimerization and thus activation of the signaling pathway, leading to the elongation of embryos. In summary, the results presented here, for the first time, provide a structural basis for the ability of certain synthetic bis-xylosides to promote FGF8-mediated FGFR activation *in vivo*. It is, however, important to keep in mind that the GAG multivalency may not be necessary for FGF/FGFR pairs that form ternary complexes on the same GAG chain, allowing FGFRs to slide along the chain to form an active signaling complex. Efforts are currently underway to elucidate the requirement of specific sulfate groups for the activation of FGF8 signaling and the nature of interaction among GAG, FGF8 and FGFR in the formation of signaling complex.

2.5 Supplemental data

Table 2.S1. Structures of additional mono-xylosides tested in zebrafish embryos. None of these mono-xylosides gave elongation phenotype at 12 hpf.

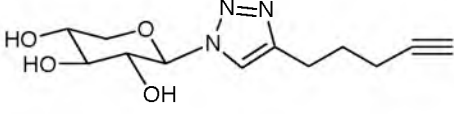
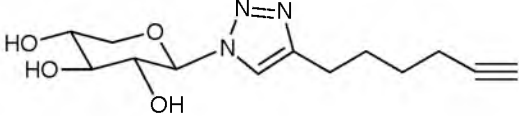
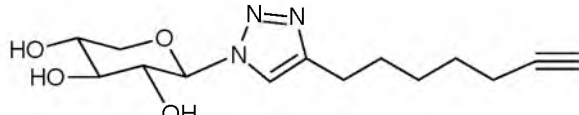
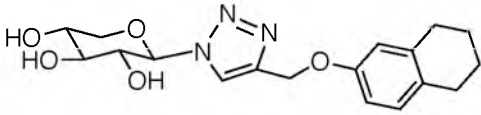
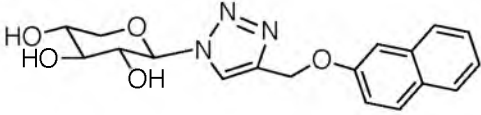
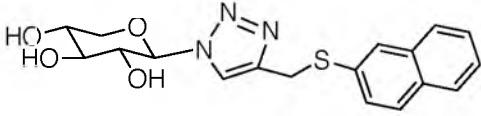
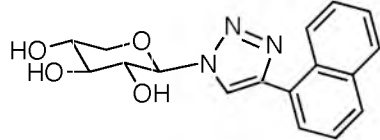
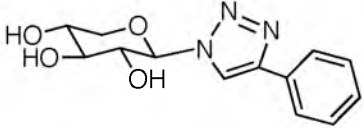
Number	Structure
XXI	
XXII	
XXIII	
XXIV	
XXV	
XXVI	
XXVII	
XXVIII	

Table 2.S1 continued

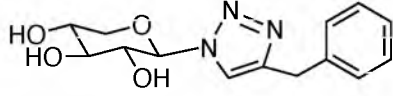
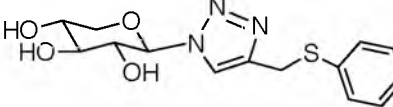
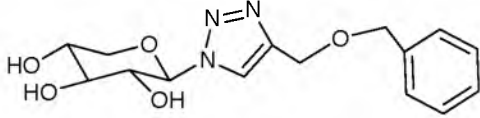
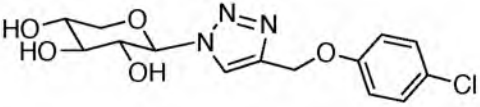
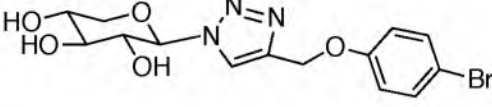
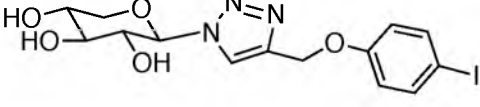
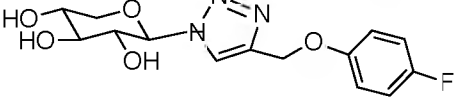
Number	Structure
XXIX	
XXX	
XXXI	
XXXII	
XXXIII	
XXXIV	
XXXV	

Table 2.S2. Effect of bis-xylosides and mono-xylosides on the elongation phenotype at 12 hpf and on *mkp3* expression at 8 hpf.

*Percentages indicate the fraction of elongated embryos

**Percentages indicate the fraction of embryos with expanded *mkp3* expression

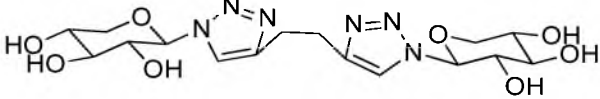


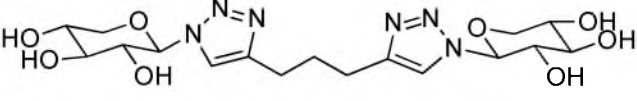

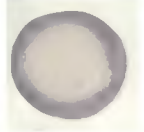
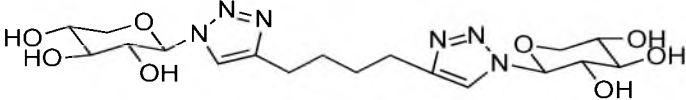


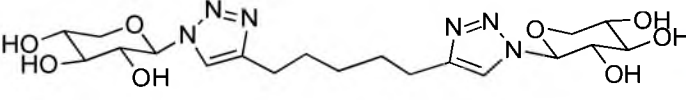


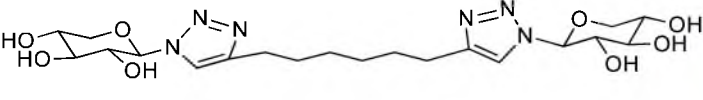


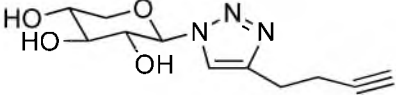


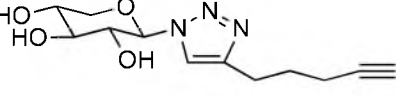


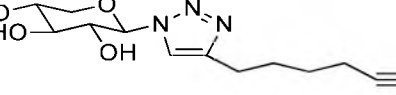


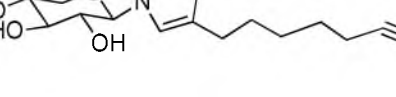
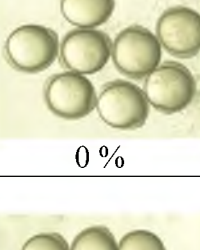


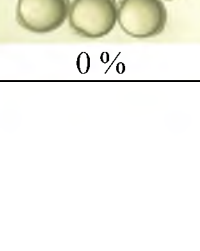
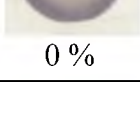
Structures of injected xylosides	12 hpf phenotype*	<i>mkp3</i> expression on 8 hpf embryos**
	 5 %	 2 %
	 15 %	 10 %
	 28 %	 20 %
	 82 %	 80 %
	 89 %	 90 %

Table 2.S2 Continued

Structures of injected xylosides	12 hpf phenotype*	mkp3 expression on 8 hpf embryos**
	 <p>0 %</p>	 <p>0 %</p>
	 <p>0 %</p>	 <p>0 %</p>
	 <p>0 %</p>	 <p>0 %</p>
	 <p>0 %</p>	 <p>0 %</p>
	 <p>0 %</p>	 <p>0 %</p>

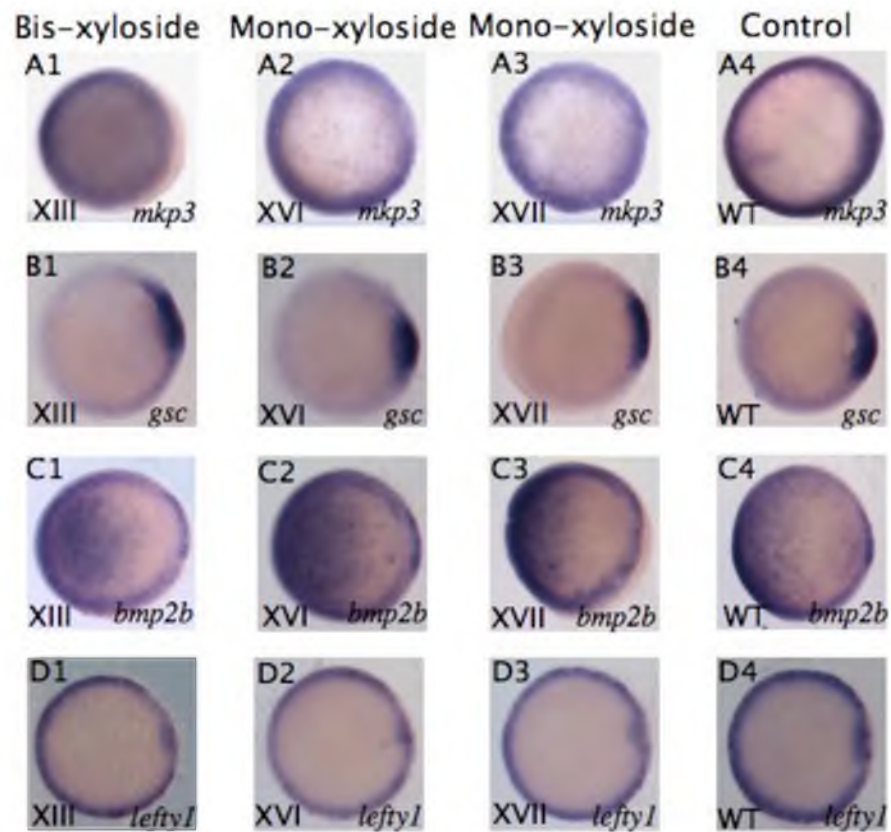


Figure 2.S1. Developmental signaling in embryos injected with bis-xyloside **XIII** and mono-xylosides **XVI**, **XVII**. A-D: Embryos injected with bis-xyloside **XIII** (A1-D1), mono-xyloside injected **XVI** (A2-D2), mono-xyloside **XVII** (A3-D3) and control embryos (A4-D4) *in situ* hybridized at 8 hpf with probes for the FGF target gene *mkp3* (A), dorsal marker *gsc* (B), BMP ligand *bmp2b* (C) and Nodal target gene *lefty1* (D). Animal pole views, dorsal right.

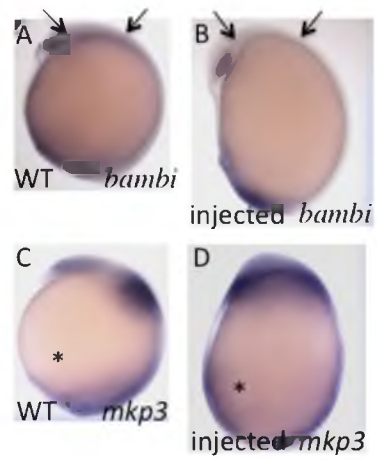


Figure 2.S2. Expression patterns of *bambi* and *mkp3* at 12 hpf. Expression of the BMP target *bambi* in the border of the nonneural ectoderm (arrows) is downregulated in bis-xyloside II-treated embryos (B) compared to WT (A). Expression of the FGF target gene *mkp3* in the ventral ectoderm (asterisks) is upregulated in bis-xyloside II-treated embryos (D) compared to WT (C).

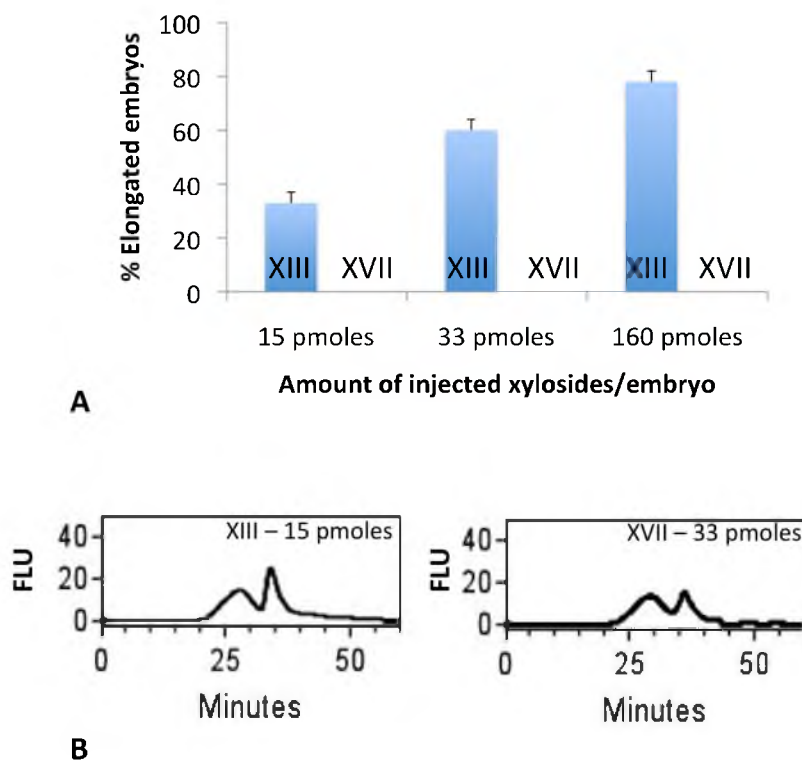


Figure 2.S3. Injection of bis-xyloside **XIII** and mono-xyloside **XVII** to zebrafish embryos at different concentrations. **A:** Bis-xyloside **XIII** and mono-xyloside **XVII** were injected to zebrafish embryos at 15, 33 and 160 pmoles/embryo. Percentage of elongated embryos increased with increased concentrations of injected bis-xyloside. Mono-xyloside did not cause elongation phenotype at all tested concentrations. **B:** Fluorescent detection of GAG chains primed in embryos by biotinylated bis-xyloside **XIII** (15 pmoles/embryo) and biotinylated mono-xyloside **XVII** (33 pmoles/embryo), after purification, complexing with streptavidin-Alexa Fluor 350 and elution from an HPLC-size exclusion column.

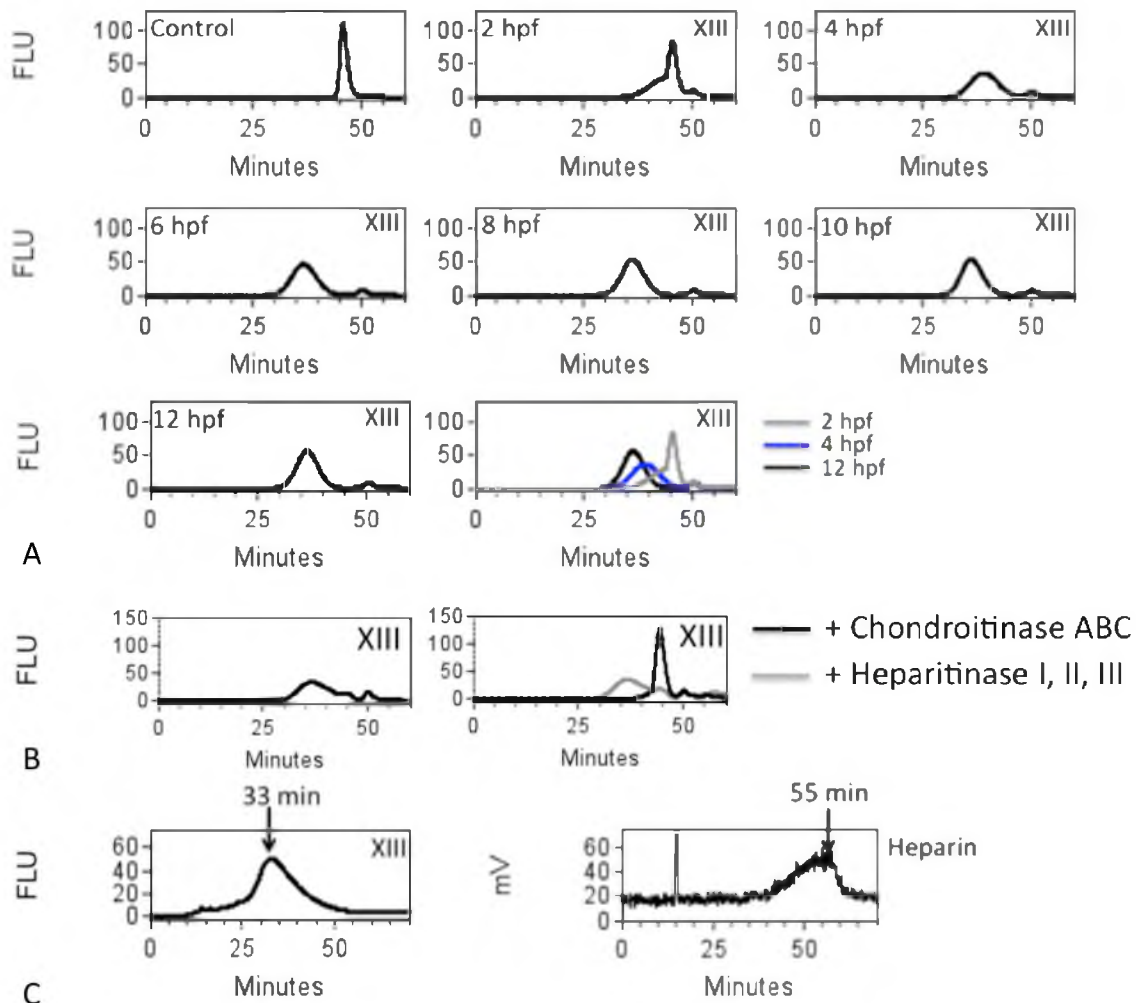


Figure 2.S4. Structural analysis of GAG chains primed by xylosides. A: Priming of GAGs in embryos by bis-xyloside XIII over time. GAG chains primed by the biotinylated bis-xyloside XIII at 2, 4, 6, 8, 10 and 12 hpf ($n = 100$ per time point) were purified, mixed with $0.125 \mu\text{g}$ S-AF350 and analyzed using an HPLC-size exclusion column with fluorescence detector. The chromatographic profiles suggested that the amount of GAGs increased over time. B: Fluorescent detection of GAG chains primed by biotinylated bis-xyloside XIII at 6 hpf before and after treatment with chondroitinase ABC or heparitinases I, II and III to determine the relative proportion of HS and CS/DS, respectively. C: Comparison of DEAE elution profiles of bis-xyloside XIII-primed GAG chains and heparin. GAG chains primed by bis-xyloside XIII purified from embryos at 10 hpf were complexed with S-AF350 and analyzed using an HPLC-DEAE ion-exchange column with fluorescence detector. Heparin was radiolabeled with $[^{35}\text{S}]$ -PAPS and 3-O-sulfotransferase and analyzed on the HPLC-DEAE column with radiodetector. Samples were eluted with a linear NaCl gradient of 0.2 M to 1 M over 80 min at 1 ml/min flow rate. Bis-xyloside primed GAG chains from 10 hpf embryos have significantly lower sulfation density than heparin.

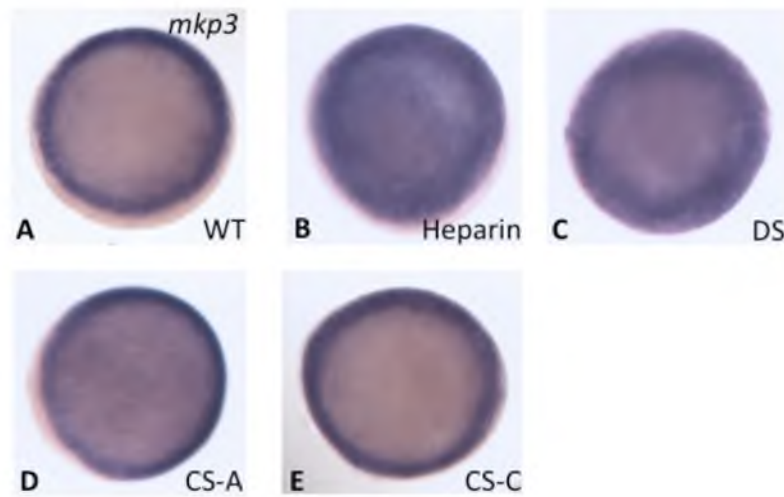


Figure 2.S5. Expression pattern of FGF signaling target gene *mkp3* in embryos injected with different GAG types. Water (A, control), heparin (B), dermatan sulfate (DS) (C), chondroitin sulfate A (CS-A) (D) or chondroitin sulfate C (CS-C) (E) were injected into 4 hpf embryos at 1 ng/embryo. *In situ* hybridization with a *mkp3* probe was carried out at 8 hpf. *mkp3* expression was expanded in embryos injected with heparin (27/35) and DS (29/40), whereas fewer embryos have expanded *mkp3* expression upon treatment with CS-A (5/45) or CS-C (7/43). Animal pole views.

2.6 References

1. Perrimon, N.; Bernfield, M., Specificities of Heparan Sulphate Proteoglycans in Developmental Processes. *Nature* **2000**, *404* (6779), 725-8.
2. Carey, D. J., Syndecans: Multifunctional Cell-Surface Co-Receptors. *Biochem J* **1997**, *327*, 1-16.
3. De Cat, B.; David, G., Developmental Roles of the Glypicans. *Semin Cell Dev Biol* **2001**, *12* (2), 117-25.
4. Lee, J. S.; Chien, C. B., When Sugars Guide Axons: Insights from Heparan Sulphate Proteoglycan Mutants. *Nat Rev Genet* **2004**, *5* (12), 923-35.
5. Muir, H., The Nature of the Link between Protein and Carbohydrate of a Chondroitin Sulphate Complex from Hyaline Cartilage. *Biochem J* **1958**, *69* (2), 195-204.
6. Lindahl, U.; Cifonelli, J. A.; Lindahl, B.; Roden, L., The Role of Serine in the Linkage of Heparin to Protein. *J Biol Chem* **1965**, *240*, 2817-20.
7. Raman, K., Kuberan, B., Chemical Tumor Biology of Heparan Sulfate Proteoglycans. *Current Chemical Biology* **2010**, *4* (1), 20-31.
8. Bishop, J. R.; Schuksz, M.; Esko, J. D., Heparan Sulphate Proteoglycans Fine-Tune Mammalian Physiology. *Nature* **2007**, *446* (7139), 1030-7.
9. Sanderson, R. D.; Bernfield, M., Molecular Polymorphism of a Cell Surface Proteoglycan: Distinct Structures on Simple and Stratified Epithelia. *Proc Natl Acad Sci U S A* **1988**, *85* (24), 9562-6.
10. Langford, J. K.; Stanley, M. J.; Cao, D.; Sanderson, R. D., Multiple Heparan Sulfate Chains Are Required for Optimal Syndecan-1 Function. *J Biol Chem* **1998**, *273* (45), 29965-71.
11. Gopal, S.; Bober, A.; Whiteford, J. R.; Multhaupt, H. A.; Yoneda, A.; Couchman, J. R., Heparan Sulfate Chain Valency Controls Syndecan-4 Function in Cell Adhesion. *J Biol Chem* **2010**, *285* (19), 14247-58.
12. Yayon, A.; Klagsbrun, M.; Esko, J. D.; Leder, P.; Ornitz, D. M., Cell Surface, Heparin-Like Molecules Are Required for Binding of Basic Fibroblast Growth Factor to Its High Affinity Receptor. *Cell* **1991**, *64* (4), 841-8.
13. Rapraeger, A. C.; Krufka, A.; Olwin, B. B., Requirement of Heparan Sulfate for Bfgf-Mediated Fibroblast Growth and Myoblast Differentiation. *Science* **1991**, *252* (5013), 1705-8.

14. Allen, B. L.; Rapraeger, A. C., Spatial and Temporal Expression of Heparan Sulfate in Mouse Development Regulates Fgf and Fgf Receptor Assembly. *J Cell Biol* **2003**, *163* (3), 637-48.
15. Bao, X.; Nishimura, S.; Mikami, T.; Yamada, S.; Itoh, N.; Sugahara, K., Chondroitin Sulfate/Dermatan Sulfate Hybrid Chains from Embryonic Pig Brain, Which Contain a Higher Proportion of L-Iduronic Acid Than Those from Adult Pig Brain, Exhibit Neuritogenic and Growth Factor Binding Activities. *J Biol Chem* **2004**, *279* (11), 9765-76.
16. Nakamura, M.; Uehara, Y.; Asada, M.; Honda, E.; Nagai, N.; Kimata, K.; Suzuki, M.; Imamura, T., Sulfated Glycosaminoglycans Are Required for Specific and Sensitive Fibroblast Growth Factor (Fgf) 19 Signaling Via Fgf Receptor 4 and Betaklotho. *J Biol Chem* **2011**, *286* (30), 26418-23.
17. Mohammadi, M.; Olsen, S. K.; Ibrahimi, O. A., Structural Basis for Fibroblast Growth Factor Receptor Activation. *Cytokine Growth Factor Rev* **2005**, *16* (2), 107-37.
18. Guimond, S.; Maccarana, M.; Olwin, B. B.; Lindahl, U.; Rapraeger, A. C., Activating and Inhibitory Heparin Sequences for Fgf-2 (Basic Fgf). Distinct Requirements for Fgf-1, Fgf-2, and Fgf-4. *J Biol Chem* **1993**, *268* (32), 23906-14.
19. Ornitz, D. M.; Yayon, A.; Flanagan, J. G.; Svahn, C. M.; Levi, E.; Leder, P., Heparin Is Required for Cell-Free Binding of Basic Fibroblast Growth Factor to a Soluble Receptor and for Mitogenesis in Whole Cells. *Mol Cell Biol* **1992**, *12* (1), 240-7.
20. Okayama, M.; Kimata, K.; Suzuki, S., The Influence of P-Nitrophenyl Beta-D-Xyloside on the Synthesis of Proteochondroitin Sulfate by Slices of Embryonic Chick Cartilage. *J Biochem* **1973**, *74* (5), 1069-73.
21. Yost, H. J., Inhibition of Proteoglycan Synthesis Eliminates Left-Right Asymmetry in *Xenopus Laevis* Cardiac Looping. *Development* **1990**, *110* (3), 865-74.
22. Kuberan, B.; Ethirajan, M.; Victor, X. V.; Tran, V.; Nguyen, K.; Do, A., "Click" Xylosides Initiate Glycosaminoglycan Biosynthesis in a Mammalian Cell Line. *Chembiochem* **2008**, *9* (2), 198-200.
23. Garud, D. R.; Tran, V. M.; Victor, X. V.; Koketsu, M.; Kuberan, B., Inhibition of Heparan Sulfate and Chondroitin Sulfate Proteoglycan Biosynthesis. *J Biol Chem* **2008**, *283* (43), 28881-7.
24. Westerfield, M., *The Zebrafish Book. A Guide for the Laboratory Use of Zebrafish (Danio Rerio)*; University of Oregon Press: Eugene, 2000.

25. Dorsky, R. I.; Sheldahl, L. C.; Moon, R. T., A Transgenic Lef1/Beta-Catenin-Dependent Reporter Is Expressed in Spatially Restricted Domains Throughout Zebrafish Development. *Dev Biol* **2002**, *241* (2), 229-37.
26. Tsang, M.; Maegawa, S.; Kiang, A.; Habas, R.; Weinberg, E.; Dawid, I. B., A Role for Mkp3 in Axial Patterning of the Zebrafish Embryo. *Development* **2004**, *131* (12), 2769-79.
27. Stachel, S. E.; Grunwald, D. J.; Myers, P. Z., Lithium Perturbation and Goosecoid Expression Identify a Dorsal Specification Pathway in the Pregastrula Zebrafish. *Development* **1993**, *117* (4), 1261-74.
28. Nikaido, M.; Tada, M.; Saji, T.; Ueno, N., Conservation of Bmp Signaling in Zebrafish Mesoderm Patterning. *Mech Dev* **1997**, *61* (1-2), 75-88.
29. Schebesta, M.; Lien, C. L.; Engel, F. B.; Keating, M. T., Transcriptional Profiling of Caudal Fin Regeneration in Zebrafish. *ScientificWorldJournal* **2006**, *6*, 38-54.
30. Meno, C.; Ito, Y.; Saijoh, Y.; Matsuda, Y.; Tashiro, K.; Kuhara, S.; Hamada, H., Two Closely-Related Left-Right Asymmetrically Expressed Genes, Lefty-1 and Lefty-2: Their Distinct Expression Domains, Chromosomal Linkage and Direct Neuralizing Activity in Xenopus Embryos. *Genes Cells* **1997**, *2* (8), 513-24.
31. Thisse, C.; Thisse, B.; Schilling, T. F.; Postlethwait, J. H., Structure of the Zebrafish Snail1 Gene and Its Expression in Wild-Type, Spadetail and No Tail Mutant Embryos. *Development* **1993**, *119* (4), 1203-15.
32. Araki, I.; Brand, M., Morpholino-Induced Knockdown of Fgf8 Efficiently Phenocopies the Acerebellar (Ace) Phenotype. *Genesis* **2001**, *30* (3), 157-9.
33. Victor, X. V.; Nguyen, T. K.; Ethirajan, M.; Tran, V. M.; Nguyen, K. V.; Kuberan, B., Investigating the Elusive Mechanism of Glycosaminoglycan Biosynthesis. *J Biol Chem* **2009**, *284* (38), 25842-53.
34. Johnsson, R.; Mani, K.; Ellervik, U., Synthesis and Biology of Bis-Xylosylated Dihydroxynaphthalenes. *Bioorg Med Chem* **2007**, *15* (8), 2868-77.
35. Kelly, G. M.; Erezyilmaz, D. F.; Moon, R. T., Induction of a Secondary Embryonic Axis in Zebrafish Occurs Following the Overexpression of Beta-Catenin. *Mech Dev* **1995**, *53* (2), 261-73.
36. Furthauer, M.; Van Celst, J.; Thisse, C.; Thisse, B., Fgf Signalling Controls the Dorsoventral Patterning of the Zebrafish Embryo. *Development* **2004**, *131* (12), 2853-64.
37. Feldman, B.; Gates, M. A.; Egan, E. S.; Dougan, S. T.; Rennebeck, G.; Sirotkin, H. I.; Schier, A. F.; Talbot, W. S., Zebrafish Organizer Development and Germ-Layer Formation Require Nodal-Related Signals. *Nature* **1998**, *395* (6698), 181-5.

38. Myers, D. C.; Sepich, D. S.; Solnica-Krezel, L., Bmp Activity Gradient Regulates Convergent Extension During Zebrafish Gastrulation. *Dev Biol* **2002**, *243* (1), 81-98.
39. Onichtchouk, D.; Chen, Y. G.; Dosch, R.; Gawantka, V.; Delius, H.; Massague, J.; Niehrs, C., Silencing of Tgf-Beta Signalling by the Pseudoreceptor Bambi. *Nature* **1999**, *401* (6752), 480-5.
40. Sun, L.; Tran, N.; Tang, F.; App, H.; Hirth, P.; McMahon, G.; Tang, C., Synthesis and Biological Evaluations of 3-Substituted Indolin-2-Ones: A Novel Class of Tyrosine Kinase Inhibitors That Exhibit Selectivity toward Particular Receptor Tyrosine Kinases. *J Med Chem* **1998**, *41* (14), 2588-603.
41. Itoh, N., The Fgf Families in Humans, Mice, and Zebrafish: Their Evolutional Processes and Roles in Development, Metabolism, and Disease. *Biol Pharm Bull* **2007**, *30* (10), 1819-25.
42. Kudoh, T.; Tsang, M.; Hukriede, N. A.; Chen, X.; Dedekian, M.; Clarke, C. J.; Kiang, A.; Schultz, S.; Epstein, J. A.; Toyama, R.; Dawid, I. B., A Gene Expression Screen in Zebrafish Embryogenesis. *Genome Res* **2001**, *11* (12), 1979-87.
43. Bernfield, M.; Kokenyesi, R.; Kato, M.; Hinkes, M. T.; Spring, J.; Gallo, R. L.; Lose, E. J., Biology of the Syndecans: A Family of Transmembrane Heparan Sulfate Proteoglycans. *Annu Rev Cell Biol* **1992**, *8*, 365-93.
44. Lin, X.; Buff, E. M.; Perrimon, N.; Michelson, A. M., Heparan Sulfate Proteoglycans Are Essential for Fgf Receptor Signaling During Drosophila Embryonic Development. *Development* **1999**, *126* (17), 3715-23.
45. Fritz, T. A.; Lugemwa, F. N.; Sarkar, A. K.; Esko, J. D., Biosynthesis of Heparan Sulfate on Beta-D-Xylosides Depends on Aglycone Structure. *J Biol Chem* **1994**, *269* (1), 300-7.

CHAPTER 3

ENZYMATIC SYNTHESIS OF FGF8-BINDING HS MOTIFS

3.1 Overview

In Chapter 2, our results demonstrated the importance of GAG multivalency in the FGF8 signaling pathway in zebrafish embryos. In developing embryos, endogenously produced GAG chains need to be at least dimerized to form two ternary complexes with FGF8 and FGFR, leading to the activation of FGF8-mediated signaling pathway. Furthermore, heparin and dermatan sulfate, but not chondroitin sulfate A and C, can have the same effect on FGF8 signaling. These findings suggest that even though specific structures are required for GAG-FGF8 interactions, promiscuity is also involved, i.e., different structures can have the same function.

This chapter outlines effort to elucidate the structural requirements of HS for its interactions with FGF8 and how these FGF8-binding HS structures are assembled *in vivo*. In order to achieve this goal, one needs to analyze the structures of HS molecules that activate FGF8 signaling and cause elongation phenotype in zebrafish embryos. However, the amounts of HS produced in developing zebrafish embryos are extremely low, making it impossible to derive any meaningful structural information about endogenously produced HS in the embryos. Therefore, a more practical approach was employed to answer these questions that would also provide more specific information regarding HS-FGF8 structure-activity relationships. A library of HS oligosaccharides carrying specific sulfation with defined sizes was enzymatically synthesized. This library was tested in zebrafish embryos considering the elongation phenotype as a FGF8 activity indicator. In this assay, the HS oligosaccharides, which cause the elongation phenotype, contain the structural parameters that are important for HS-FGF8 interactions.

In order to assemble this HS oligosaccharide library, several intermediate studies

were performed. *N*-acetylheparosan, polysaccharide HS backbone, is isolated from *E.coli* K5. This backbone was then fragmented with heparitinase I to obtain size-defined oligosaccharides. In parallel, we prepared uniformly and atom-specifically ¹³C-labeled polysaccharide backbones (*I*). These labeled backbones provided high-resolution NMR signal and distinct mass spectrometric data, allowing one to distinguish exogenous and endogenous HS. The details of this study were reported in Section 3.2. In the next step, HS biosynthetic enzymes including *N*-deacetylase *N*-sulfotransferase (NDST-2), C5-epimerase (C5-Epi), 2-*O*-sulfotransferase (2-OST), 6-*O*-sulfotransferase (6-OST1, 6-OST2a, 6-OST2b, 6-OST3) and 3-*O*-sulfotransferase (3-OST1, 3-OST3a) were expressed using baculovirus system and purified. Each enzyme isoform can have distinct substrate specificity. Therefore, the action of each isoform was studied to provide a guidance to assemble distinct HS oligosaccharides. The study on the enzymatic actions of 3-OST3a and 3-OST1 was reported in Section 3.3 (2). Not only different isoforms of the same enzyme can have distinct substrate specificity but also enzymes can generate distinct structures depending on the order of enzymatic modifications. Therefore, we specifically investigated the actions of NDST-2, C5-Epi and 2-OST in concurrent and sequential manners to elucidate the possible mechanism by which the FGF-1 HS binding motifs are assembled. This study was reported in Section 3.4 (3). Finally, with all the above information, HS oligosaccharides with different sizes and structures were enzymatically synthesized. All structures were thoroughly analyzed by liquid chromatography coupled with mass spectrometry. This oligosaccharide library was tested on zebrafish embryos for their effect on FGF8 signaling. With these results, we were able to reveal the

minimum size, the specific structures and the biogenesis pathway of FGF8-binding HS motifs *in vivo*. These results were reported in Section 3.5.

3.2 Characterization of uniformly and atom-specifically ^{13}C -labeled
heparin and heparan sulfate polysaccharide precursors using
 ^{13}C NMR spectroscopy and ESI mass spectrometry

Manuscript reproduced with permission from:

Nguyen, T. K., Tran, V. M., Victor, X. V., Skalicky, J. J., and Kuberan, B. (2010) Characterization of uniformly and atom-specifically (^{13}C)-labeled heparin and heparan sulfate polysaccharide precursors using (^{13}C) NMR spectroscopy and ESI mass spectrometry, *Carbohydr Res* 345, 2228-2232.

© 2010 Elsevier Ltd.



Characterization of uniformly and atom-specifically ^{13}C -labeled heparin and heparan sulfate polysaccharide precursors using ^{13}C NMR spectroscopy and ESI mass spectrometry

Thao K. N. Nguyen^a, Vy M. Tran^a, Xylophone V. Victor^b, Jack J. Skalicky^c, Balagurunathan Kuberan^{a,b,d,*}

^a Department of Bioengineering, University of Utah, Salt Lake City, UT 84112, United States

^b Department of Medicinal Chemistry, University of Utah, Skaggs Hall Rm#307, 30 South 2000 East, Salt Lake City, UT 84112, United States

^c Department of Biochemistry, University of Utah, Salt Lake City, UT 84112, United States

^d Interdepartmental Program in Neuroscience, University of Utah, Salt Lake City, UT 84112, United States

ARTICLE INFO

Article history:

Received 25 June 2010

Received in revised form 30 July 2010

Accepted 17 August 2010

Available online 21 August 2010

Keywords:

Glycosaminoglycan

Heparan sulfate

Heparin

Isotopes

Heparanomics

NMR spectroscopy

ABSTRACT

The biological actions of heparin and heparan sulfate, two structurally related glycosaminoglycans, depend on the organization of the complex heparanome. Due to the structural complexity of the heparanome, the sequence of variably sulfonated uronic acid and glucosamine residues is usually characterized by the analysis of smaller oligosaccharide and disaccharide fragments. Even characterization of smaller heparin and heparan sulfate oligosaccharide or disaccharide fragments using simple 1D ^1H NMR spectroscopy is often complicated by the extensive signal overlap. ^{13}C NMR signals, on the other hand, overlap less and therefore, ^{13}C NMR spectroscopy can greatly facilitate the structural elucidation of the complex heparanome and provide finer insights into the structural basis for biological functions. This is the first report of the preparation of anomeric carbon-specific ^{13}C -labeled heparin and heparan sulfate precursors from the *Escherichia coli* K5 strain. Uniformly ^{13}C - and ^{15}N -labeled precursors were also produced and characterized by ^{13}C NMR spectroscopy. Mass spectrometric analysis of enzymatically fragmented disaccharides revealed that anomeric carbon-specific labeling efforts resulted in a minor loss/scrambling of ^{13}C in the precursor backbone, whereas uniform labeling efforts resulted in greater than 95% ^{13}C isotope enrichment in the precursor backbone. These labeled precursors provided high-resolution NMR signals with great sensitivity and set the stage for studying the heparanome–proteome interactions.

© 2010 Elsevier Ltd. All rights reserved.

1. Introduction

Heparan sulfate (HS), a member of the glycosaminoglycan (GAG) family, is a linear, sulfated polysaccharide composed of repeating disaccharide units comprising glucosamine and hexuronic acid (*ido*- or *gluco*-). Highly anionic HS is widely distributed on the cell surface and in the extracellular matrix. Interactions of HS sequences with various proteins have been implicated in many physiological and pathological processes such as their participation in cell–cell and cell–matrix interactions, cell proliferation, cell migration and cell differentiation, anti-coagulation, inflammation, tumor metastasis, and various infections.^{1,2} However, the structure–function relationships of HS chains are difficult to establish because of their structural complexity arising from their highly variable length and composition.³ During HS biosynthesis, a number of enzymes incompletely modify a nascent chain comprised of alternating glucuronic acid and *N*-acetylglucosamine residues. The resulting heterogeneity in HS fine structure, however, appears to

be a key factor in determining the function of the HS chain, possibly because it confers specificity for interactions with HS-binding proteins.

There are a number of methods through which HS–protein interactions can be studied, but one of the most powerful approaches is NMR spectroscopy. NMR spectroscopy provides crucial structural and conformational information useful in identifying precise contact points between interacting molecules and can also be used as an assay for identifying binding partners. Furthermore, NMR spectroscopy can also be used to detect modifications made by HS biosynthetic enzymes on precursor molecules and to study the biosynthetic process. However, high concentrations of HS chains are required for such studies due to the low natural abundance of nuclei with a net spin (^{13}C and ^{15}N). The preparation of HS biomolecules enriched with NMR-active nuclei would improve the detection and facilitate the analysis of structure–function relationships. Thus, the goal of this study is to prepare HS structures with atom-specific ^{13}C labels at the anomeric centers of each sugar residue and also to prepare ^{15}N -enriched and uniformly ^{13}C -labeled HS precursors.

Escherichia coli K5 strain naturally synthesizes *N*-acetylheparosan (heparosan), a non-sulfated polysaccharide that resembles

* Corresponding author. Tel.: +1 801 587 9474; fax: +1 801 585 9119.
E-mail address: KUBY@pharm.utah.edu (B. Kuberan).

the unmodified, nascent HS chain.⁴ Thus, the preparation of isotope-enriched HS precursors can easily be accomplished by growing the *E. coli* strain K5 in a minimal media containing ¹⁵N-labeled ammonium salts and ¹³C-labeled glucose as the principal nitrogen source and carbon source, respectively. Several groups including our group recently published the preparation of isotope-enriched HS precursors for performing subsequent structural analysis.^{5–7} We report herein the first preparation of atom-specifically ¹³C-labeled HS precursor polysaccharides at the anomeric carbons. Differentially isotope-enriched HS precursor polysaccharides were isolated, quantified, and characterized using NMR spectroscopy. They were also analyzed using ESI-qTOFMS to determine the extent of isotope incorporation.

2. Results and discussions

The intrinsically narrow range of proton chemical shifts has significant spectral overlap, particularly in GAG chains, and makes ¹H NMR analysis challenging.⁸ On the other hand, ¹³C chemical shifts have a much wider range providing an opportunity to characterize complex HS/heparin chains using ¹³C NMR spectroscopy. However, NMR-active ¹³C nuclei are less abundant. Therefore, it is necessary to develop a strategy to prepare ¹³C isotope-enriched HS structures to fully exploit recent advances in NMR techniques to further our understanding of the structural basis for the biological actions of heparanome.

2.1. Preparation of differentially ¹³C-labeled HS precursors

N-Acetylheparosan, a capsular polysaccharide synthesized by the *E. coli* K5 strain, has the same structure as the non-sulfated and non-epimerized HS backbone. Therefore, this polymer has been used in the production of antithrombin III-binding HS oligosaccharides and polysaccharides.^{9–12} Our group recently reported the use of the *E. coli* K5 strain for the production of ¹⁵N-labeled HS polysaccharide and oligosaccharide precursors.⁶ Zhang and co-workers produced uniformly ¹³C-, ¹⁵N-labeled HS polymers using a similar strategy for enzymatic modifications.⁵ They subsequently characterized the solution structures of these uniformly labeled HS polymers. However, one of the main disadvantages of uniformly ¹³C-labeled HS is that direct detection and assignment of ¹³C signals may not be straightforward due to the presence of one-bond ¹³C–¹³C couplings between adjacent carbons. One potential approach to overcome this difficulty is to produce atom-specific ¹³C-labeled HS precursors by utilizing an appropriate ¹³C-labeled glucose as a metabolic source for the backbone synthesis by the *E. coli* K5 strain. However, uniformly ¹³C-labeled glucose is less expensive than atom-specific ¹³C-labeled glucose. Therefore, at the outset, we optimized the growth conditions of the *E. coli* K5 strain in a minimal medium containing uniformly ¹³C-labeled glucose and ¹⁵N-labeled ammonium sulfate or ¹⁵N-labeled ammonium chloride. We found that the overall yield of uniformly ¹³C-, ¹⁵N-labeled *N*-acetylheparosan is much higher when the *E. coli* K5 strain was grown in the presence of ¹⁵N-labeled ammonium sulfate (yield ~100 mg/L of culture) than in the presence of ¹⁵N-labeled ammonium chloride (yield ~30 mg/L of culture). After optimizing growth conditions to obtain the maximum amount of *N*-acetylheparosan polysaccharides using minimal media, we then turned our attention to prepare atom-specifically ¹³C-labeled HS precursors by growing the *E. coli* K5 strain in a minimal medium containing [1-¹³C]-D-glucose as a carbon source and ¹⁵N-labeled ammonium sulfate as a nitrogen source. Differentially isotope-enriched *N*-sulfoheparosan polysaccharides were obtained from the respective *N*-acetylheparosan polysaccharides by *N*-deacetylation and *N*-sulfonation as reported in the literature.^{13,14}

2.2. Structural analysis of uniformly or atom-specifically ¹³C-labeled HS precursor polysaccharides

Regular *N*-sulfoheparosan and differentially isotope-enriched *N*-sulfoheparosan polysaccharides and regular *N*-sulfoheparosan (**1**, **2**, and **3**, Fig. 1) were exhaustively digested with recombinant heparitinase I. The disaccharide products obtained were purified from the digestion mixture using 3000 MWCO Amicon centrifugal filter columns. The flow-through carrying the disaccharide components was dried in a speed-vac system and subsequently reconstituted in deionized water prior to mass spectrometric analysis. ESI-qTOFMS was utilized in the disaccharide analysis to determine the isotope enrichment.¹⁵ The mass spectrum of a given analyte typically consists of a sum of signals of various possible naturally occurring isotopic compositions. Thus, the monoisotopic patterns of the molecular ions of the given analyte provide further insights into the fine structure, the isotopic distribution, and the extent of isotopic enrichment. Therefore, it is important to have high-resolution mass spectra for which one needs a mass spectrometer with TOF or FT-ICR capability. MS analysis revealed the presence of significant peaks at *m/z* values of 416.3520, 418.3559, and 429.3921 for the molecular ions corresponding to the disaccharides derived from polysaccharides **1**, **2**, and **3**, respectively (see Figs. 1 and 2). Based on the monoisotopic pattern, the isotopic purity of uniformly ¹³C-, ¹⁵N-labeled *N*-sulfoheparosan, polysaccharide **3**, was found to be greater than 95%, whereas the isotopic purity of atom-specifically ¹³C-labeled at the anomeric carbon of each sugar building block of *N*-sulfoheparosan, polysaccharide **2** was found to be ~70%. Thus, anomeric atom-specific ¹³C-labeling efforts resulted in a partial isotopic loss that could not be overcome by altering the amounts of ¹³C-labeled glucose added to the minimal medium. Nevertheless, this is still significant enough to conduct NMR experiments to obtain critical structural information about glycosidic linkages which would not otherwise be possible with the polysaccharide **1**. In addition to MS analysis, various NMR experiments were performed on these polysaccharides to obtain 1D ¹³C NMR (Fig. 3), 2D [¹³C–¹³C] COSY (Fig. 4), and [¹³C, ¹H] HSQC NMR spectra (Fig. 5). These NMR spectra confirmed the identity and the isotopic purity of differentially isotope-enriched *N*-sulfoheparosan polysaccharides **2** and **3**. Our ¹³C and ¹H chemical shift assignments are in good agreement with those previously reported in the literature (Table 1) considering the variations in NMR experimental conditions. Using intra-residue ¹³C-spin connectivities from 2D [¹³C–¹³C] COSY experiments, we assigned the peaks by a standard sequential assignment procedure.

3. Concluding remarks

It is essential to elucidate both the primary sequence and the 3D conformation of HS structures of a biological origin to understand HS structure–function relationships. However, these structures are available only in a limited quantity, and this scarcity challenges our ability to characterize these complex molecules using traditional approaches. While MS analysis allows one to characterize oligosaccharide and disaccharide molecular weights, sulfation densities and sulfation patterns, NMR analysis aids the characterization of the intact heparanome at the polymer level in terms of conformation, microstructure, and dynamic solution properties. However, one of the major limitations of NMR spectroscopy is that its low sensitivity because of the low magnetogyric ratio and the low natural abundance of NMR-active isotopes, ¹³C (1.1%) and ¹⁵N (0.37%). Therefore, the production of HS chains enriched with various isotopes will provide further insights into their sequence through MS-based fragmentation approaches and conformational dynamics through multi-dimensional NMR spectroscopy. Thus, the isotopic

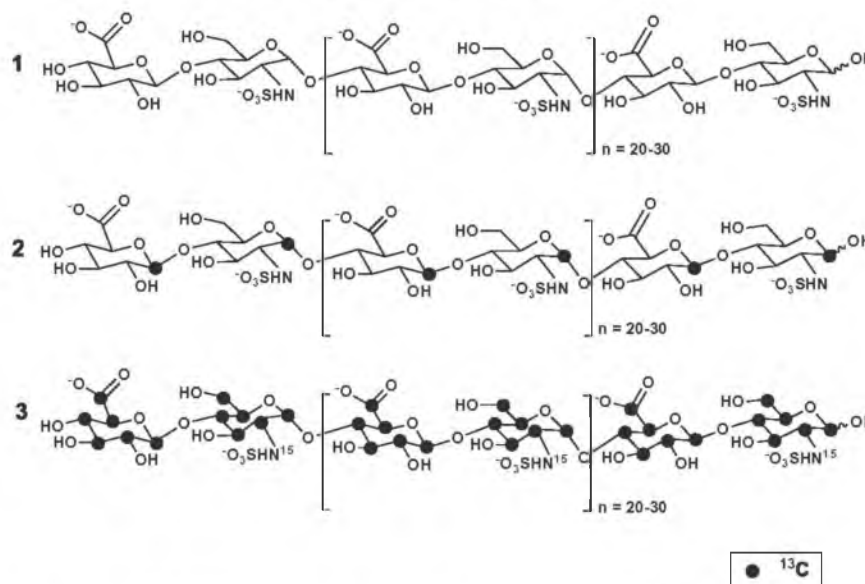


Figure 1. Structures of the HS precursor chains prepared without isotope enrichment (**1**) or with isotope enrichment (**2, 3**). The locations of ^{13}C -isotopes are indicated by filled dark circles.

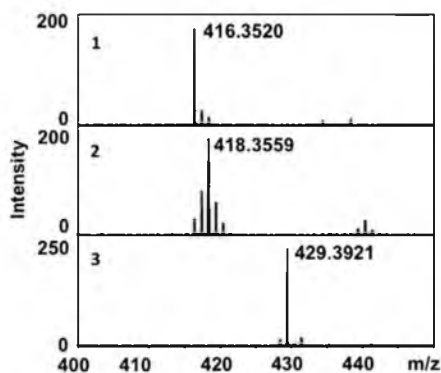


Figure 2. ESI-mass spectra of the disaccharides obtained from their corresponding heparan sulfate precursors with the natural isotope abundance **1** ($m/z = 416.35$), with atom-specific ^{13}C -labels at anomeric carbon **2** ($m/z = 418.36$) and with uniform ^{13}C and ^{15}N -labels **3** ($m/z = 429.39$).

enrichment techniques described herein for the production of HS chains along with the recent technological advances in NMR probe design, miniaturization of the separation techniques and softer MS ionization methods will overcome any remaining barriers in the structural analysis of HS in the coming decade. However, one note of caution is that the enzymatic approach does not have the capability to generate HS structures with discrete domain organizations as found in nature. Therefore, similar isotopic enrichment techniques need to be developed to prepare HS chains of a cellular or biological origin for structural biology studies.

In summary, uniform ^{13}C labeling facilitated the assignment of ^1H and ^{13}C chemical shifts using $[^{13}\text{C}\text{--}^{13}\text{C}]$ COSY and $[^{13}\text{C}\text{--}^1\text{H}]$ HSQC

spectra. However, it is important to note that the measurements of exact distance in HS chains with uniform ^{13}C labels will be significantly complicated because of the presence of several one-bond $^{13}\text{C}\text{--}^{13}\text{C}$ couplings between adjacent carbon atoms. Therefore, we also prepared atom-specific ^{13}C -labeled HS chains that can facilitate the measurement of long distance weak couplings in the presence of strong interactions. Nevertheless, armed with differentially, uniformly or atom-specifically labeled HS chains, we can deduce the structural parameters required for the binding of a given HS structure to a protein target at a much higher molecular resolution than what is currently possible.

4. Experimental

4.1. Materials

Solid pronase from *Streptomyces griseus* and mung bean nuclease was purchased from Sigma–Aldrich Chemical Co. (St. Louis, MO, USA). Heparitinase I from *Flavobacterium heparinum* was a generous gift from Professor Robert D. Rosenberg (BIDMC, Harvard Medical School). Sodium salts of unsaturated disaccharide standards, $\Delta\text{U-GlcNS}$ and $\Delta\text{U-GlcNAc}$ were obtained from Iduron Co. (Manchester, England, UK). $[1,2,3,4,5,6\text{--}^{13}\text{C}_6]\text{-D-glucose}$, $[1\text{--}^{13}\text{C}]\text{-D-glucose}$, $^{15}\text{NH}_4\text{Cl}$ and $(^{15}\text{NH}_4)_2\text{SO}_4$ were obtained from Sigma–Aldrich Chemical Co. Water was purified using a Milli-Q filtration apparatus (Millipore Co., Bedford, MA, USA). Fast-flow DEAE-Sepharose was obtained from GE Healthcare (Amersham, Uppsala, Sweden). All other chemicals, including MS grade and NMR solvents, were obtained from Sigma–Aldrich Chemical Co. and Cambridge Isotope Laboratories, Inc. (Andover, MA, USA), respectively. Polypropylene chromatographic columns (2.5×20 cm) were purchased from Bio-Rad Life Sciences (Hercules, CA, USA). NMR tubes were purchased from Sigma–Aldrich Chemical Co. The *E. coli* strain K5 [O10:K5 (L):H4] was obtained from ATCC.

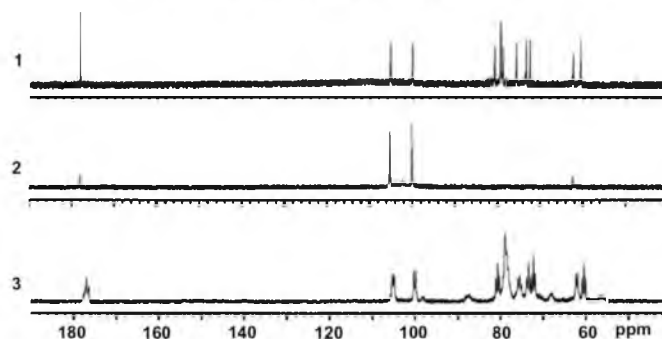


Figure 3. Comparative 1D [^{13}C] 100 MHz NMR spectra of the HS precursors with natural abundance (1) atom-specifically ^{13}C -labeled HS precursors at anomeric carbons (2) and uniformly ^{13}C - and ^{15}N -labeled HS precursors (3). All NMR spectra were acquired in D_2O at 25 °C. The values of ^1H chemical shifts are referenced to the external 4,4-dimethyl-4-silapentane-1-sulfonic acid (DSS) and ^{13}C using an indirect reference.

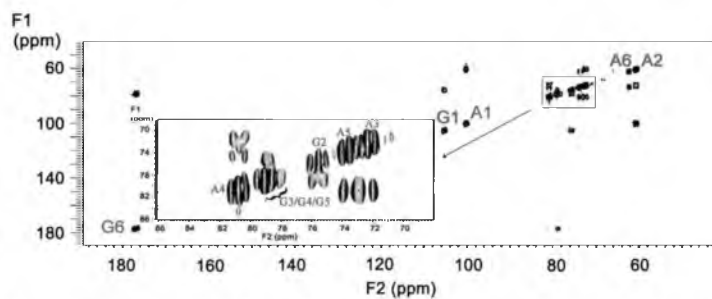


Figure 4. 2D [^{13}C - ^{13}C] COSY spectrum of the uniformly ^{13}C - and ^{15}N -labeled HS precursors. A represents glucosamine and G represents glucuronic acid.

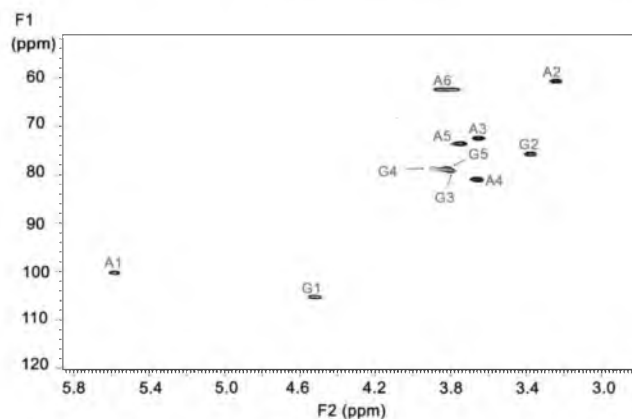


Figure 5. 2D [^{13}C - ^1H] HSQC spectrum of the uniformly ^{13}C - and ^{15}N -labeled HS precursors. A represents glucosamine and G represents glucuronic acid.

4.2. Isolation of differentially ^{13}C -labeled *N*-acetylheparosan

[1,2,3,4,5,6- ^{13}C , ^{15}N] *N*-Acetylheparosan was prepared from cultures of the *E. coli* K5 strain grown in a minimal media containing 4 g/L of [1,2,3,4,5,6- $^{13}\text{C}_6$]- α -glucose and 2 g/L ($^{15}\text{NH}_4$) $_2\text{SO}_4$

or $^{15}\text{NH}_4\text{Cl}$. The bacterial primary cultures were grown in 100 mL of LB broth for 24 h at 37 °C with shaking (250 rpm) and harvested by centrifuging at 5000 rpm for 30 min. The pellet from the 100-mL primary cultures was used to inoculate 1 L of minimal medium in a 3-L Erlenmeyer flask containing 4 g/L

Table 1
¹H and ¹³C chemical shifts of HS precursors in D₂O at 25 °C^a

Position ^b	¹ H Chemical shift (ppm)	¹³ C Chemical shift (ppm)
A1	5.58	100.30
A2	3.24	60.77
A3	3.65	72.48
A4	3.65	81.11
A5	3.75	73.61
A6	3.84/3.79	62.65
G1	4.52	105.33
G2	3.38	75.83
G3	3.80	79.96
G4	3.89	78.70
G5	3.82	79.06
G6	—	176.85

^a Chemical shifts are given in ppm, ¹H chemical shifts is measured indirectly with reference to DSS in D₂O at 25 °C. ¹³C is measured indirectly with reference to ¹H using a chemical shift ratio of 0.25144.

^b A represents glucosamine and G represents glucuronic acid. The numerical suffix corresponds to the carbon position starting with the anomeric carbon as 1.

[1,2,3,4,5,6-¹³C₆]-D-glucose as the principal carbon source and 2 g/L (¹⁵NH₄)₂SO₄ or ¹⁵NH₄Cl as the principal nitrogen source. The cultures were incubated at 37 °C for 48 h with shaking (250 rpm) and then autoclaved. The autoclaved medium was adjusted to pH 7.0 and treated with protease for 12 h at 37 °C with gentle shaking (50 rpm). The insoluble material was removed by centrifugation (5000 rpm, 30 min), and the resulting supernatant was diluted to two times the original volume with deionized water. The diluted supernatant was then loaded onto a 50-ml DEAE-Sepharose column, previously equilibrated with wash buffer (20 mM NaOAc, 100 mM NaCl, pH 6). The column was washed three times (10 column volumes/wash) with wash buffer. The heparosan polysaccharide was eluted with 6 column volumes of elution buffer (20 mM NaOAc, 0.6 M NaCl, pH 6). The eluate was adjusted to 1.0 M NaCl, and 4 volumes of 99% EtOH were added to precipitate the desired polysaccharide. After 24 h at 4 °C, the resulting [¹³C, ¹⁵N] *N*-acetylheparosan was recovered by centrifugation (5000 rpm, 30 min, 4 °C) and removal of the supernatant, and was finally allowed to air-dry overnight. The amount of purified heparosan obtained was determined using a carbazole assay for uronic acids with the aid of glucuronolactone as a standard. The assay was performed in triplicate. In a similar manner, the anomeric carbon-specific ¹³C-labeled polysaccharide was obtained from the *E. coli* K5 strain grown in the minimal medium containing 1 g/L [¹⁻¹³C]-D-glucose.

4.3. Preparation of *N*-sulfoheparosan

Regular *N*-acetylheparosan, anomeric atom-specifically ¹³C-labeled heparosan or uniformly ¹³C, ¹⁵N-labeled heparosan was dissolved in 2.5 M NaOH, stirred for 12 h at 55 °C, then cooled to ice-cold temperature and adjusted to pH 7. The fully *N*-deacetylated product was *N*-sulfonated with the Et₃N-SO₃ as described before^{13,14} and purified to obtain polysaccharides **1**, **2**, and **3** (Fig. 1).

4.4. NMR acquisition

1D [¹³C] and 2D [¹³C-¹³C] COSY spectra were recorded at 100 MHz on a Varian Mercury 400 MHz spectrometer. 2D [¹³C-¹H]

HSQC spectra were recorded at 125 MHz on a Varian Inova 500 MHz spectrometer (Varian, Palo Alto, USA). NMR measurements were performed at 25 °C for acquiring 1D [¹³C] spectra and 2D [¹³C-¹³C] COSY spectra whereas 2D [¹³C-¹H] HSQC spectra were acquired at 37 °C. Samples (~10 mg) were lyophilized from deuterium oxide (D₂O) and finally dissolved in 0.4 mL of D₂O (99.9% deuterium).

4.5. Isotopomer analysis of disaccharides using LC-ESI-TOFMS

MS analyses were performed on a Bruker ESI-TOFMS instrument. The samples containing disaccharides, obtained from the digestion of polysaccharides with heparitinase I, were processed and dissolved in 1:1 H₂O-CH₃CN containing 5 mM Bu₃NH₂OAc for the isotopomer analysis using mass spectrometry.¹⁵ Mass spectra were collected by the direct infusion of samples containing disaccharides at a flow rate of 5 μL/min. The electrospray interface was set in the negative-ionization mode with a collision energy of 7.0 eV, a capillary potential of 3500 V and a source temperature of 180 °C. Nitrogen was used as a drying gas (4 L/min) and nebulizer (0.4 bar). Mass spectra were processed using Data Analysis 2.2 software (Bruker Daltonics Inc., Billerica, MA).

Acknowledgments

This work was supported by the National Institutes of Health grant (GM075168), Mizutani Foundation for Glycoscience Award and American Heart Association National Scientist Development Award to B.K. We acknowledge the funding support from NIH, grant RR06262, for NMR instrumentation awarded to the University of Utah Health Sciences NMR Center. T.K.N.N. received a graduate fellowship from the Vietnam Education Foundation. We thank Karthik Raman for careful reading of the manuscript.

Reference

- Raman, K.; Kuberan, B. *Curr. Chem. Biol.* **2010**, *4*, 20–31.
- Cummings, R. D. *Mol. Biosyst.* **2009**, *5*, 1087–1104.
- Raguraman, A.; Mosier, P. D.; Desai, U. R. *J. Med. Chem.* **2006**, *49*, 3553–3562.
- Vann, W. F.; Schmidt, M. A.; Jann, B.; Jann, K. *Eur. J. Biochem.* **1981**, *116*, 359–364.
- Zhang, Z.; McCalkum, S. A.; Xie, J.; Nieto, L.; Corzana, F.; Jimenez-Barbero, J.; Chen, M.; Liu, J.; Linhardt, R. J. *J. Am. Chem. Soc.* **2008**, *130*, 12998–13007.
- Sigulinsky, C.; Babu, P.; Victor, X. V.; Kuberan, B. *Carbohydr. Res.* **2010**, *345*, 250–256.
- Mobli, M.; Nilsson, M.; Almond, A. *Glycoconjugate J.* **2008**, *25*, 401–414.
- Korir, A. K.; Larive, C. K. *Anal. Bioanal. Chem.* **2009**, *393*, 155–169.
- Kuberan, B.; Beeler, D. L.; Lawrence, R.; Lech, M.; Rosenberg, R. D. *J. Am. Chem. Soc.* **2003**, *125*, 12424–12425.
- Kuberan, B.; Beeler, D. L.; Lech, M.; Wu, Z. L.; Rosenberg, R. D. *J. Biol. Chem.* **2003**, *278*, 52613–52621.
- Kuberan, B.; Lech, M. Z.; Beeler, D. L.; Wu, Z. L.; Rosenberg, R. D. *Nat. Biotechnol.* **2003**, *21*, 1343–1346.
- Lindahl, U.; Li, J. P.; Kusche-Gullberg, M.; Salmivirta, M.; Alaranta, S.; Veromaa, T.; Emeis, J.; Roberts, I.; Taylor, C.; Oreste, P.; Zoppetti, G.; Naggi, A.; Torri, G.; Casu, B. *J. Med. Chem.* **2005**, *48*, 349–352.
- Yates, E. A.; Santini, F.; Guerrini, M.; Naggi, A.; Torri, G.; Casu, B. *Carbohydr. Res.* **1996**, *294*, 15–27.
- Casu, B.; Grazioli, G.; Razi, N.; Guerrini, M.; Naggi, A.; Torri, G.; Oreste, P.; Tursi, F.; Zoppetti, G.; Lindahl, U. *Carbohydr. Res.* **1994**, *263*, 271–284.
- Kuberan, B.; Lech, M.; Zhang, L.; Wu, Z. L.; Beeler, D. L.; Rosenberg, R. D. *J. Am. Chem. Soc.* **2002**, *124*, 8707–8718.

3.3 A synthetic heparan sulfate oligosaccharide library reveals the novel enzymatic action of D-glucosaminyl 3-O-sulfotransferase-3a

Manuscript reproduced with permission from:

Nguyen, T. K., Arungundram, S., Tran, V. M., Raman, K., Al-Mafraji, K., Venot, A., Boons, G. J., and Kuberan, B. (2012) A synthetic heparan sulfate oligosaccharide library reveals the novel enzymatic action of D-glucosaminyl 3-O-sulfotransferase-3a, *Mol Biosyst* 8, 609-614.

© 2012 The Royal Society of Chemistry

A synthetic heparan sulfate oligosaccharide library reveals the novel enzymatic action of D-glucosaminyl 3-O-sulfotransferase-3a†Thao Kim Nu Nguyen,^a Sailaja Arungundram,^b Vy My Tran,^a Karthik Raman,^a Kanar Al-Mafraji,^a Andre Venot,^b Geert-Jan Boons^b and Balagurunathan Kuberan^{*acd}

Received 3rd June 2011, Accepted 3rd November 2011

DOI: 10.1039/c1mb05221g

Heparan sulfate (HS) glucosaminyl 3-O-sulfotransferases sulfate the C3-hydroxyl group of certain glucosamine residues on heparan sulfate. Six different 3-OST isoforms exist, each of which can sulfate very distinct glucosamine residues within the HS chain. Among these isoforms, 3-OST1 has been shown to play a role in generating ATIII-binding HS anticoagulants whereas 3-OST2, 3-OST3, 3-OST4 and 3OST-6 have been shown to play a vital role in generating gD-binding HS chains that permit the entry of herpes simplex virus type 1 into cells. 3-OST5 has been found to generate both ATIII- and gD-binding HS motifs. Previous studies have examined the substrate specificities of all the 3-OST isoforms using HS polysaccharides. However, very few studies have examined the contribution of the epimer configuration of neighboring uronic acid residues next to the target site to 3-OST action. In this study, we utilized a well-defined synthetic oligosaccharide library to examine the substrate specificity of 3-OST3a and compared it to 3-OST1. We found that both 3-OST1 and 3-OST3a preferentially sulfate the 6-O-sulfated, N-sulfoglucosamine when an adjacent iduronyl residue is located to its reducing side. On the other hand, 2-O-sulfation of this uronyl residue can inhibit the action of 3-OST3a on the target residue. The results reveal novel substrate sites for the enzyme actions of 3-OST3a. It is also evident that both these enzymes have promiscuous and overlapping actions that are differentially regulated by iduronyl 2-O-sulfation.

Introduction

Heparan sulfate (HS) is a highly sulfated polysaccharide that is located on cell surfaces as well as in the extracellular matrix (ECM). The nascent HS chain consists of repeating units of N-acetyl glucosamine (GlcNAc) and glucuronic acid (GlcA). This backbone subsequently undergoes a series of modifications by various HS modifying enzymes located in the Golgi. GlcNAc residues can be N-deacetylated and N-sulfated by N-deacetylase-N-sulfotransferase (NDST). GlcA can be epimerized to iduronic acid (IdoA) by C5-epimerase. Additionally, a number of O-sulfotransferases (OST) can add sulfate groups

to the C6 (by 6-OST) and C3 (by 3-OST) carbons of glucosamine (GlcN) residues and to the C2 carbon (by 2-OST) of IdoA or GlcA residues.¹ These modifications create the enormous diversity that confers a wide array of biological functions. Among these modifications, 3-O-sulfation has been shown to play a vital role in creating HS chains that function as anticoagulants and as entry receptors for herpes simplex virus type 1 (HSV-1).^{2–5} It has also been shown that 3-O-sulfation has been associated with both cancer and embryonic development.^{6–9} Six different isoforms of 3-OST have been identified [3-OST1, 2, 3 (3a and 3b splice variants), 4, 5, and 6] and shown to generate distinct HS structures.^{10–18} 3-OST3a has a broad expression profile and is present in many different tissues including heart, placenta, lungs, liver and kidneys.¹¹ One of its pathological functions is to create binding sites for viral gD glycoprotein and initiate the entry of HSV-1 into cells.⁵ 3-OST1 is expressed in heart, brain, lungs and kidneys.¹¹ 3-OST1 has been shown to play a vital role in generating ATIII-binding HS anticoagulants.¹⁹ However, it has been also shown that mice deficient in 3-OST1 still have normal hemostasis.^{20,21} Therefore, it is important to carefully examine the contribution of other 3-OST isoforms to this crucial function of HS.

Though the substrate specificity of 3-OST1 has been rigorously studied, the substrate specificity of other isoforms including

^a Department of Bioengineering, University of Utah, Salt Lake City, Utah, USA 84112^b Complex Carbohydrate Research Center, University of Georgia, Athens, Georgia, USA 30603^c Department of Medicinal Chemistry, University of Utah, 30 S 2000 E, Skaggs Hall Room 307, Salt Lake City, Utah, USA 84112. E-mail: kuby@pharm.utah.edu; Fax: +1 801-585-9119; Tel: +1 801-587-9474^d Interdepartmental Program in Neuroscience, University of Utah, Salt Lake City, Utah, USA 84112

† Electronic supplementary information (ESI) available. See DOI: 10.1039/c1mb05221g

3-OST3a has not been examined extensively. The Rosenberg group has shown that 3-OST3a preferentially acts on GlcNH₂, GlcNH₂6S and GlcNS residues that have an IdoA2S residue at their non-reducing side.^{10,15,22} Furthermore, earlier studies reported the crystal structures of 3-OST 1, 3, 5, and identified two amino acid residues that are responsible for the specific activity of 3-OST3a on the IdoA2S-GlcNH₂/NS ± 6S.²³ However, it is still unknown whether the epimer configuration of the neighboring uronic acid residue, *i.e.* GlcA or IdoA, located at the reducing side of the target site, influences the action of 3-OST3a. This structural information could not be obtained previously because commonly used fragmentation approaches such as heparitinase digestion or nitrous acid treatment cleaved the chains at the reducing side of the target GlcN residue. In this study, we utilized a library of chemically synthesized, well-defined oligosaccharides to study the effect of precursor structures, in particular the influence of epimer configuration of adjacent uronyl residues, on the action of 3-OST3a. We found that 3-OST3a preferentially sulfates the GlcNS6S residue when an IdoA residue is located to its reducing side. On the other hand, 2-*O*-sulfation of this IdoA inhibits the action of 3-OST3a on the target residue.

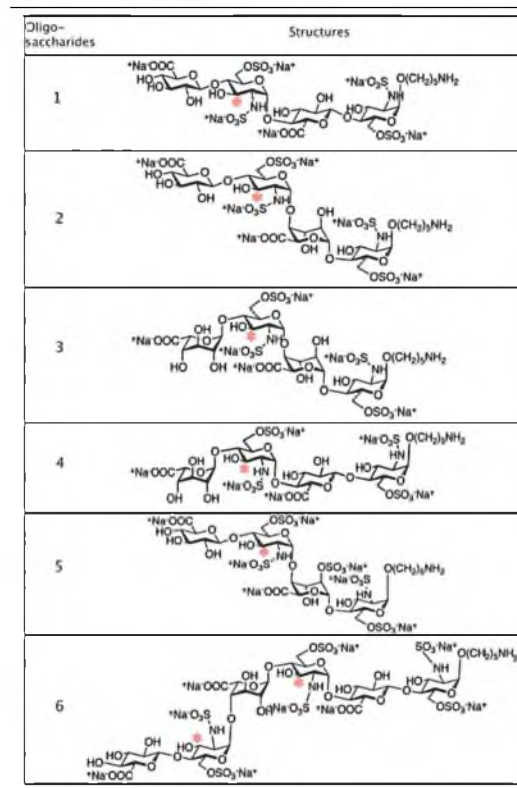
Results

It has previously been shown that 3-OST3a can sulfate GlcNH₂, GlcNH₂6S and GlcNS that are located to the reducing side of IdoA2S.^{10,15} However, all previous substrate specificity studies relied on the analysis of 3-*O*-sulfotransferase modified heparan sulfate polysaccharides that were fragmented using nitrous acid or heparitinases. The heterogeneity of heparan sulfate makes it difficult to thoroughly analyze all the modified products. Moreover, enzymatic digestion leads to a loss of epimer configuration and chemically-induced chain scission occasionally causes isomerisation, thus complicating the study of the effect of neighboring uronic acid residues located next to the target glucosamine residues. In this study, we utilized a library of well-defined tetra- and hexa-saccharides to study the effect of precursor structures on the enzymatic action of 3-OST3a (Table 1). We also compared the enzymatic action of 3-OST3a to that of 3-OST1. This library of oligosaccharides was previously synthesized and extensively studied by the Boons group.²⁴ By utilizing HPLC coupled to a radiometry detector and capillary LC coupled to electrospray ionization-time-of-flight MS (ESI-TOF-LC-MS), we could detect and distinguish all possible modified products.

Six different oligosaccharides containing GlcA or IdoA at different locations were chosen for this study (Table 1). The first four oligosaccharides are tetrasaccharides containing either a GlcA or IdoA adjacent to the expected modification site (marked with an asterisk, Table 1). The sequences of these tetrasaccharides are GlcA/IdoA-GlcNS6S-GlcA/IdoA-GlcNS6S. Oligosaccharide **5** contains a 2-*O*-sulfated iduronic acid residue in its sequence: GlcA-GlcNS6S-IdoA2S-GlcNS6S. Oligosaccharide **6** is a hexasaccharide with the following sequence: GlcA-GlcNS6S-IdoA-GlcNS6S-GlcA-GlcNS6S.

These six oligosaccharides were modified with either 3-OST3a or 3-OST1 in the presence of [³⁵S]PAPS as the sulfate donor. The 3-*O*-sulfated products could then be detected due

Table 1 Structures of oligosaccharides examined as potential substrates for 3-OST3a and 3-OST1. Potential 3-OST substrate sites are marked with asterisks



to the addition of radiolabeled sulfate (³⁵S]SO₄²⁻). HPLC analysis showed that only oligosaccharides **2**, **3** and **6** were radiolabeled by 3-OST3a (Fig. 1 and Fig. S1A, ESI†). Thus, it is clear that 3-OST3a can only act on three substrates: GlcA-GlcNS6S-IdoA-GlcNS6S (**2**), IdoA-GlcNS6S-IdoA-GlcNS6S²⁴ and GlcA-GlcNS6S-IdoA-GlcNS6S-GlcA-GlcNS6S (**6**). On the other hand, 3-OST1 modification was detected on oligosaccharides **1**, **2**, **3**, **5**, and **6** (Fig. 2 and Fig. S1B, ESI†). Thus, oligosaccharides **2**, **3** and **6** were modified by both isoforms whereas oligosaccharides **1** and **5** were exclusively modified by 3-OST1. Our finding that oligosaccharide **5** is the substrate for 3-OST1 but not for 3-OST3a is consistent with earlier findings that 3-OST1 modifies GlcNS6S residues that are flanked by GlcA at their non-reducing sides and IdoA2S residues at their reducing side.^{19,25} Furthermore, it is interesting to note that the reducing end GlcNS6S residue in oligosaccharide **5** is not modified by 3-OST3a even though it is located adjacent to IdoA2S. It has previously been observed that 3-OST1 modification preferentially occurs on the internal GlcNS residues whereas reducing end terminal GlcNS fails to undergo modification.²⁵ Liu *et al.* have shown that 3-OST1 can act on HS structures that lack IdoA residues.²⁶ This is consistent with our observation that oligosaccharide **1**, which lacks IdoA, is a substrate for 3-OST1. On the other hand, oligosaccharide **3** is also a substrate for

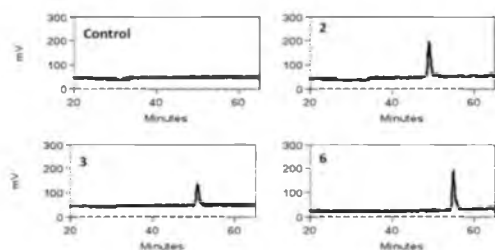


Fig. 1 Radiochromatograms of oligosaccharide products generated by modification with 3-OST3a and [35 S]PAPS. Radiochromatograms indicated that oligosaccharides **2**, **3** and **6** are substrates for 3-OST3a whereas other oligosaccharides are not substrates.

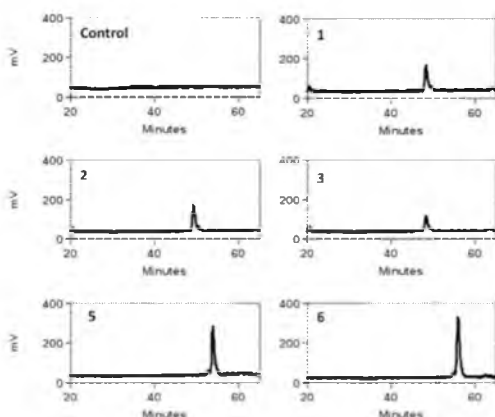


Fig. 2 Radiochromatograms of oligosaccharide products generated by modification of oligosaccharides **1**, **2**, **3**, **5**, and **6** by 3-OST1 and [35 S]PAPS.

3-OST1, albeit with much less [35 S] incorporation (Fig. S1, ESI †). This suggests that 3-OST1 prefers GlcNS6S residues that contain GlcA at the non-reducing side. It has been reported in several studies that 3OST1 and 3OST3a act on distinct sites within HS chains. Surprisingly, earlier studies have not found that 3-OST1 and 3-OST3 can act on the same oligosaccharide—as in the case of oligosaccharides **2**, **3**, and **6**. Based on these interesting observations, we next focused our efforts to locate the 3-OST3a modification site within these oligosaccharides. Oligosaccharides **2** and **3** have one potential modification site whereas oligosaccharide **6** has two potential modification sites. However, the radiolabeled results could not pinpoint which

GlcNS6S residues on the oligosaccharides were modified upon 3-*O*-sulfation by 3OST3a.

To determine which residue was modified, the oligosaccharides were treated with 3-OST3a again in the presence of non-radioactive [32 S]PAPS. The modified oligosaccharide products were then digested with heparitinase I, II and III to disaccharides and analyzed by LC-MS. Heparitinases catalyze the eliminative cleavage of heparin and heparan sulfate at the α (1,4)-glycosidic linkage between the glucosamine and the uronic acid.^{27,28} Since all oligosaccharides were terminated with the aminopentyl linker, cleavage with heparitinase created specific disaccharides species: a disaccharide containing no unsaturated bond, a disaccharide containing 4,5-unsaturated uronic acid (Δ UA), and a disaccharide containing both the aminopentyl linker and the 4,5-unsaturated uronic acid. For clarification, the potential modifications of oligosaccharide **2** and its disaccharides upon heparitinase digestion are presented in Fig. S2 (ESI †). Due to the mass differences among these cleavage products, we could distinguish all possible modified disaccharides from unmodified disaccharides and were able to pinpoint the 3-*O*-sulfation site (Table 2). MS data of 3-*O*-sulfated disaccharides revealed the precise location of 3-*O*-sulfation sites within the oligosaccharides **2**, **3** and **6** (Fig. 3). MS spectra of unmodified disaccharides as well as intact 3-*O*-sulfated oligosaccharide products are shown in Fig. S3 and S4 (ESI †). In the case of oligosaccharides **2** and **3**, one 3-*O*-sulfated disaccharide with $m/z = 593.96$ was found, indicating that 3-OST3a sulfated the penultimate GlcNS6S residue from the non-reducing end of the oligosaccharide (Fig. 3). For oligosaccharide **6**, two 3-*O*-sulfated disaccharides with $m/z = 593.96$ and 575.97 were found, indicating that 3-OST3a sulfated both the penultimate residue from the non-reducing end and the internal GlcNS6S residue. Since the only difference between these two disaccharides is the hydroxyl group at the C4 position of the uronic acid residue, we expect that the ionization to be similar or close to similar. The fact that the relative intensity of the peak with $m/z = 593.96$ is far higher than that of the peak with $m/z = 575.97$ suggests that the penultimate GlcNS6S residue is preferred over the internal GlcNS6S residue by 3-OST3a (Fig. 3). However, one may have to use isotope enriched disaccharides as internal standards to estimate quantitatively differential preference. It is interesting to note that the penultimate GlcNS6S residue has IdoA at its reducing side whereas the less preferred internal GlcNS6S residue, the third residue from the aminopentyl linker, has GlcA at its reducing side.

Current work demonstrates that 3-OST3a preferentially sulfates GlcA/IdoA-GlcNS6S-IdoA (Fig. 4) and that the presence of an IdoA residue at the reducing side of the target GlcNS6S promotes 3-OST3a activity. 3-OST3a could sulfate

Table 2 Potential 3-*O*-sulfated disaccharides resulting from 3-OST3a modified oligosaccharides with their expected mass

Oligosaccharide	Structure	Possible modified disaccharide product	Exact mass
2	GlcA-GlcNS6S-IdoA-GlcNS6S-(CH ₂) ₅ NH ₂	GlcA-GlcNS6S3S	594.98
		Δ UA-GlcNS6S3S-(CH ₂) ₅ NH ₂	662.06
3	IdoA-GlcNS6S-IdoA-GlcNS6S-(CH ₂) ₅ NH ₂	IdoA-GlcNS6S3S	594.98
		Δ UA-GlcNS6S3S-(CH ₂) ₅ NH ₂	662.06
6	GlcA-GlcNS6S-IdoA-GlcNS6S-GlcA-GlcNS6S-(CH ₂) ₅ NH ₂	GlcA-GlcNS6S3S	594.98
		Δ UA-GlcNS6S3S	576.97
		Δ UA-GlcNS6S3S-(CH ₂) ₅ NH ₂	662.06

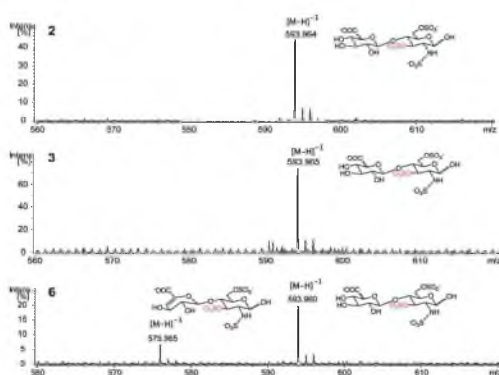


Fig. 3 MS spectra of 3-*O*-sulfated disaccharide products. The expected molecular weights of possible disaccharide products are presented in Table 2.

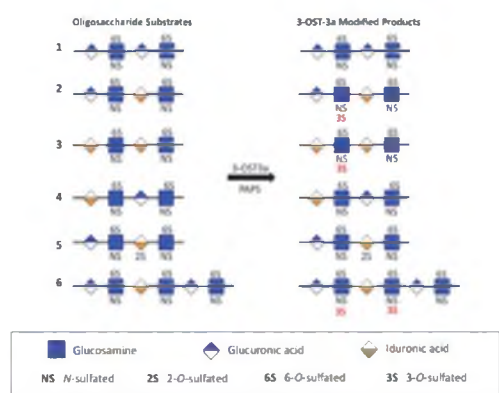


Fig. 4 List of oligosaccharides tested as substrates for 3-OST3a and their modified products.

the sequence, GlcA-GlcNS6S-IdoA, in the oligosaccharide **2**, but not the sequence, GlcA-GlcNS6S-IdoA2S, in the oligosaccharide **5**, which suggests that 2-*O*-sulfation of the IdoA, at the reducing side of the target site, is inhibitory for 3-OST3a. It is also interesting to note that 3-OST3a could sulfate IdoA-GlcNS6S-GlcA (**6**), albeit less preferentially, only if the target site was located downstream of a GlcA-GlcNS6S-IdoA sequence. It is possible that there could be a conformational change, after 3-OST3a sulfates the first glucosamine residue, in the oligosaccharide structure that may allow the enzyme to slide along the oligosaccharide sequence and continue to sulfate the next glucosamine residue on the reducing side in the oligosaccharide **6**.

Discussion

The substrate specificities of the 3OST isoforms have been extensively studied before. However, in these studies, heparitinase treatment resulted in the loss of stereochemical information of the proximal uronyl residues next to the target residue. Furthermore, the employment of a nitrous acid degradation technique in earlier

studies resulted in the removal of the uronyl residue at the reducing side of the target residue. Therefore, the influence of the epimer configuration of adjacent uronyl residues could not be elucidated until now. In addition, the heterogeneous nature of HS precursors used in those earlier studies exacerbated the difficulties involved in elucidating the influence of epimer configuration. Therefore, it is essential to use defined oligosaccharides to elucidate the substrate specificity of the 3-OST isoforms in order to lay a foundation for uncovering their physiological functions. In the present study, we systematically investigated the substrate specificity of 3-OST3a and compared its specificity to that of 3-OST1 using well-defined oligosaccharide precursors that had different epimer configurations.

In this study, we expressed and purified 3-OST3a and 3-OST1 recombinant enzymes using a baculovirus system. We then radiolabeled a library of synthetic oligosaccharides with these enzymes in the presence of [³⁵S]PAPS. The reaction mixture was then analyzed using HPLC. It was found that oligosaccharide structures with the following sequence were preferentially modified by 3-OST3a: GlcA/IdoA-GlcNS6S-IdoA and less preferentially IdoA-GlcNS6S-GlcA. It was also found that 3-OST3a failed to modify the oligosaccharides that consisted of the following sequences: GlcA-GlcNS6S-IdoA2S and GlcA-GlcNS6S-GlcA. These sequence requirements have not been reported previously.

After the identification of novel sequence requirements for 3-OST3a, we focused our efforts to compare the differential substrate preferences of 3-OST3a and 3-OST1. It is surprising to note that both 3-OST1 and 3-OST3a modified oligosaccharides **2**, **3** and **6**. Thus, both of these isoforms preferred an iduronyl residue at the reducing side of the target residue. Furthermore, oligosaccharide **4**, carrying IdoA-GlcNS6S-GlcA, was not a substrate for either of these isoforms. This suggests that the presence of GlcA at the reducing side of the target residue is unfavorable for 3-OST enzyme action. Nevertheless, oligosaccharide **1** was moderately modified by 3-OST1 but not by 3-OST3a. This suggests that there are subtle differences in the substrate specificity between these enzyme isoforms. It is also interesting that both oligosaccharides **2** and **5** were substrates for 3-OST1 whereas only the oligosaccharide **2** was the substrate for 3-OST3a. The only difference between these two oligosaccharides is the presence of the 2-*O*-sulfate group on the IdoA residue, located at the reducing side of the target residue. Additionally, even though oligosaccharide **4**, carrying IdoA-GlcNS6S-GlcA sequence, was not at all modified by 3-OST3a, the same sequence in oligosaccharide **6** was modified, albeit less efficiently. Based on the results presented here, we propose that both 3-OST1 and 3-OST3a have a significant overlap in their substrate specificity and that their activity is differentially regulated by 2-*O*-sulfation (Fig. 5).

In summary, the action of 3-OST1 and 3-OST3a on the HS substrates depends on the epimer configuration and the 2-*O*-sulfation. It is important to note that even though polymers are the substrates for HS biosynthetic enzymes *in vivo*, polymers cannot be helpful in elucidating the influence of adjacent uronic acid configuration. Therefore, oligomeric substrates are utilized instead in this study to be able to pinpoint the influence of epimer configuration on the action of 3-OST

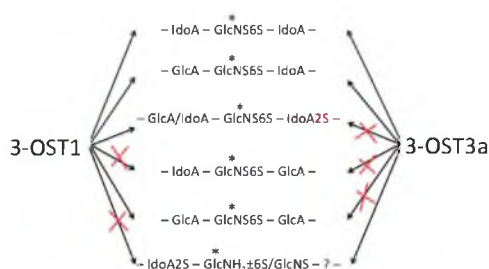


Fig. 5 Schematic model of the action of 3-OST1 and 3-OST3a at the target sites (*) representing the influence of neighbouring epimer configuration and 2-*O*-sulfate group.

enzymes. Future studies will focus on examining the substrate specificities of other 3OST isoforms and studying the influence of 6-*O*-sulfation with the aid of additional synthetic HS oligosaccharides.

Materials and methods

Materials

Oligosaccharides that were used in the current study were synthesized and characterized in an earlier report.²⁴ Heparitinase (Hep) I, II, and III were cloned and expressed in *E. coli* BL21. The DEAE-sepharose gel was purchased from Amersham Biosciences. The analytical strong-anion exchange column and capillary reverse phase C18 column were purchased from various commercial vendors. [³⁵S]Na₂SO₄ and Ultima-FloAP scintillation fluid were purchased from Perkin Elmer Life and Analytical Sciences. [³⁵S]PAPS was prepared as reported earlier.²⁹ [³²S]PAPS was purchased from Sigma-Aldrich. HS disaccharide standards were purchased from Iduron and Sigma-Aldrich. Insect cell Sf-900 SFM medium was purchased from Invitrogen. Dibutylamine was used as an ion-pairing agent in LC-MS analysis.³⁰ All other reagents and solvents were from Sigma-Aldrich unless otherwise stated.

Expression of 3-OST3a

The 3-OST3a recombinant enzyme was expressed using a baculovirus system. 20 ml of 3-OST3a viral stock was added to 1×10^9 Sf9 cells in 1 L Sf-900 SFM medium. Infected cells were shaken at 90 rpm in a humidified shaker-incubator maintained at 28 °C for 4 days. The cell suspension was then centrifuged at $1000 \times g$ for 30 min to pellet cells. PIPES and phenylmethylsulfonyl fluoride were added to the supernatant to a final concentration of 10 mM and 1 mM respectively. The supernatant was then adjusted to pH 7.0, chilled on ice for 30 min, and subsequently centrifuged at $4000 \times g$ for 30 min. The solution was diluted twice with water, filtered and loaded onto a 100-ml column of ToyoPearl AF-heparin 650M. The column was washed with 600 ml of PCG-50 (10 mM PIPES, pH 7.0, 1% glycerol, 0.2% CHAPS, 50 mM NaCl) and eluted with a 450 ml linear gradient of 50–1000 mM NaCl in PCG. The elution of the protein was monitored by measuring its absorbance at 280 nm. The protein containing fractions were pooled and concentrated using an Amicon YM-10 filter.

3-OST1 recombinant enzyme was also expressed and purified in a similar manner for comparative studies.

Enzymatic modification of synthetic oligosaccharide substrates

All reactions were performed in a buffer consisting of 25 mM MES (pH 7.0), 0.02% Triton X-100, 2.5 mM MgCl₂, 2.5 mM MnCl₂, 1.25 mM CaCl₂ and 0.75 mg ml⁻¹ BSA. 5 μg of an oligosaccharide was incubated with 10 μl 3-OST3a or 3-OST1 ($\sim 20 \mu\text{g ml}^{-1}$) in the presence of [³⁵S]PAPS (0.5×10^7 CPM) or [³²S]PAPS (10 μg) in a 50 μl reaction. The radioactive samples were then analyzed using analytical SAX-HPLC coupled with an in-line radiometry detector. The oligosaccharides were eluted with a linear gradient of 0 to 1 M NaCl in 70 mM phosphate buffer (pH 3.0) for 60 min. HS disaccharide standards were co-injected and detected at 232 nm. The non-radioactive samples were digested with Hep I, II and III, and analyzed using liquid chromatography mass spectrometry (LC-MS). Disaccharides were separated on a capillary C18 column (0.3 × 250 mm) using a linear gradient of acetonitrile at a flow rate of 5 μl min⁻¹ over 70 min. 5 mM dibutylamine was used as an ion-pairing agent. C18-HPLC was coupled to an electrospray ionization time-of-flight MS (Bruker Daltonics, USA) and analyzed in the negative ion mode under the following conditions: cone gas 50 l h⁻¹, nozzle temperature 130 °C, drying gas (N₂) flow 450 l h⁻¹, spray tip potential 2.3 kV, and nozzle potential 35 V.

This work was supported by National Institutes of Health grants (GM075168 and HL107152), Mizutani Foundation for Glycoscience Award, and American Heart Association National Scientist Development Award (0830360N) to BK. TN also acknowledges support from a graduate fellowship from the Vietnam Education Foundation.

Notes and references

- H. Habuchi, O. Habuchi and K. Kimata, *Glycoconjugate J.*, 2004, **21**, 47–52.
- L. H. Lam, J. E. Silbert and R. D. Rosenberg, *Biochem. Biophys. Res. Commun.*, 1976, **69**, 570–577.
- M. Hook, I. Bjork, J. Hopwood and U. Lindahl, *FEBS Lett.*, 1976, **66**, 90–93.
- U. Lindahl, G. Backstrom, L. Thunberg and I. G. Leder, *Proc. Natl. Acad. Sci. U. S. A.*, 1980, **77**, 6551–6555.
- D. Shukla, J. Liu, P. Blaiklock, N. W. Shworak, X. Bai, J. D. Esko, G. H. Cohen, R. J. Eisenberg, R. D. Rosenberg and P. G. Spear, *Cell*, 1999, **99**, 13–22.
- A. B. Cadwallader and H. J. Yost, *Dev. Dyn.*, 2006, **235**, 3423–3431.
- K. Kamimura, J. M. Rhodes, R. Ueda, M. McNeely, D. Shukla, K. Kimata, P. G. Spear, N. W. Shworak and H. Nakato, *J. Cell Biol.*, 2004, **166**, 1069–1079.
- C. Bui, M. Ouzzine, I. Talhaoui, S. Sharp, K. Prydz, M. W. Coughtrie and S. Fournel-Gigleux, *FASEB J.*, 2010, **24**, 436–450.
- K. Miyamoto, K. Asada, T. Fukutomi, E. Okochi, Y. Yagi, T. Hasegawa, T. Asahara, T. Sugimura and T. Ushijima, *Oncogene*, 2003, **22**, 274–280.
- J. Liu, Z. Shriver, P. Blaiklock, K. Yoshida, R. Sasisekharan and R. D. Rosenberg, *J. Biol. Chem.*, 1999, **274**, 38155–38162.
- N. W. Shworak, J. Liu, L. M. Petros, L. Zhang, M. Kobayashi, N. G. Copeland, N. A. Jenkins and R. D. Rosenberg, *J. Biol. Chem.*, 1999, **274**, 5170–5184.
- A. F. Moon, S. C. Edavettal, J. M. Krahn, E. M. Munoz, M. Negishi, R. J. Linhardt, J. Liu and L. C. Pedersen, *J. Biol. Chem.*, 2004, **279**, 45185–45193.
- J. Chen and J. Liu, *Biochim. Biophys. Acta*, 2005, **1725**, 190–200.

- 14 N. Razi and U. Lindahl, *J. Biol. Chem.*, 1995, **270**, 11267–11275.
- 15 J. Liu, N. W. Shworak, P. Sinay, J. J. Schwartz, L. Zhang, L. M. Fritze and R. D. Rosenberg, *J. Biol. Chem.*, 1999, **274**, 5185–5192.
- 16 R. Lawrence, T. Yabe, S. Hajmohammadi, J. Rhodes, M. McNeely, J. Liu, E. D. Lamperti, P. A. Toselli, M. Lech, P. G. Spear, R. D. Rosenberg and N. W. Shworak, *Matrix Biol.*, 2007, **26**, 442–455.
- 17 R. Lawrence, B. Kuberan, M. Lech, D. L. Beeler and R. D. Rosenberg, *Glycobiology*, 2004, **14**, 467–479.
- 18 H. Mochizuki, K. Yoshida, M. Gotoh, S. Sugioka, N. Kikuchi, Y. D. Kwon, A. Tawada, K. Maeyama, N. Inaba, T. Hiruma, K. Kimata and H. Narimatsu, *J. Biol. Chem.*, 2003, **278**, 26780–26787.
- 19 J. Liu, N. W. Shworak, L. M. Fritze, J. M. Edelberg and R. D. Rosenberg, *J. Biol. Chem.*, 1996, **271**, 27072–27082.
- 20 N. W. Shworak, S. Hajmohammadi, A. I. de Agostini and R. D. Rosenberg, *Glycoconjugate J.*, 2002, **19**, 355–361.
- 21 S. Hajmohammadi, K. Enyoji, M. Princivalle, P. Christi, M. Lech, D. Beeler, H. Rayburn, J. J. Schwartz, S. Barzegar, A. I. de Agostini, M. J. Post, R. D. Rosenberg and N. W. Shworak, *J. Clin. Invest.*, 2003, **111**, 989–999.
- 22 Z. L. Wu, M. Lech, D. L. Beeler and R. D. Rosenberg, *J. Biol. Chem.*, 2004, **279**, 1861–1866.
- 23 D. Xu, A. F. Moon, D. Song, L. C. Pedersen and J. Liu, *Nat. Chem. Biol.*, 2008, **4**, 200–202.
- 24 S. Arungundram, K. Al-Mafraji, J. Asong, F. E. Leach, 3rd, I. J. Amster, A. Venot, J. E. Turnbull and G. J. Boons, *J. Am. Chem. Soc.*, 2009, **131**, 17394–17405.
- 25 B. Kuberan, M. Z. Lech, D. L. Beeler, Z. L. Wu and R. D. Rosenberg, *Nat. Biotechnol.*, 2003, **21**, 1343–1346.
- 26 J. Chen, C. L. Jones and J. Liu, *Chem. Biol.*, 2007, **14**, 986–993.
- 27 E. D. Korn and A. N. Payza, *J. Biol. Chem.*, 1956, **223**, 859–864.
- 28 A. Linker and P. Hovingh, *J. Biol. Chem.*, 1965, **240**, 3724–3728.
- 29 E. B. Lansdon, A. J. Fisher and I. H. Segel, *Biochemistry*, 2004, **43**, 4356–4365.
- 30 B. Kuberan, M. Lech, L. Zhang, Z. L. Wu, D. L. Beeler and R. D. Rosenberg, *J. Am. Chem. Soc.*, 2002, **124**, 8707–8718.

Supplementary Information

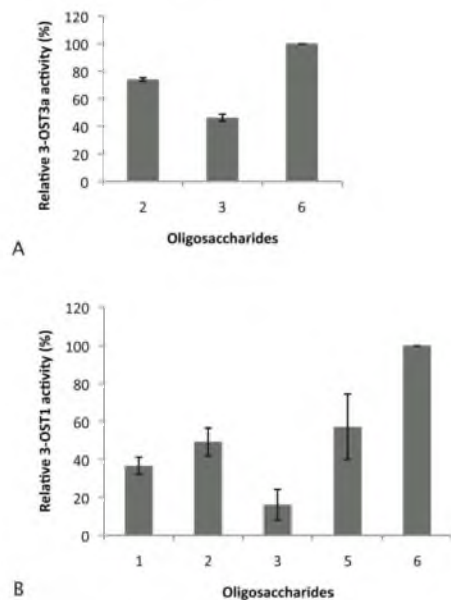


Figure S1. Relative activity of 3-OST1 (**A**) and 3-OST3a (**B**) on synthetic oligosaccharides. The values presented are calculated from the AUC of 3-*O*-sulfated oligosaccharide product peaks that are shown in Figures 1 and 2. Data has been normalized to the AUC for oligosaccharide **6**. The error bar indicates the standard error of the mean (SEM) from three independent experiments.

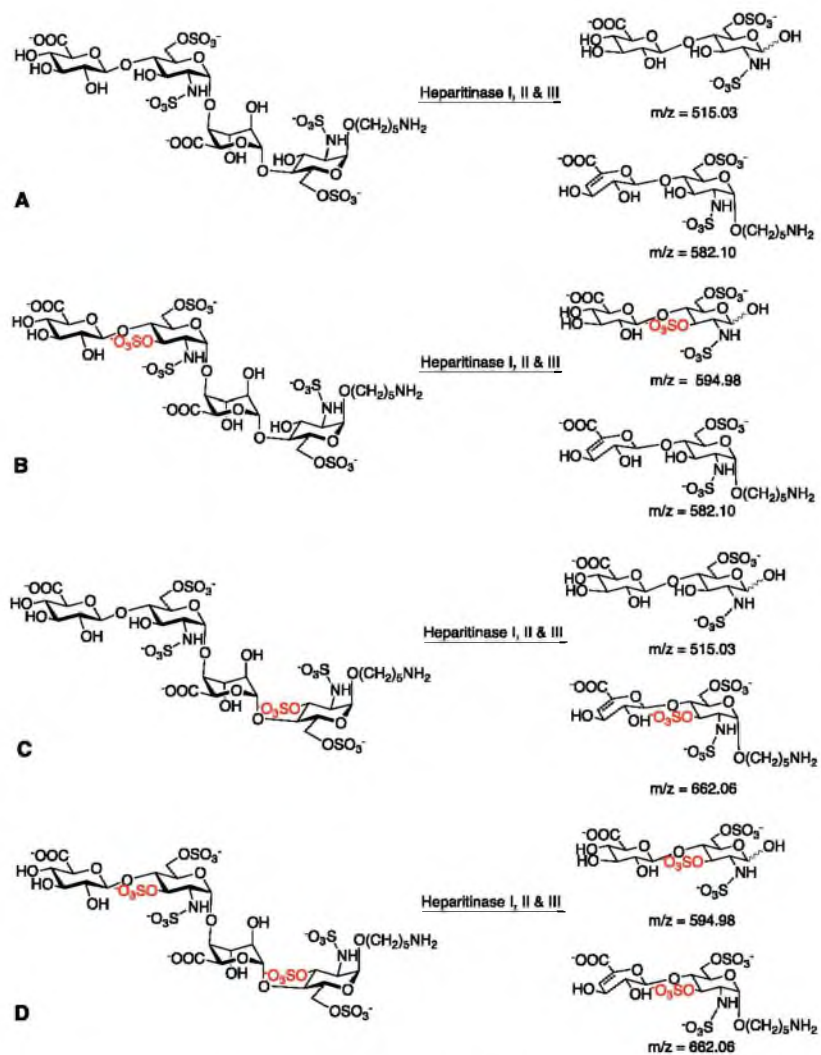


Figure S2. Theoretical 3-OST3a modification sites on oligosaccharide 2 and their respective disaccharide products upon digestion with heparitinase I, II & III. **A.** No 3-*O*-sulfate groups are added to the oligosaccharide. **B.** One 3-*O*-sulfate group is added to the first GlcNS6S residue. **C.** One 3-*O*-sulfate group is added to the second GlcNS6S residue. **D.** 3-*O*-sulfate groups are added to both GlcNS6S residues.

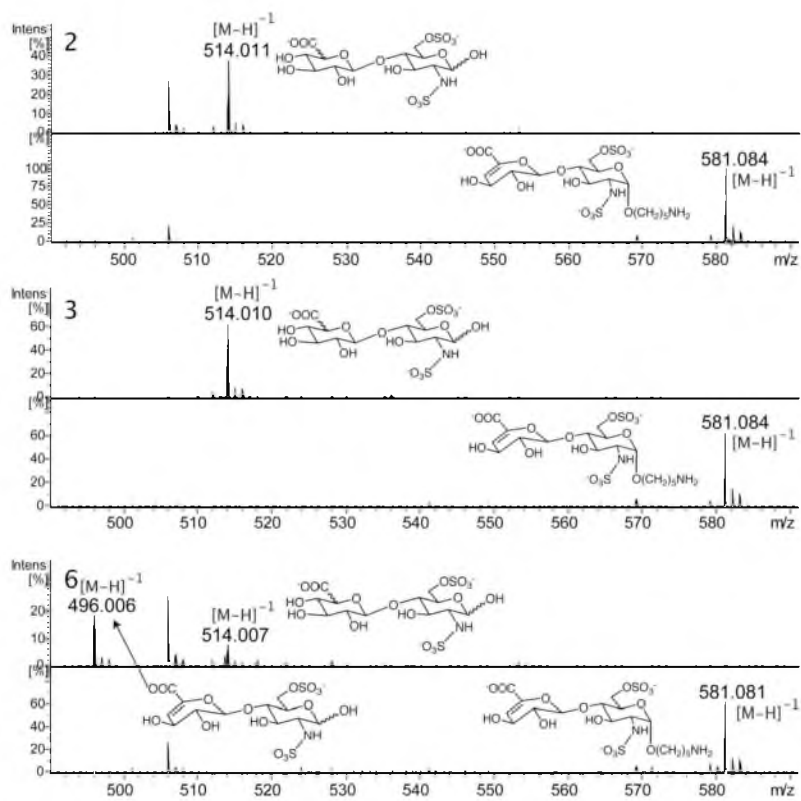


Figure S3. MS spectra of non-3-O-sulfated disaccharide products of oligosaccharides **2**, **3**, and **6**.

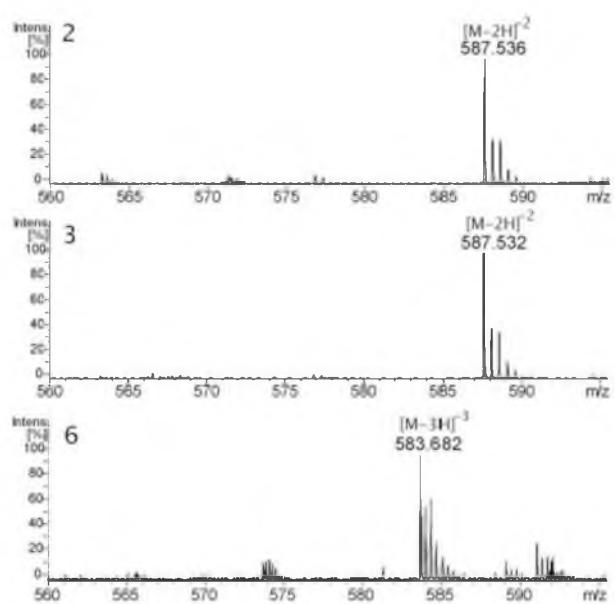


Figure S4. MS spectra of intact 3-O-sulfated oligosaccharide products derived from oligosaccharide substrates **2**, **3** and **6**.

3.4 Investigating the mechanism of the assembly of FGF1-binding
heparan sulfate motifs

Manuscript reproduced with permission from:

Nguyen, T. K., Raman, K., Tran, V. M., and Kuberan, B. (2011) Investigating the mechanism of the assembly of FGF1-binding heparan sulfate motifs, *FEBS Lett* 585, 2698-2702.

© 2011 Federation of European Biochemical Societies. Published by Elsevier B.V.



FEBS
Letters

journal homepage: www.FEBSLetters.org



Investigating the mechanism of the assembly of FGF1-binding heparan sulfate motifs

Thao Kim Nu Nguyen^a, Karthik Raman^a, Vy My Tran^a, Balagurunathan Kuberan^{a,b,c,*}

^a Department of Bioengineering, University of Utah, Salt Lake City, UT 84112, USA

^b Department of Medicinal Chemistry, University of Utah, Salt Lake City, UT 84112, USA

^c Interdepartmental Program in Neuroscience, University of Utah, Salt Lake City, UT 84112, USA

ARTICLE INFO

Article history:

Received 17 June 2011

Revised 19 July 2011

Accepted 20 July 2011

Available online 26 July 2011

Edited by Wilhelm Just

Keywords:

Heparan sulfate

FGF

GAGOSOMES

Biosynthesis

Sulfotransferase

Enzymatic modification

Proteoglycan

Signaling

ABSTRACT

Heparan sulfate (HS) chains play crucial biological roles by binding to various signaling molecules including fibroblast growth factors (FGFs). Distinct sulfation patterns of HS chains are required for their binding to FGFs/FGF receptors (FGFRs). These sulfation patterns are putatively regulated by biosynthetic enzyme complexes, called GAGOSOMES, in the Golgi. While the structural requirements of HS-FGF interactions have been described previously, it is still unclear how the FGF-binding motif is assembled in vivo. In this study, we generated HS structures using biosynthetic enzymes in a sequential or concurrent manner to elucidate the potential mechanism by which the FGF1-binding HS motif is assembled. Our results indicate that the HS chains form ternary complexes with FGF1/FGFR when enzymes carry out modifications in a specific manner.

© 2011 Federation of European Biochemical Societies. Published by Elsevier B.V. All rights reserved.

1. Introduction

Heparan sulfate (HS) is a linear, sulfated polysaccharide that consists of repeating units of glucosamine (GlcN) and glucuronic acid (GlcA) or iduronic acid (IdoA). As the nascent HS undergoes elongation, a series of modifications occurs on the backbone. N-acetyl glucosamine (GlcNAc) residues are N-deacetylated and N-sulfated by N-deacetylase-N-sulfotransferase (NDST), whereas GlcA residues are epimerized to IdoA by C5-epimerase. Additionally, a variety of O-sulfotransferases (OST) can add sulfate groups to the C6 (6-OST) and C3 (3-OST) carbons of GlcN residues and the C2 carbon (2-OST) of IdoA residues. It is also possible for 2-OST to add sulfate groups, albeit less preferentially, to the C2 carbon of GlcA residues [1]. To further augment this structural diversity, HS has a domain-like architecture composed of highly sulfated domains (NS domains), non-sulfated domains (NA domains), and partially sulfated domains (NA/NS domains). This immense structural complexity is believed to regulate the interac-

tions of HS with several protein targets including growth factors and cytokines [2].

One of the most commonly studied HS–protein interactions is that of HS and FGF. The FGF family plays a major role in several fundamental biological processes including cell proliferation, cell differentiation and cell migration [3,4]. Twenty two different FGFs and four FGFR genes have been discovered in humans [4]. FGF1 (acidic FGF) and FGF2 (basic FGF) were the first FGFs isolated [5,6]. FGF1 is able to bind to all FGFRs while FGF2 can only bind to FGFR1b, 1c, 2c, 3c and 4 [7]. HS potentiates FGF signaling by acting as a co-receptor and facilitates the formation of biologically relevant HS/FGF/FGFR ternary complexes. It facilitates the dimerization of FGFRs and thereby regulates downstream signaling pathways [8–10].

There have been many studies that have investigated the structural requirements of HS–FGF interactions. It has been shown that the minimal HS sequence that can bind to FGF2 requires 2-O-sulfated IdoA and N-sulfated GlcN residues [11–13]. Highly sulfated non-reducing end HS oligosaccharides were also found to bind FGF-2 with a high affinity [14]. Similarly, short, highly sulfated, HS chains isolated from porcine liver and intestine could induce FGF-2 mediated signaling efficiently [15]. However, while the structure of the FGF binding motif has been discovered previously,

* Corresponding author at: University of Utah, 30 S 2000 E, Skaggs Hall Room 307, Salt Lake City, UT 84112, USA. Fax: +1 801 585 9119.

E-mail address: KUBY@pharm.utah.edu (B. Kuberan).

it is still unclear how such specific binding motifs arise within the intact HS chain. One proposed model points to the existence of GAGOSOMES – macromolecular enzyme complexes that reside within the Golgi where HS biosynthetic enzymes act on nascent HS chains to generate growth factor binding motifs [16,17]. However, it is unclear as to how these enzymes modify a growing HS chain. Do all the enzymes in a GAGOSOME act concurrently or sequentially on a growing HS chain to generate biologically active structures?

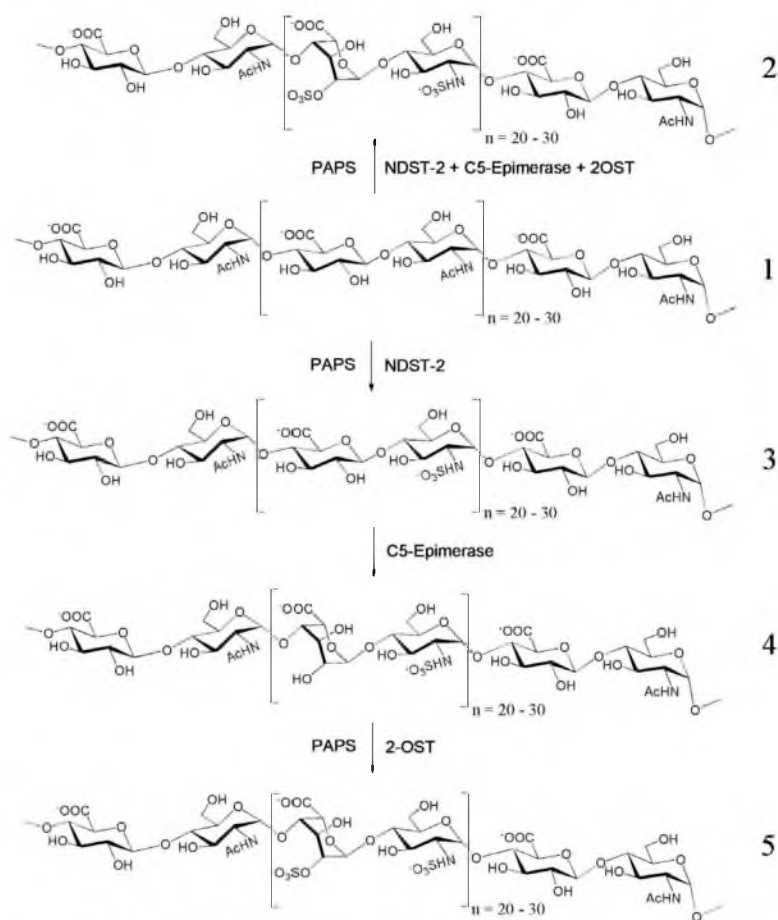
In this study, we aim to elucidate the natural action of HS biosynthetic enzymes by utilizing HS/FGF/FGFR interactions as a tool. To do this, we prepared N-sulfated, epimerized and 2-O-sulfated HS structures by conducting enzymatic modifications concurrently or sequentially. The resulting HS structures were examined in a gel mobility shift assay to determine their ability to form ternary complexes with FGF1 and FGFR1 or FGFR2. The results of this study outline a snapshot of the series

of biosynthetic events that may take place in GAGOSOMES to generate diverse HS structures.

2. Materials and methods

2.1. Materials

Recombinant HS biosynthetic enzymes, NDST-2, C5-epimerase and 2-OST, were expressed using a baculovirus system and purified as previously described [18]. Heparitinase I, II, and III were cloned and expressed as previously described. Completely desulfated, N-sulfated heparin **6** (CDSNS) was prepared as previously described [19]. The heparosan polysaccharide **1** was prepared from *Escherichia coli* K5 strain as reported previously [20]. The DEAE-sepharose gel was purchased from Amersham Biosciences. The SAX column (250 × 4.6 mm, 5 μm particle size) was purchased from Phenomenex Inc. [³⁵S]Na₂SO₄ and Ultima-FloAP were



Scheme 1. Concurrent and sequential action of HS biosynthetic enzymes NDST, C5-epimerase and 2-OST.

purchased from Perkin Elmer Life and Analytical Sciences. [^{35}S]PAPS was prepared as reported earlier [21]. [^{32}S]PAPS was purchased from Sigma–Aldrich. HS disaccharide standards were purchased from Iduron and Sigma–Aldrich. Human FGF1, FGFR1 α (IIIc) and FGFR2 α (IIIc) were purchased from R&D Systems. All other reagents and solvents were obtained from Sigma–Aldrich.

2.2. Preparation of N-sulfated, epimerized and 2-O-sulfated HS polysaccharides

All reactions were performed in a buffer consisting of 25 mM MES (pH 7.0), 0.02% Triton X-100, 2.5 mM MgCl_2 , 2.5 mM MnCl_2 , 1.25 mM CaCl_2 and 0.75 mg/ml BSA [22]. In the concurrent reaction, 20 μg of heparosan 1 was incubated with 10 μl each of NDST-2, C5-epi and 2-OST ($\sim 20 \mu\text{g/ml}$), and with 5 μl of [^{35}S]PAPS ($1 \times 10^7 \text{CPM}$)/100 μg of [^{32}S]PAPS in a 200 μl reaction. The reaction was incubated for 24 h at 37 $^\circ\text{C}$. The reaction was terminated by heating for 2 min at 96 $^\circ\text{C}$. The samples were diluted with one volume of 0.016% Triton X-100 and loaded onto a mini DEAE-sepharose column (0.3 ml) that had been pre-equilibrated with 2 ml of wash buffer (20 mM NaOAc, 0.1 M NaCl and 0.01% Triton X-100, pH 6.0). After washing with 9 ml of wash buffer, the bound polysaccharide was eluted with 1.8 ml of elution buffer (20 mM NaOAc, 1 M NaCl, pH 6.0). The eluate was then desalted and concentrated to 100 μl final volume. In the sequential reaction, 20 μg of heparosan 1 was first incubated with NDST-2 and [^{32}S]PAPS. The sample was purified, desalted, concentrated and used as the substrate for the next reaction with C5-epimerase. Finally, the resulting product was 2-O-sulfated by 2-OST in the presence of [^{35}S]PAPS/[^{32}S]PAPS. CDSNS polysaccharide 6 was 2-O-sulfated by 2-OST in the presence of [^{35}S]PAPS or [^{32}S]PAPS and the resulting product 7 was used as a control in the gel mobility shift assay.

2.3. Disaccharide analysis of the polysaccharides

Radioactive samples were digested with heparitinase I, II, and III overnight at 37 $^\circ\text{C}$ and analyzed using strong anion-exchange (SAX)-HPLC coupled with an in-line radiometry/UV detector. The disaccharides were eluted with a linear gradient of 0–800 mM NaCl (pH 3.5) for 35 min and 2 M NaCl (pH 3.5) for 10 min. HS disaccharide standards were co-injected and detected at 232 nm. Non-radioactive samples were analyzed using liquid chromatography–mass spectrometry (LC–MS). Disaccharides were separated on a C18 column (0.3 \times 250 mm, Vydac, USA) using a gradient from 0% to 100% of acetonitrile at a flow rate of 5 $\mu\text{l}/\text{min}$ over 70 min.

5 mM dibutylamine was used as an ion-pairing agent. Capillary HPLC coupled to an electrospray ionization time-of-flight MS (Bruker Daltonics, USA) was used in the negative ion mode at the following conditions: cone gas 50 l/h, nozzle temperature 130 $^\circ\text{C}$, drying gas (N_2) flow 450 l/h, spray tip potential 2.3 kV, and nozzle potential 35 V.

2.4. Gel mobility shift assay

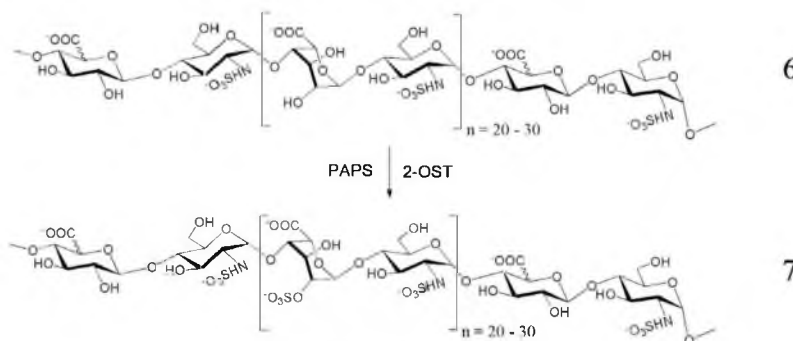
Enzymatically modified polysaccharide (1 μg), FGF (250 ng), and FCFR (500 ng) were mixed in 20 μl of binding buffer (137 mM NaCl, 2.7 mM KCl, 4.3 mM Na_2HPO_4 , 10 mM MgCl_2 , 1.4 mM KH_2PO_4 and 12% glycerol) and incubated at 23 $^\circ\text{C}$ for 30 min to facilitate complex formation [22]. The entire mixture was loaded onto a native 4.5% polyacrylamide gel (20 \times 25 cm). The gel was subjected to electrophoresis at 100 V for 6 h at 4 $^\circ\text{C}$. The gel was then dried, exposed to a phosphor screen overnight and imaged by a Typhoon PhosphorImager system.

3. Results

The primary objective of the current study is to elucidate how the FGF binding motif is generated in the Golgi. In order to determine whether the different modifications present in the FCF binding motif are created by enzymatic modifications that may occur sequentially or concurrently, three different polysaccharides products were prepared in a sequential or concurrent approach as outlined in the Schemes 1 and 2 using biosynthetic enzymes:

- (1) Polysaccharide 2: Heparosan 1 was treated with NDST-2, C5-Epimerase and 2-OST all together.
- (2) Polysaccharide 5: Heparosan 1 was first treated with NDST-2, then C5-epimerase and followed finally by 2-OST.
- (3) Polysaccharide 7: Completely desulfated, N-sulfated (CDSNS) heparin 6 was treated with 2-OST in the presence of [^{35}S]PAPS to produce the polysaccharide 7 for use in the control experiment.

Polysaccharides 2, 5 and 7 were characterized by SAX-HPLC (Fig. 1) by comparing their disaccharide compositions with the aid of co-injected disaccharide standards. While polysaccharide 2 had two radiolabeled disaccharides, $\Delta\text{UA-GlcNS}$ and $\Delta\text{UA2S-GlcNS}$, polysaccharide 5 had only one radiolabeled $\Delta\text{UA2S-GlcNS}$ disaccharide because it was N-sulfated using non-radioactive [^{32}S]PAPS. Similarly, polysaccharide 7 only contained the radioactive $\Delta\text{UA2S-GlcNS}$ disaccharide.



Scheme 2. Enzymatic 2-O-sulfation of CDSNS-heparin polysaccharide.

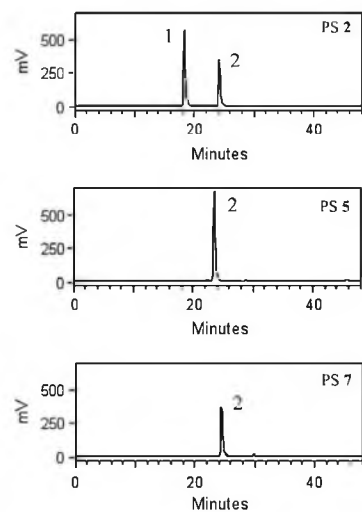


Fig. 1. Disaccharide analysis of concurrently modified polysaccharide 2, sequentially modified polysaccharide 5 and positive control polysaccharide 7. The disaccharide peaks were determined with the aid of co-injected disaccharide standards: (1) Δ UA-GlcNS, (2) Δ UA2S-GlcNS.

Sequential and concurrent modifications were carried out in the presence of [32 S]PAPS so that we could utilize LC-MS analysis to estimate the non-sulfated disaccharide content (Fig. 2). MS data suggested that the amount of Δ UA2S-GlcNS disaccharide was significantly higher in both the sequentially modified polysaccharide 5 and the positive control polysaccharide 7 in comparison to the concurrently modified polysaccharide 2.

Once the polysaccharides were characterized, they were tested in a gel mobility shift assay to determine whether they could form the ternary complex with FGF1 and FGFR1 or FGFR2 (Fig. 3). A shift in the mobility of the radiolabeled-polysaccharide indicates the

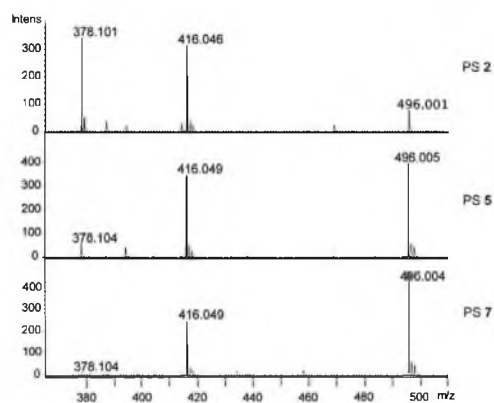


Fig. 2. MS spectra of disaccharides from concurrently modified polysaccharide 2, sequentially modified polysaccharide 5 and positive control polysaccharide 7. The following disaccharides were detected: Δ UA-GlcNAc (m/z 378.1), Δ UA-GlcNS (m/z 416.0) and Δ UA2S-GlcNS (m/z 496.0).

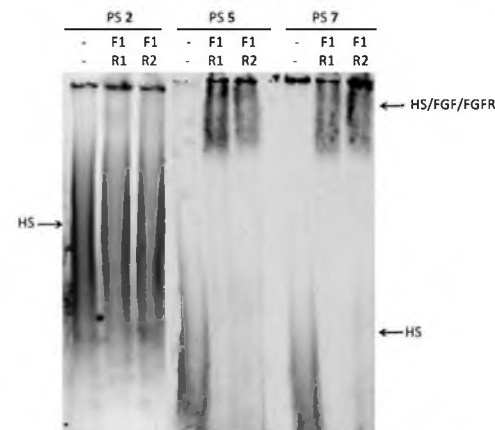


Fig. 3. Gel mobility shift assay to test the formation of the HS/FGF/FGFR ternary complex. Polysaccharide 2, 5 and 7 were used in combinations with FGF1 (F1) and FGFR1 (R1) or FGF1 and FGFR2 (R2). A shift in the mobility of radio-labeled polysaccharides indicates ternary complex formation. Only polysaccharides 5 and 7 could form the ternary complex with FGF1/FGFR1 and FGF1/FGFR2.

formation of the ternary complex. Based on the data shown in Fig. 3, only polysaccharides 5 and 7 could form the ternary complex significantly with FGF1/FGFR1 and FGF1/FGFR2.

4. Discussion

The FGF family members play a major role in various biological processes including organogenesis, wound healing, and nervous system development and function [4]. Disrupted FGF signaling is also present in a variety of human pathologies including Crouzon's syndrome, Pfeiffer's syndrome, and Apert's syndrome [3]. It is well known that heparan sulfate acts as a co-receptor for FGF/FGFR mediated cell signaling [8–10]. Various studies have reported that both specific sulfation patterns and the extent of sulfation of HS are key parameters that determine the formation of the HS/FGF/FGFR ternary complex [11–13,15]. However, it is still unclear how the FGF binding motif on HS is assembled in the Golgi. Therefore, this work aims to elucidate whether the FGF binding motif is assembled by enzyme actions that occur sequentially or concurrently.

In this investigation, three different enzymatically synthesized polysaccharides were utilized for binding studies with FGF1 and FGFRs. The obtained data confirmed that NDST-2, C5-epimerase and 2-OST can act on heparosan concurrently. When acting concurrently, these enzymes did not generate a significant amount of the disulfated Δ UA2S-GlcNS disaccharide. However, when the enzymes were added sequentially, this disaccharide was abundant in the modified product.

After the structural characterization of the synthesized products, a gel mobility shift assay was performed with FGF1 and FGFR1 or FGFR2 to determine which polysaccharides could form the ternary complex. Surprisingly, only polysaccharides 5 and 7 could form the ternary complex with FGF1/FGFR1 and FGF1/FGFR2. While it is possible that polysaccharide 2 may form a few weak complexes that are intangible in this gel mobility shift assay, it is evident that polysaccharide 5 has significantly higher binding affinity compared to polysaccharide 2 resulting in tangible complexes under the electrophoretic conditions. Differential binding ability of these polysaccharides with FGF/FGFR may perhaps be

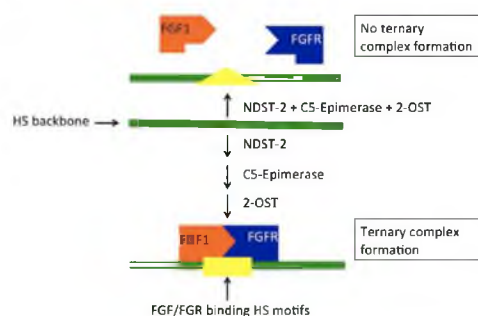


Fig. 4. Plausible schematic model of the assembly of FGF/FGFR binding HS motifs. HS chains can form ternary complexes with FGF and FGFR only when they are modified by HS biosynthetic enzymes in a sequential manner.

quantitatively deduced through sophisticated biophysical methods such as surface plasmon resonance. Interestingly, an earlier study has shown that more potent ATIII-binding HS anticoagulant structure is generated when HS biosynthetic enzymes act concurrently [18]. The current study points to a fundamental difference in the sulfation patterns produced by HS biosynthetic enzymes when they act sequentially or concurrently on the polysaccharide backbone. Natural heparan sulfate has a domain-like organization whereby some segments of the chain are highly sulfated (NS domains), some segments have little to no sulfation (NA domains), and some segments are partially sulfated (NA/NS domains). By sequentially modifying heparosan, it is likely that the resulting polysaccharides 5 and 7 have an extended sulfation pattern that mimics natural HS whereas polysaccharide 2 has a more random sulfation pattern that is not present in the natural FGF1-binding HS domain. Furthermore, polysaccharide 2 was found to migrate slower than polysaccharide 5 during gel electrophoresis, indicating that the overall sulfation density of the polysaccharide 2 is much less than that of the polysaccharides 5 and 7.

Based on the results from this study, we can predict that the production of the FGF1/FGFR binding motif proceeds in a sequential manner in the Golgi. As the nascent HS chain passes through GAGOSOMES, it is modified in a specific order by HS biosynthetic enzymes (Fig. 4). However, the factors that modulate this orderly action remain unknown. A number of factors can affect the order of modification including: the specific location of these enzymes, the limited concentration of PAPS or the effect of sulfation patterns on the enzymatic action of other sulfotransferases. Future studies will further probe the biosynthesis of the FGF/FGFR binding motif in HS by using fluorescence assisted colocalization experiments to track nascent HS chains as they are modified by GAGOSOMES.

Acknowledgements

This work was supported by the National Institutes of Health grants (GM075168 and NS057144) and American Heart Associa-

tion National Scientist development award (0830360N) to B.K. In addition, T.N. acknowledges funding support from the Vietnam Education Foundation.

References

- [1] Esko, J.D. and Lindahl, U. (2001) Molecular diversity of heparan sulfate. *J. Clin. Invest.* 108, 169–173.
- [2] Raman, K. and Kuberan, B. (2010) Chemical tumor biology of heparan proteoglycans. *Curr. Chem. Biol.* 4, 20–31.
- [3] Beenken, A. and Mohammadi, M. (2009) The FGF family: biology, pathophysiology and therapy. *Nat. Rev. Drug Discov.* 8, 235–253.
- [4] Itoh, N. (2007) The Fgf families in humans, mice, and zebrafish: their evolutionary processes and roles in development, metabolism, and disease. *Biol. Pharm. Bull.* 30, 1819–1825.
- [5] Klagsbrun, M. and Baird, A. (1991) A dual receptor system is required for basic fibroblast growth factor activity. *Cell* 67, 229–231.
- [6] Burgess, W.H. and MacIag, T. (1989) The heparin-binding (fibroblast) growth factor family of proteins. *Annu. Rev. Biochem.* 58, 575–606.
- [7] Coutts, J.C. and Gallagher, J.T. (1995) Receptors for fibroblast growth factors. *Immunol. Cell Biol.* 73, 584–589.
- [8] Allen, B.L. and Rapraeger, A.C. (2003) Spatial and temporal expression of heparan sulfate in mouse development regulates FGF and FGF receptor assembly. *J. Cell Biol.* 163, 637–648.
- [9] Gallagher, J.T. (2001) Heparan sulfate: growth control with a restricted sequence menu. *J. Clin. Invest.* 108, 357–361.
- [10] Mohammadi, M., Olsen, S.K. and Ibrahim, O.A. (2005) Structural basis for fibroblast growth factor receptor activation. *Cytokine Growth Factor Rev.* 16, 107–137.
- [11] Maccarana, M., Casu, B. and Lindahl, U. (1993) Minimal sequence in heparin/heparan sulfate required for binding of basic fibroblast growth factor. *J. Biol. Chem.* 268, 23898–23905.
- [12] Guilmond, S., Maccarana, M., Olwin, B.B., Lindahl, U. and Rapraeger, A.C. (1993) Activating and inhibitory heparin sequences for FGF-2 (basic FGF): distinct requirements for FGF-1, FGF-2, and FGF-4. *J. Biol. Chem.* 268, 23906–23914.
- [13] Turnbull, J.E., Ferrig, D.G., Ke, Y., Wilkinson, M.C. and Gallagher, J.T. (1992) Identification of the basic fibroblast growth factor binding sequence in fibroblast heparan sulfate. *J. Biol. Chem.* 267, 10337–10341.
- [14] Naimy, H., Buczek-Thomas, J.A., Nugent, M.A., Leymarie, N. and Zaia, J. (2011) Highly sulfated nonreducing end-derived heparan sulfate domains bind fibroblast growth factor-2 with high affinity and are enriched in biologically active fractions. *J. Biol. Chem.* 286, 19311–19319.
- [15] Jastrebova, N., Vanwildemeersch, M., Lindahl, U. and Spillmann, D. (2010) Heparan sulfate domain organization and sulfation modulate FGF-induced cell signaling. *J. Biol. Chem.* 285, 26842–26851.
- [16] Carlsson, P., Presto, J., Spillmann, D., Lindahl, U. and Kjellen, L. (2008) Heparin/heparan sulfate biosynthesis: processive formation of N-sulfated domains. *J. Biol. Chem.* 283, 20008–20014.
- [17] Victor, X.V., Nguyen, T.K., Ehirajan, M., Tran, V.M., Nguyen, K.V. and Kuberan, B. (2009) Investigating the elusive mechanism of glycosaminoglycan biosynthesis. *J. Biol. Chem.* 284, 25842–25853.
- [18] Kuberan, B., Lech, M.Z., Beeler, D.L., Wu, Z.L. and Rosenberg, R.D. (2003) Enzymatic synthesis of antithrombin III-binding heparan sulfate pentasaccharide. *Nat. Biotechnol.* 21, 1343–1346.
- [19] Yates, E.A., Santini, F., Guerrini, M., Naggi, A., Torri, G. and Casu, B. (1996) ^1H and ^{13}C NMR spectral assignments of the major sequences of twelve systematically modified heparin derivatives. *Carbohydr. Res.* 294, 15–27.
- [20] Nguyen, T.K., Tran, V.M., Victor, X.V., Skalicky, J.J. and Kuberan, B. (2010) Characterization of uniformly and atom-specifically (^{13}C)-labeled heparin and heparan sulfate polysaccharide precursors using (^{13}C) NMR spectroscopy and ESI mass spectrometry. *Carbohydr. Res.* 345, 2228–2232.
- [21] Lansdon, E.B., Fisher, A.J. and Segel, I.H. (2004) Human 3'-phosphoadenosine 5'-phosphosulfate synthetase (isoform 1, brain): kinetic properties of the adenosine triphosphate sulfurylase and adenosine 5'-phosphosulfate kinase domains. *Biochemistry* 43, 4356–4365.
- [22] Wu, Z.L., Zhang, L., Yabe, T., Kuberan, B., Beeler, D.L., Love, A. and Rosenberg, R.D. (2003) The involvement of heparan sulfate (HS) in FGF1/HS/FGFR1 signaling complex. *J. Biol. Chem.* 278, 17121–17129.

3.5 *In vitro* synthesis of HS library and screening for FGF8-binding HS motifs in zebrafish embryos

3.5.1 Introduction

Heparan sulfate (HS) is a linear and highly sulfated polysaccharide that plays crucial roles in a number of biological processes through binding to various proteins, including FGF8. Therefore, it is important to study the structure-function relationships of HS in these interactions in order to fully understand the biological processes governed by HS. However, one of the major problems in the GAG field is the tremendous difficulty in synthesizing bioactive HS molecules. The Rosenberg lab has developed an enzymatic approach to assemble antithrombin-III-binding pentasaccharides in a much shorter time with a higher yield than a typical chemical synthesis process (4, 5). In the enzymatic approach, recombinant HS modifying enzymes were utilized to modify *N*-acetylated oligosaccharides into homogenous bioactive HS oligosaccharides, mimicking the HS biosynthetic processes in the Golgi apparatus.

In this study, HS oligosaccharides with different sizes and structures were enzymatically synthesized to study the structure-function relationships of HS-FGF8 interactions. FGF signaling pathways play critical roles in cell proliferation, migration and differentiation during embryonic development (6, 7). HS has been found to act as a co-receptor for FGFs and their cognate receptors (8, 9). Many studies have investigated the structure-function relationships for HS in its interactions with FGFs and FGFRs. However, most studies examined the interactions among FGF1/2, FGFR1/2 and heparin (10, 11). Furthermore, FGF8 is one of the FGFs expressed earliest during development and plays crucial roles in limb, central nervous system, kidney and cardiac outflow tract

development (6). Very little is known about the size and structural requirements of HS for its interactions with FGF8/FGFR. Therefore, in this study, enzymatically synthesized HS oligosaccharides were utilized to study HS-FGF8 interactions *in vivo* to deduce such requirements as well as the biogenesis pathway of FGF8-binding HS motifs.

3.5.2 Materials and methods

3.5.2.1 Preparation of N-acetyl and N-sulfo oligosaccharides

N-acetyl heparosan polysaccharide was prepared from *E.coli* strain K5 following a published report (12). *N*-sulfo heparosan was prepared as described in literature (13). Heparosan (1 g) was treated with 2.5 M NaOH, added up to a total volume of 100 ml. The reaction was stirred at 55°C overnight and then neutralized to pH 7.0. Subsequently, 5 g of sodium carbonate and 5 g of triethylamine sulfotrioxide were added. The reaction was stirred at 48°C for 2 days. *N*-sulfo heparosan was then purified through DEAE sepharose column, precipitated with ethanol and lyophilized.

N-Acetyl heparosan (NA) and *N*-sulfo heparosan (NS) were then partially digested into oligosaccharides using heparitinase enzyme for a very short time (usually less than 10 min) at 37°C. The reactions were terminated by boiling for 2 min. The oligosaccharide mixtures were separated on a semipreparative Carbowac column (PA1 9 mm x 250 mm). The oligosaccharides with different degrees of polymerization (Dp) were eluted with a gradient of 1 M NaCl (pH 3.5) for 180 min at a flow rate of 2 ml/min and monitored by absorbance at 232 nm. The fractions containing each size-defined oligosaccharide were pooled together and desalted using a G-25 column (1.5 cm x 50 cm).

3.5.2.2 Expression of HS biosynthetic enzymes

The NDST-2, C5-Epimerase, 2-OST, 6-OST1 recombinant enzymes were expressed using a baculovirus system following the protocol described below. The viral stock (20 ml) was added to 1×10^9 Sf9 cells in 1 L of Sf-900 SFM medium. Infected insect cells were shaken at 90 rpm at 28°C for 4 days and then centrifuged at 1000 x g for 30 min to pellet the cells. The supernatant was collected and added with PIPES (pH 7.0) and phenylmethylsulfonyl fluoride to a final concentration of 10 mM and 1 mM, respectively. The supernatant was chilled on ice for 30 min, and subsequently centrifuged at 4000 x g for 30 min. The enzyme was purified through a 100-ml column of ToyoPearl AF-heparin 650M. The column was washed with 600 ml of PCG-50 (10 mM PIPES, pH 7.0, 1 % glycerol, 0.2 % CHAPS, 50 mM NaCl). The enzyme was eluted from the column with a 450 ml linear gradient of 50 – 1000 mM NaCl in PCG and monitored by measuring its absorbance at 280 nm. The fractions containing the enzyme were pooled and concentrated using an Amicon YM-10 filter.

3.5.2.3 Enzymatic modifications

Fifty μ g of heparosan or oligosaccharide (Dp 4-14) was incubated with 20 μ l of enzyme (~1 mg/ml) and 100 μ g of PAPS in a total volume of 100 μ l. The reactions were performed at 37°C for 24 h in a buffer consisting of 25 mM MES (pH 7.0), 0.02 % Triton X-100, 2.5 mM MgCl₂, 2.5 mM MnCl₂, 1.25 mM CaCl₂ and 0.75 mg/ml BSA. With C5-epimerase, the reactions were carried out in D₂O. The reaction mixtures were purified through a mini DEAE-sepharose column (0.2 ml) that had been pre-equilibrated with wash buffer (20 mM NaOAc, 0.1 M NaCl and 0.01 % Triton X-100, pH 6.0). After

washing with 6 ml of wash buffer, the bound HS was eluted with 1.2 ml of elution buffer (20 mM NaOAc, 1 M NaCl, pH 6.0). The polysaccharide samples were desalted and concentrated with 3000 MWCO Amicon columns. The oligosaccharide samples were desalted through a G-25 column (1.5 cm x 50 cm). The fractions containing oligosaccharides were detected by measuring UV absorbance at 232 nm, the corresponding fractions were pooled and then lyophilized.

3.5.2.4 Mass spectrometry analysis of oligosaccharides

The oligosaccharides were analyzed using a capillary C18-HPLC column (0.3 x 30 mm) coupled to an electrospray ionization time-of-flight MS (Bruker Daltonics, USA). The oligosaccharides were eluted with a linear gradient of acetonitrile at a flow rate of 5 μ l/min for 30 min. Dibutylammonium acetate (5 mM) was used as an ion-pairing agent. The MS was acquired in the negative ion mode at the following conditions: cone gas flow rate at 50 L/h, nozzle temperature at 130°C, drying gas (N₂) flow rate at 450 L/h, spray tip potential at 2.3 kV and nozzle potential at 35 V.

3.5.2.5 Injection of HS oligosaccharides into zebrafish embryos

One nl of each oligosaccharide (1 ng/nl) was injected into the animal pole of dome-stage embryos at 4 hpf. The phenotypes of these embryos were compared to those of WT embryos that had been injected with 1% phenol red.

3.5.2.6 RNA *in situ* hybridization

Mkp3 antisense digoxigenin-labeled probe was generated from cDNA clones using a T7 RNA polymerase-based labeling kit (14). Embryos were fixed overnight in 4 % PFA, and then washed with PBST (0.1 % Tween-20 phosphate buffer saline). Whole mount *in situ* hybridization experiments were performed as previously described (15). Embryos were then stained with BM Purple for imaging.

3.5.3 Results and discussion

3.5.3.1 Polysaccharides containing N-sulfation and one type of O-sulfation can activate FGF8 signaling in zebrafish embryos

In order to understand the overall structural requirements of HS for its interactions with FGF8, we tested a HS polysaccharide library in zebrafish embryos. A HS polysaccharide library was assembled by modifying *N*-sulfo heparosan (NS) with HS biosynthetic enzymes as discussed in Section 3.5.2. Enzymes were added concurrently or sequentially in specific orders as noted in Table 3.4. Each HS structure was tested in zebrafish embryos for FGF8 activity, considering the elongation phenotype as a FGF8 activity indicator (Figure 3.1). The results showed that all tested HS structures caused elongation phenotype in zebrafish embryos at 12 hpf, indicating the promiscuity of HS-FGF8 interactions. The results also indicated that *N*-sulfation and one type of *O*-sulfation are sufficient to activate FGF8 signaling pathway in zebrafish embryos.

Table 3.4 Assembly of HS polysaccharide structures. The order of HS modification is indicated in the table.

NS	C5-Epimerase	2-OST	6-OST1 and 3	3-OST1 and 3a
NS6S			1 st	
NSEpi6S	1 st		2 nd	
NSEpi2S3S	1 st	2 nd		3 rd
NSEpi2S6S	1 st	2 nd	3 rd	
NSEpi3S2S	1 st	3 rd		2 nd
NSEpi3S6S	1 st		3 rd	2 nd
NSEpi6S3S	1 st		2 nd	3 rd
NSEpi2S+3S	1 st	2 nd		2 nd
NSEpi2S+6S	1 st	2 nd	2 nd	
NSEpi3S+6S	1 st		2 nd	2 nd
NSEpi6S3S2S	1 st	4 th	2 nd	3 rd

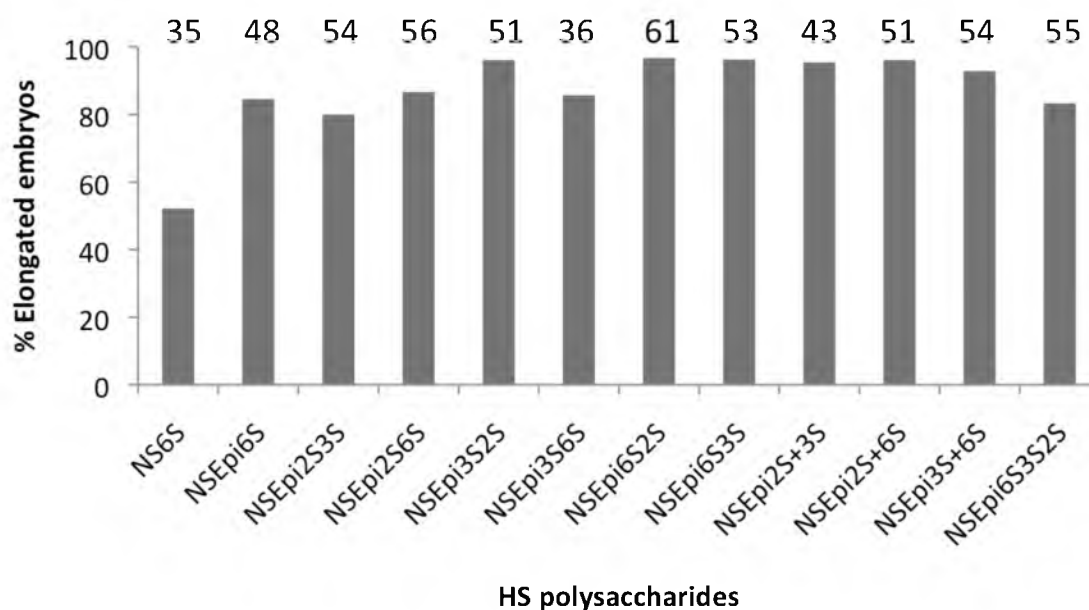


Figure 3.1 HS polysaccharides caused elongation phenotype in developing zebrafish embryos at 12 hpf. Each HS polysaccharide was injected into the animal pole of dome-stage embryos at 4 hpf (1 ng/embryo). Total number of embryos injected with oligosaccharides is indicated on each bar.

3.5.3.2 Nonsulfated oligosaccharides cannot activate FGF8

signaling in zebrafish embryos

Results obtained from polysaccharide experiments indicated that *in vitro* enzymatically synthesized HS could activate FGF8 signaling in zebrafish embryos. However, structural analysis of polysaccharides could not provide more specific information of the minimum sizes of HS that can activate FGF8 signaling. Therefore, we fragmented the *N*-acetyl heparosan polymer (NA) into oligosaccharides by heparitinase I digestion. *N*-acetyl heparosan oligosaccharides were then separated on a strong-anion exchange column and purified through G-25 column (Figure 3.2). Each oligosaccharide (Dp4 – Dp14) was injected into zebrafish embryos at 4 hpf and the embryos were screened for the elongation phenotype at 12 hpf (Figure 3.3). All of these oligosaccharides caused elongation phenotype in less than 5 % of injected embryos, indicating that nonsulfated oligosaccharides with their chain length of up to 14-mer are not efficient in activating FGF8 signaling pathway in zebrafish embryos.

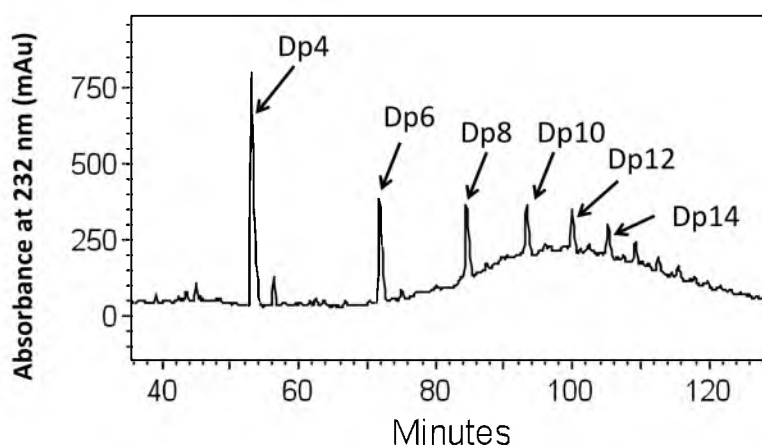


Figure 3.2 Separation of *N*-acetyl (NA) oligosaccharides on a strong anion exchange column. The oligosaccharides with different degrees of polymerization (Dp) were eluted with a linear gradient of 0 - 1 M NaCl (pH 3.5) over 180 min at a flow rate of 2 ml/min and monitored by UV absorbance at 232 nm.

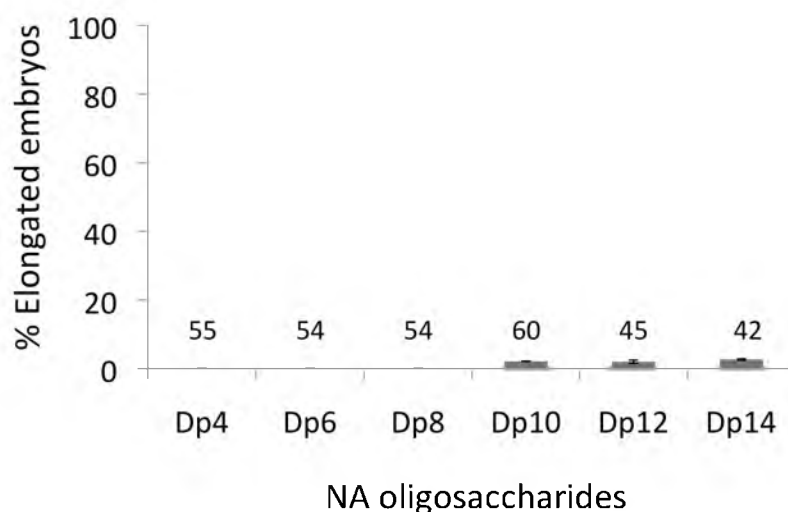


Figure 3.3 *N*-acetyl oligosaccharides (NA) with their chain length of up to 14-mer did not cause elongation phenotype in zebrafish embryos at 12 hpf. Each oligosaccharide was injected into the animal pole of dome-stage embryos at 4 hpf (1 ng/embryo). Mean \pm SEM from 3 experiments are presented. Total number of embryos injected with oligosaccharides is indicated on each bar.

3.5.3.3 *N*-sulfo oligosaccharides with their chain length of 20-mer and longer can activate FGF8 signaling significantly

The next question is whether *N*-sulfated oligosaccharides can activate FGF8 signaling and if so, what is the minimum size that can have the effect. *N*-sulfo heparosan oligosaccharides (NS) were prepared as described in Section 3.5.2. The oligosaccharides that were utilized were listed in Table 3.5. Mass spectral profiles of these oligosaccharides were shown in Table 3.6. These oligosaccharides were injected into zebrafish embryos at 4 hpf and the embryos were screened for elongation phenotype at 12 hpf (Figure 3.4). The results showed that the minimum size of HS that can cause elongation phenotype is 14-mer (11%); however, a significant percentage of the elongation phenotype was observed with Dp20 (63%).

Table 3.5 NS oligosaccharides utilized in the study.

Number	Oligosaccharide	Structure
1	NS Dp4	
2	NS Dp6	
3	NS Dp8	
4	NS Dp10	
5	NS Dp12	
6	NS Dp14	
7	NS Dp16	
8	NS Dp18	

Table 3.5 continued

Number	Oligo-saccharide	Structure
9	NS Dp20	
10	NS Dp22	
11	NS Dp24	

Table 3.6 MS profiles of NS oligosaccharides before and after epimerization by C5-epimerase.

Number	NS + C5-Epi	MS profile
2a	NSEpi Dp6	<p>Intens. [%]</p> <p>25 20 15 10 5 0</p> <p>624.58 625.08 625.58 626.09</p> <p>[M-2H]²⁻</p> <p>2</p> <p>100 80 60 40 20 0</p> <p>625.58 625.08 626.08 626.58 627.08</p> <p>[M-2H]²⁻</p> <p>2a</p> <p>622 623 624 625 626 627 628 629 630 m/z</p>
3a	NSEpi Dp8	<p>Intens. [%]</p> <p>100 80 60 40 20 0</p> <p>833.11 833.61 834.11 834.61 835.11</p> <p>[M-2H]²⁻</p> <p>3</p> <p>100 80 60 40 20 0</p> <p>834.12 834.62 835.12 836.12</p> <p>[M-2H]²⁻</p> <p>3a</p> <p>830 831 832 833 834 835 836 837 838 m/z</p>

Table 3.6 continued

Number	NS + C5-Epi	MS profile
4a	NSEpi Dp10	<p>Mass spectra for compound 4a. The top trace (labeled '4') shows peaks at m/z 694.07, 694.40, 694.74, 695.07, and 695.40. The bottom trace (labeled '4a') shows peaks at m/z 694.09, 694.42, 694.76, 695.10, 695.43, 695.76, 696.10, and 696.435. Both traces show a [M-3H]³⁻ ion.</p>
5a	NSEpi Dp12	<p>Mass spectra for compound 5a. The top trace (labeled '5') shows peaks at m/z 833.12, 833.45, 833.78, 834.12, and 834.45. The bottom trace (labeled '5a') shows peaks at m/z 833.11, 833.45, 833.78, 834.12, 834.45, and 834.79. Both traces show a [M-3H]³⁻ ion.</p>
6a	NSEpi Dp14	<p>Mass spectra for compound 6a. The top trace (labeled '6') shows peaks at m/z 972.12, 972.45, 972.79, 973.12, 973.45, and 973.79. The bottom trace (labeled '6a') shows peaks at m/z 972.13, 972.47, 972.80, 973.13, 973.47, 973.80, and 974.14. Both traces show a [M-3H]³⁻ ion.</p>

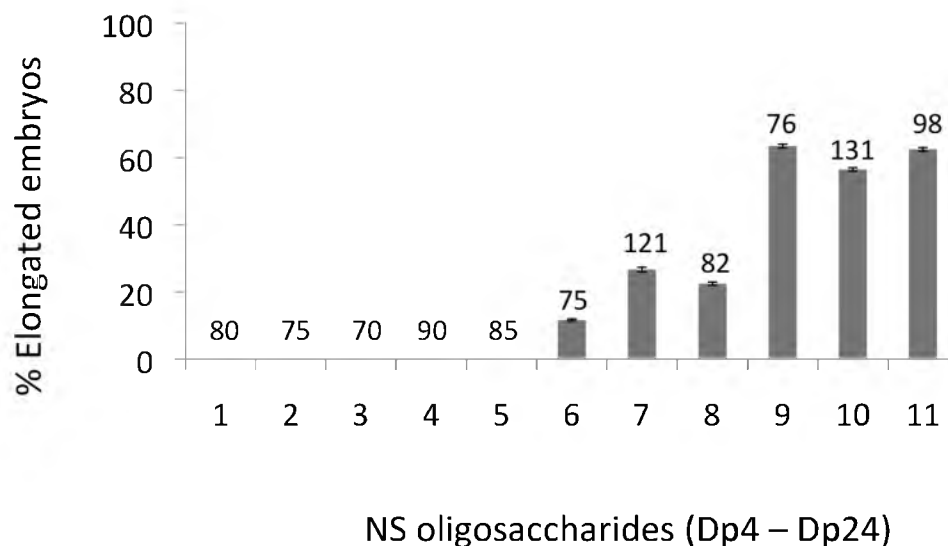


Figure 3.4 *N*-sulfo heparosan (NS) oligosaccharides with a chain length of 20-mer or longer caused the elongation phenotype in a significant number of treated embryos at 12 hpf. Each oligosaccharide was injected into the animal pole of dome-stage embryos at 4 hpf (1 ng/embryo). Mean \pm SEM from 3 experiments are presented. The oligosaccharides are labeled as shown in Table 3.5. Total number of embryos injected with oligosaccharides is indicated on each bar.

3.5.3.4 C5-Epimerization alone is not sufficient to activate FGF8

signaling significantly in zebrafish embryos

The next question is whether epimerized NS oligosaccharides carrying iduronyl residues can activate FGF8 signaling more effectively than unepimerized NS oligosaccharides carrying no iduronyl residues. It has been known that IdoA is required for FGF1/FGF2-mediated growth promoting activity (16, 17). We prepared epimerized NS oligosaccharides (NSEpi Dp6 – Dp14) by C5-epimerase as described in Section 3.5.2. The reactions were carried out in deuterium so that the epimer content can be characterized by the hydrogen/deuterium exchange-LC-MS approach published earlier by our group (18). Mass spectral profiles of both substrates and products of these reactions were shown in Table 3.6. These oligosaccharides were injected into zebrafish embryos at

4 hpf and the embryos were screened for elongation phenotype at 12 hpf (Figure 3.5). NSEpi oligosaccharides did not increase the percentage of elongated embryos significantly compared to NS oligosaccharides, indicating that iduronic acid alone is not sufficient to activate FGF8 signaling in zebrafish embryos.

3.5.3.5 N-sulfated, epimerized and 2-O-sulfated deca-saccharide can activate FGF8 signaling significantly in zebrafish embryos

The next question is whether 2-*O*-sulfation can have an effect on FGF8 signaling. We prepared epimerized, 2-*O*-sulfated NS oligosaccharides (NSEpi2S Dp6 – Dp12) by modifying K5NS oligosaccharides with C5-epimerase and 2-OST concurrently in D₂O. Mass spectral profiles of NSEpi2S oligosaccharide products of these reactions are shown in Table 3.7. These oligosaccharides were injected into zebrafish embryos at 4 hpf and the embryos were screened for the elongation phenotype at 12 hpf (Figure 3.6). NSEpi2S Dp10 (4b) and Dp12 (5b) caused elongation phenotype in 92.8% and 95.1% of treated embryos while NSEpi2S Dp8 (3b) only caused elongation phenotype in 13.1%. These three oligosaccharides were subsequently tested in different dosages (Figure 3.7). The results showed that 10-mer is the critical size for NSEpi2S oligosaccharide that can activate FGF8 signaling in zebrafish embryos.

3.5.3.6 N-sulfated, 6-O-sulfated hexa-saccharide can activate FGF8 signaling significantly in zebrafish embryos

Another question is whether 6-*O*-sulfation can have an effect on FGF8 signaling. We prepared 6-*O*-sulfated NS oligosaccharides (NS6S Dp6 – Dp10) by modifying NS

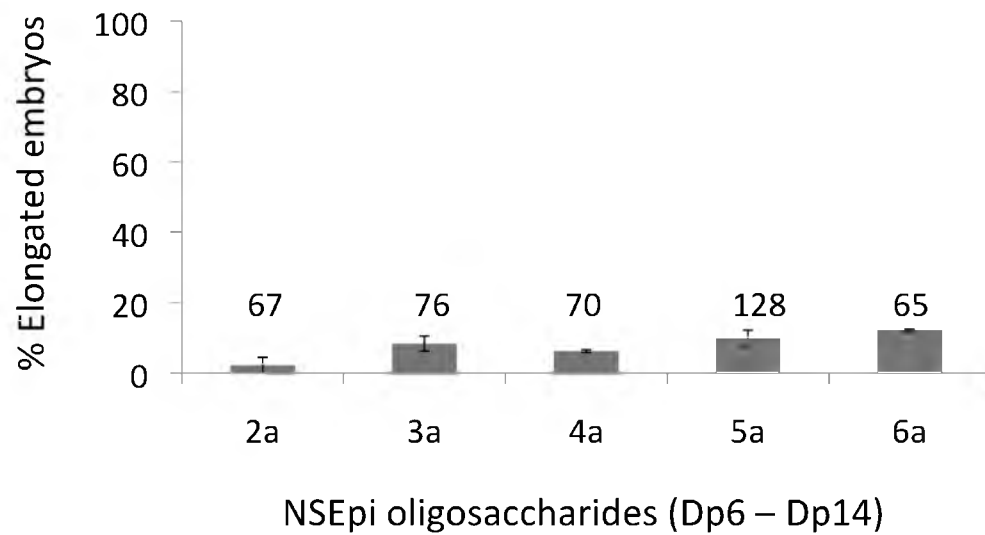


Figure 3.5 NSEpi oligosaccharides did not have a significant effect on FGF8 signaling in zebrafish embryos. Each NSEpi oligosaccharide was injected into the animal pole of dome-stage embryos at 4 hpf (1 ng/embryo). Mean \pm SEM from 3 experiments are presented. The oligosaccharides are labeled as shown in Table 3.6. Total number of embryos injected with oligosaccharides is indicated on each bar.

Table 3.7 MS profiles of NSEpi2S oligosaccharides.

Number	NS + C5-Epi + 2-OST	Structure
2b	NSEpi 2S Dp6	<p>Mass spectrum for NSEpi 2S Dp6. The x-axis is m/z (495-499) and the y-axis is Intensity [%] (0-100). The base peak is at m/z 496.34. Other significant peaks are labeled at m/z 496.01, 496.68, 497.01, 497.34, and 497.68. The spectrum is labeled '2b' in the top right corner.</p>
3b	NSEpi 2S Dp8	<p>Mass spectrum for NSEpi 2S Dp8. The x-axis is m/z (495-499) and the y-axis is Intensity [%] (0-100). The base peak is at m/z 496.51. Other significant peaks are labeled at m/z 496.01, 496.26, 496.76, 497.01, 497.26, and 497.51. The spectrum is labeled '3b' in the top right corner.</p>
4b	NSEpi 2S Dp10	<p>Mass spectrum for NSEpi 2S Dp10. The x-axis is m/z (495.5-498.5) and the y-axis is Intensity [%] (0-100). The base peak is at m/z 496.82. Other significant peaks are labeled at m/z 496.22, 496.42, 496.62, 497.02, 497.22, 497.42, and 497.62. The spectrum is labeled '4b' in the top right corner.</p>
5b	NSEpi 2S Dp12	<p>Mass spectrum for NSEpi 2S Dp12. The x-axis is m/z (911-917) and the y-axis is Intensity [%] (0-100). The base peak is at m/z 913.78. Other significant peaks are labeled at m/z 913.11, 913.44, 914.11, 914.45, 914.78, 915.11, and 915.44. The spectrum is labeled '5b' in the top right corner.</p>

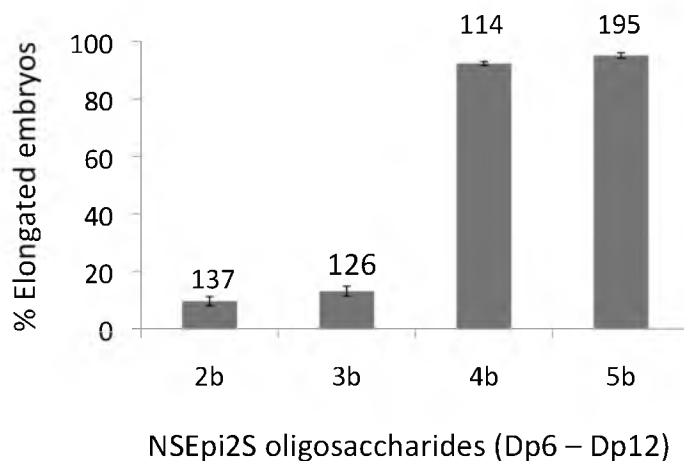


Figure 3.6 NSEpi2S 10-mer and 12-mer caused elongation phenotype in significant numbers of treated embryos at 12 hpf. Each NSEpi2S oligosaccharide was injected into the animal pole of dome-stage embryos at 4 hpf (1 ng/embryo). Mean \pm SEM from 3 experiments are presented. Total number of embryos injected with oligosaccharides is indicated on each bar. The oligosaccharides are labeled as shown in Table 3.7.

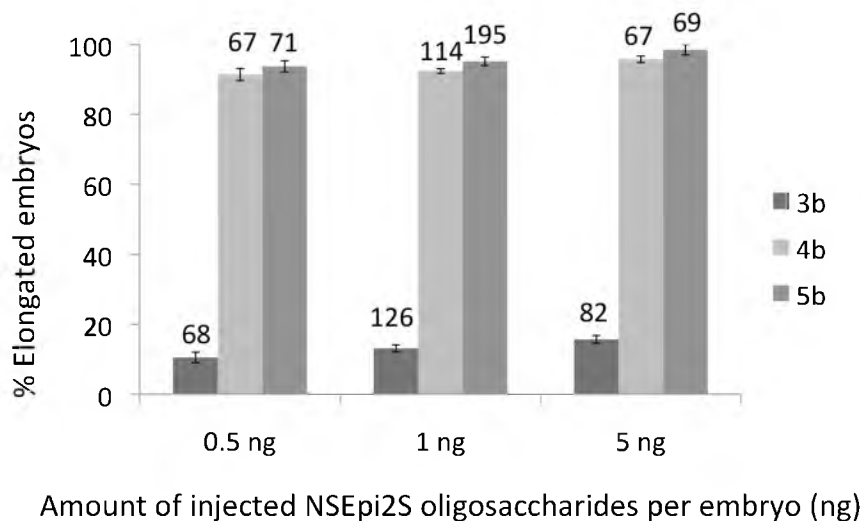


Figure 3.7 Effect of various dosages of NSEpi2S Dp8 (3b), Dp10 (4b) and Dp12 (5b) on FGF8 signaling in zebrafish embryos. Each NSEpi2S oligosaccharide was injected into the animal pole of dome-stage embryos at 4 hpf. Mean \pm SEM from 3 experiments are presented. Total number of embryos injected with oligosaccharides is indicated on each bar.

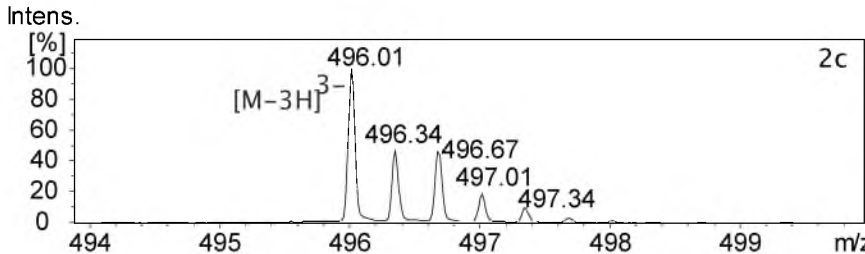
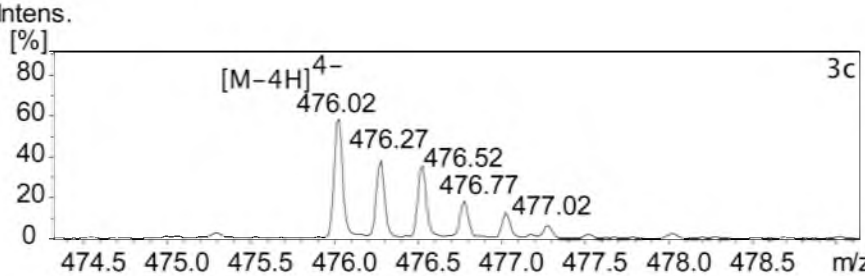
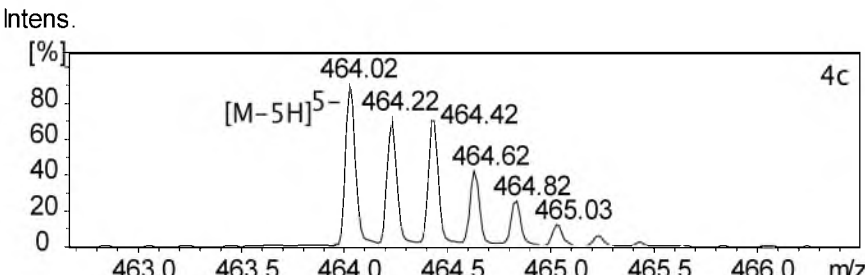
oligosaccharides with 6-OST1. Mass spectral profiles of NS6S oligosaccharide products of these reactions are shown in Table 3.8. These oligosaccharides were injected into zebrafish embryos at 4 hpf and the embryos were screened for the elongation phenotype at 12 hpf (Figure 3.8). NS6S Dp6 (2c) caused elongation phenotype in 46 % treated embryos, indicating that *N*-sulfated and 6-*O*-sulfated hexasaccharide can activate FGF8 signaling in zebrafish embryos.

3.5.3.7 The elongation phenotype caused by injection of oligosaccharides is the result of hyperactivation of FGF8 signaling

In order to confirm that oligosaccharides affect zebrafish embryos in the same pathway with cluster xylosides and heparin, expression of FGF target gene *mkp3* was analyzed. Expression of *mkp3* was found to be expanded in embryos injected with NSEpi2S Dp12 (5b) and NS6S Dp6 (2c), compared to WT (Figure 3.9). These results indicated that, similar to cluster xylosides and heparin, enzymatically synthesized oligosaccharides with specific sizes and structures can activate FGF8 signaling in zebrafish embryos.

Based on our current study, we propose the structural requirements of HS that can activate FGF8 signaling pathway *in vivo*. Polysaccharides with *N*-sulfation and any one type of *O*-sulfation can activate FGF8 signaling in zebrafish embryos. These results suggest that HS-FGF8 interactions are promiscuous and *O*-sulfation can be substituted for each other in HS polysaccharides. It does not, however, reveal the minimum size requirements for FGF8 activation. Therefore, oligosaccharides were utilized to reveal size requirements. In the case of oligosaccharides with only *N*-sulfation, FGF8 signaling

Table 3.8 MS profiles of NS6S oligosaccharides.

Number	NS + 6-OST1	Structure
2c	NS6S Dp6	 <p>Mass spectrum of NS6S Dp6 showing relative intensity (%) versus m/z. The base peak is at m/z 496.01, labeled $[M-3H]^{3-}$. Other labeled peaks are at m/z 496.34, 496.67, 497.01, and 497.34.</p>
3c	NS6S Dp8	 <p>Mass spectrum of NS6S Dp8 showing relative intensity (%) versus m/z. The base peak is at m/z 476.02, labeled $[M-4H]^{4-}$. Other labeled peaks are at m/z 476.27, 476.52, 476.77, and 477.02.</p>
4c	NS6S Dp10	 <p>Mass spectrum of NS6S Dp10 showing relative intensity (%) versus m/z. The base peak is at m/z 464.02, labeled $[M-5H]^{5-}$. Other labeled peaks are at m/z 464.22, 464.42, 464.62, 464.82, and 465.03.</p>

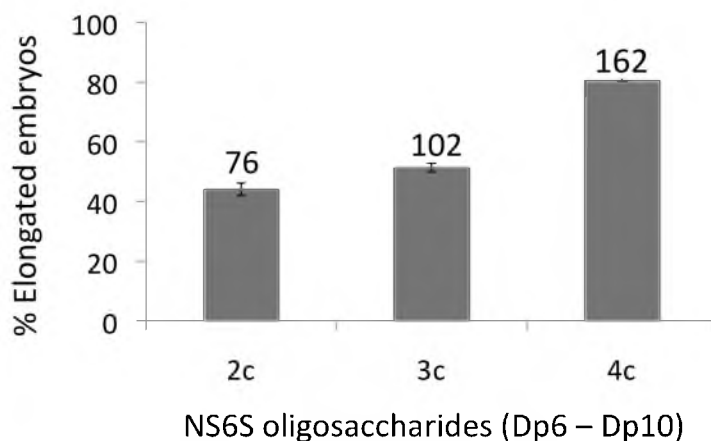


Figure 3.8 Various NS6S oligosaccharides caused elongation phenotype in a significant number of treated embryos at 12 hpf. Each NS oligosaccharide was injected into the animal pole of dome-stage embryos at 4 hpf (1 ng/embryo). Mean \pm SEM from 3 experiments are presented. The oligosaccharides are labeled as in Table 3.8. Total number of embryos injected with oligosaccharides is indicated on each bar.

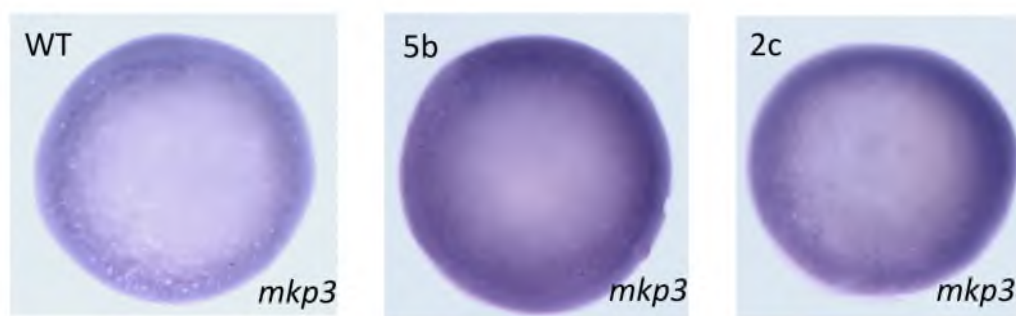


Figure 3.9 Expression pattern of FGF signaling target gene *mkp3* in WT and embryos injected with NSEpi2S Dp12 (5b) and NS6S Dp6 (2c) at 1 ng/embryo. *In situ* hybridization with a *mkp3* probe was carried out at 7 hpf. *mkp3* expression was expanded in embryos injected with 5b and 2c compared to WT embryos. Animal pole views.

is effectively hyperactivated by oligosaccharides with the chain length of 20-mer or longer. In the presence of *N*-sulfation and 2-*O*-sulfation, 10-mer is the minimum size that can affect FGF8 signaling significantly. With *N*-sulfation and 6-*O*-sulfation, 6-mer is sufficient to activate FGF8 signaling in zebrafish embryos. These results suggested that 6-*O*-sulfation is very important for HS-FGF8 interactions. However, this requirement can be compensated by longer oligosaccharides containing *N*-sulfation and 2-*O*-sulfation, revealing the promiscuity of HS-FGF8 interactions for the first time. In summary, HS with different sulfations can activate the FGF8 signaling pathway but they require different minimum sizes. In other words, HS-FGF8 interactions are promiscuous yet require specific structural attributes. One may suggest that these oligosaccharides may undergo further modifications by the endogenous HS modifying enzymes to become active in the interactions with FGF8. However, if that were the case, NS oligosaccharides should have been modified by any of the *O*-sulfotransferase enzymes and causing the effect at a much shorter chain length than 20-mer. The fact that elongation phenotype was observed with NS6S 6-mer, NSEpi2S 10-mer and NS 20-mer indicates that oligosaccharides do not undergo further modifications. However, in order to confirm this hypothesis, several experiments can be set up. Zebrafish embryos can be injected with uniformly and atom-specifically ¹³C-labeled oligosaccharides, which are distinguishable by mass from endogenous HS. These oligosaccharides can be pulled out and analyzed by LC-MS to detect any additional modifications. Alternatively, zebrafish embryos can be treated with chlorate, which has been shown as a sulfation inhibitor (19), together with oligosaccharides. If the oligosaccharides do not undergo further modifications, their effect on FGF signaling should not be altered by chlorate treatment.

In future study, the library will be expanded with 3-*O*-sulfated oligosaccharides as well as oligosaccharides modified with different enzyme isoforms and different orders of additions of enzymes to deduce additional structural features that can modulate FGF8 signaling.

3.6 References

1. Nguyen, T. K.; Tran, V. M.; Victor, X. V.; Skalicky, J. J.; Kuberan, B., Characterization of Uniformly and Atom-Specifically (13)C-Labeled Heparin and Heparan Sulfate Polysaccharide Precursors Using (13)C Nmr Spectroscopy and Esi Mass Spectrometry. *Carbohydr Res* **2010**, *345* (15), 2228-32.
2. Nguyen, T. K.; Arungundram, S.; Tran, V. M.; Raman, K.; Al-Mafraji, K.; Venot, A.; Boons, G. J.; Kuberan, B., A Synthetic Heparan Sulfate Oligosaccharide Library Reveals the Novel Enzymatic Action of D-Glucosaminyl 3-O-Sulfotransferase-3a. *Mol Biosyst* **2012**, *8* (2), 609-14.
3. Nguyen, T. K.; Raman, K.; Tran, V. M.; Kuberan, B., Investigating the Mechanism of the Assembly of Fgf1-Binding Heparan Sulfate Motifs. *FEBS Lett* **2011**, *585* (17), 2698-702.
4. Kuberan, B.; Lech, M. Z.; Beeler, D. L.; Wu, Z. L.; Rosenberg, R. D., Enzymatic Synthesis of Antithrombin Iii-Binding Heparan Sulfate Pentasaccharide. *Nat Biotechnol* **2003**, *21* (11), 1343-6.
5. Kuberan, B.; Beeler, D. L.; Lech, M.; Wu, Z. L.; Rosenberg, R. D., Chemoenzymatic Synthesis of Classical and Non-Classical Anticoagulant Heparan Sulfate Polysaccharides. *J Biol Chem* **2003**, *278* (52), 52613-21.
6. Itoh, N., The Fgf Families in Humans, Mice, and Zebrafish: Their Evolutional Processes and Roles in Development, Metabolism, and Disease. *Biol Pharm Bull* **2007**, *30* (10), 1819-25.
7. Goldfarb, M., Functions of Fibroblast Growth Factors in Vertebrate Development. *Cytokine Growth Factor Rev* **1996**, *7* (4), 311-25.
8. Gallagher, J. T.; Turnbull, J. E., Heparan Sulphate in the Binding and Activation of Basic Fibroblast Growth Factor. *Glycobiology* **1992**, *2* (6), 523-8.
9. Rapraeger, A. C.; Krufka, A.; Olwin, B. B., Requirement of Heparan Sulfate for Bfgf-Mediated Fibroblast Growth and Myoblast Differentiation. *Science* **1991**, *252* (5013), 1705-8.
10. Pellegrini, L.; Burke, D.; von Delft, F.; Mulloy, B., Crystal Structure of Fibroblast Growth Factor Receptor Ectodomain Bound to Ligand and Heparin. *Nature* **2000**, *407*, 1029-34.
11. Schlessinger, J.; Plotnikov, A. N.; Ibrahimi, O. A.; Eliseenkova, A. V.; Yeh, B. K.; Yayon, A.; Linhardt, R. J.; Mohammadi, M., Crystal Structure of a Ternary Fgf-Fgfr-Heparin Complex Reveals a Dual Role for Heparin in Fgfr Binding and Dimerization. *Mol Cell* **2000**, *6* (3), 743-50.

12. Kuberan, B.; Lech, M.; Zhang, L.; Wu, Z. L.; Beeler, D. L.; Rosenberg, R. D., Analysis of Heparan Sulfate Oligosaccharides with Ion Pair-Reverse Phase Capillary High Performance Liquid Chromatography-Microelectrospray Ionization Time-of-Flight Mass Spectrometry. *J Am Chem Soc* **2002**, *124* (29), 8707-18.
13. Naggi, A.; Torri, G.; Casu, B.; Oreste, P.; Zoppetti, G.; Li, J. P.; Lindahl, U., Toward a Biotechnological Heparin through Combined Chemical and Enzymatic Modification of the Escherichia Coli K5 Polysaccharide. *Semin Thromb Hemost* **2001**, *27* (5), 437-43.
14. Tsang, M.; Maegawa, S.; Kiang, A.; Habas, R.; Weinberg, E.; Dawid, I. B., A Role for Mkp3 in Axial Patterning of the Zebrafish Embryo. *Development* **2004**, *131* (12), 2769-79.
15. Thisse, C.; Thisse, B.; Schilling, T. F.; Postlethwait, J. H., Structure of the Zebrafish Snail1 Gene and Its Expression in Wild-Type, Spadetail and No Tail Mutant Embryos. *Development* **1993**, *119* (4), 1203-15.
16. Guimond, S.; Maccarana, M.; Olwin, B. B.; Lindahl, U.; Rapraeger, A. C., Activating and Inhibitory Heparin Sequences for Fgf-2 (Basic Fgf). Distinct Requirements for Fgf-1, Fgf-2, and Fgf-4. *J Biol Chem* **1993**, *268* (32), 23906-14.
17. Kreuger, J.; Salmivirta, M.; Sturiale, L.; Gimenez-Gallego, G.; Lindahl, U., Sequence Analysis of Heparan Sulfate Epitopes with Graded Affinities for Fibroblast Growth Factors 1 and 2. *J Biol Chem* **2001**, *276* (33), 30744-52.
18. Babu, P.; Victor, X. V.; Nelsen, E.; Nguyen, T. K.; Raman, K.; Kuberan, B., Hydrogen/Deuterium Exchange-Lc-Ms Approach to Characterize the Action of Heparan Sulfate C5-Epimerase. *Anal Bioanal Chem* **2011**, *401* (1), 237-44.
19. Brandan, E.; Hirschberg, C. B., Purification of Rat Liver N-Heparan-Sulfate Sulfotransferase. *J Biol Chem* **1988**, *263* (5), 2417-22.

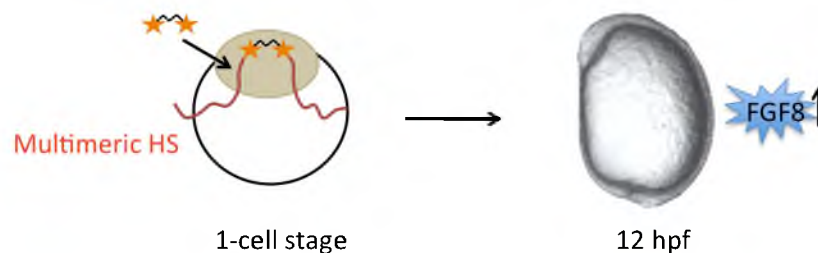
CHAPTER 4

CONCLUSIONS

4.1 Conclusions

The FGF8 signaling pathway is essential for many biological processes, and previous studies have proven the crucial role of heparan sulfate (HS) in the FGF8 signaling pathway. This dissertation was conducted to understand the biogenesis and structural characteristics of FGF8-binding heparan sulfate motifs. The study utilized zebrafish as an animal model and the elongation phenotype as a FGF8 activity indicator. In Chapter 2, the importance of HS multivalency in the activation of FGF8 signaling was illustrated using xylosides, a class of small molecules known to stimulate HS biosynthesis *in vivo* in the absence of core protein. A library of xylosides, including mono-, bis- and tris-xylosides, was used to treat zebrafish embryos at the one-cell stage. After injection, mono-, bis- and tris-xylosides stimulate the biogenesis of monomeric, dimeric and trimeric GAG chains in the Golgi apparatus, which are subsequently secreted into the extracellular matrix. Only dimeric and trimeric GAGs are capable of concurrently forming two ternary complexes with two FGF8 molecules and two FGFRs, induce FGFR dimerization and subsequently activate the downstream signaling pathway, finally causing the elongation phenotype. These results suggested a new molecular model in which endogenous multimeric HS is required for the activation of FGF8 signaling in zebrafish embryos (Figure 4.1A). In this model, at least two covalently linked GAG chains interact with two FGF8 molecules and their cognate FGFRs, thereby efficiently inducing FGFR dimerization that leads to the elongation phenotype. These results also support the 2:2:2 model (2 FGF: 2 FGFR : 2 HS) instead of the 2:2:1 model. This model was reaffirmed by the results of experiments testing syndecan-1 constructs containing zero, one, two or three HS side chains. Injection of mRNAs encoding for syndecan-1

A: Endogenous HS needs to be in a multivalent form to activate FGF8 signaling



B: Diverse HS structures can interact with FGF8 and activate signaling

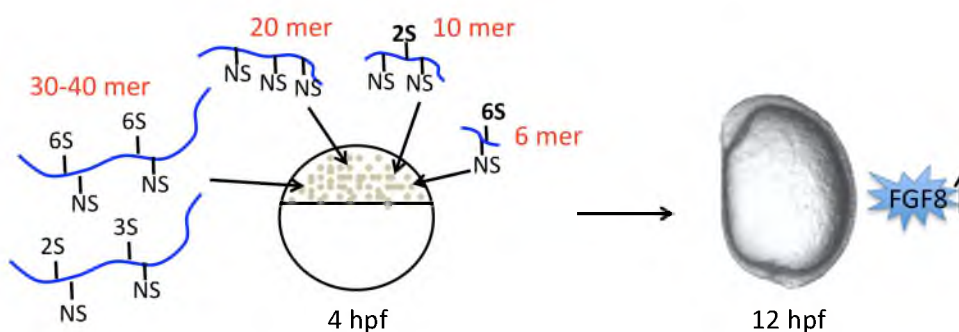


Figure 4.1 Schematic model depicting the structural requirements of HS for its interactions with FGF8. **A:** A library of xylosides was utilized to stimulate HS biosynthesis *in vivo*, where endogenous HS has been shown to require multivalency to activate FGF8 signaling in zebrafish embryos. **B:** A library of enzymatically synthesized HS polymers/oligomers was assembled *in vitro* and tested for its effect on FGF8 signaling *in vivo*. *N*-sulfo oligosaccharides can activate FGF8 signaling if their chain length is 20-mer or longer. With *N*-sulfation and 2-*O*-sulfation, a 10-mer oligosaccharide can affect FGF8 signaling significantly. With *N*-sulfation and 6-*O*-sulfation, a 6-mer oligosaccharide is sufficient to activate FGF8 signaling in zebrafish embryos.

protein capable of carrying two or three HS chains caused a significantly higher percentage of elongated embryos as compared to those carrying a single or no HS side chain. These results, once again, demonstrate the essential role of HS multivalency in activating FGF8 signaling. Moreover, heparin and dermatan sulfate but not chondroitin sulfate A and C activated FGF8 signaling in zebrafish embryos, which provides the evidence that diverse yet specific GAG structures are required for activating the FGF8 pathway.

In order to understand the specific structural requirements that dictate HS-FGF8 interactions, a library of HS oligosaccharides was enzymatically synthesized *in vitro* and tested for its effect on FGF8 signaling in zebrafish embryos, as described in Chapter 3. The results from this study allow us to deduce the structural requirements of HS for activating the FGF8 pathway. Surprisingly, the HS-FGF8 interactions are diverse, yet structurally defined promiscuity, in which varying HS structures can perform the same function. This study has shown for the first time that HS molecules with different sulfations can activate the same FGF8 signaling pathway in zebrafish embryos in a size-dependent manner. Thus, the minimum size of each structure, which can have an effect, is different, and depends on the type of sulfation. More importantly, different types of *O*-sulfation show different levels of activity. In particular, oligosaccharides with only *N*-sulfate groups need to have the chain length of 20-mer and longer to have a significant effect on FGF8 signaling. On the contrary, oligosaccharides with *N*- and 2-*O*-sulfate groups and oligosaccharides with *N*- and 6-*O*-sulfate groups only need the chain length of 10-mer and 6-mer, respectively, to have the same effect on FGF8 signaling (Figure 4.1B). This new information concerning the HS-FGF8-based structure-function relationship

presents a new picture of cellular processes in which HS structures can modulate many signaling pathways at the post-translational level and beyond.

It is interesting to note that these results on the promiscuity of HS structures in FGF8 signaling, in fact, can explain several earlier observations that suggest the compensatory effect of one type of sulfate group for another type (1-4). For example, Merry C.L. *et al.* have shown that the complete loss of 2-OST in mice is compensated by increased *N*- and 6-*O*-sulfation to maintain the overall charge density as well as HS functions. The 2-OST knock-out mice did not have the early developmental failure as observed in HS lacking embryos, suggesting that the loss of 2-OST is compensated by the increase of other types of sulfation (2). Similarly, it has been shown that in 6-OST knock-out mice, 2-*O*-sulfation is increased (1). A similar compensation effect was also observed in *Drosophila* as well (4). The loss of 2-*O*-sulfation is compensated by the increase in 6-*O*-sulfation to maintain the total charge density and vice versa. More importantly, the loss of either 2-OST or 6-OST did not cause severe phenotype as in the case of 2-OST and 6-OST double knock-out, suggesting that the compensation effect is not only observed in the content of overall charge but also in the functions of HS molecules (3). These results demonstrate that topology of charged groups rather than the exact sequence of sugar residues with fixed sulfate positions is crucial for HS functions and thus, different HS structures can have the same function. However, more severe defects were observed in 6-OST knock-out than 2-OST knock-out *Drosophila*, indicating the importance of a specific type of sulfation. This finding reaffirms our results that different types of *O*-sulfation show different levels of activity, in particular, oligosaccharides with 6-*O*-sulfate groups may require shorter chain lengths, in

comparison with oligosaccharides with 2-O-sulfate groups, to have the same effect on FGF8 signaling in zebrafish embryos.

The injected exogenous oligosaccharides are monomeric but still exhibited the same effect as that of dimeric xyloside-primed HS. However, it is important to note that HS produced in zebrafish embryos at the early stages of development is only available at extremely low concentrations and also contains a few sulfate groups. Thus, the amount of monomeric oligosaccharides injected is much more than the amount of endogenous HS produced, suggesting that during early development, zebrafish embryos need to synthesize dimeric HS in order to effectively activate FGF8 signaling at low concentration. Furthermore, these HS molecules have a higher sulfation density than GAG chains primed by xylosides *in vivo*; thus, these HS molecules possibly contain more than one FGF and FGFR binding site. Therefore, we speculate that under *in vivo* conditions, GAG chains must be multimeric so that they can facilitate ternary complex formation with FGF and FGFR, and subsequently lead to FGFR dimerization and signal transduction.

This study also led to the development of a novel *in vivo* FGF8 activity assay. To date, the only available FGF activity assay is the mitogenic activation assay in cell culture using BAF3 cells. Therefore, the FGF8 activity assay in zebrafish using the elongation phenotype as an indicator is the first *in vivo* assay for FGF8-mediated cell differentiation and cell migration processes. It is important to note that in this assay, FGF8 signaling is the primary signaling pathway affected. Once FGF signaling is hyperactivated, we would expect secondary effects on other signaling pathways such as BMP and Wnt signalings. The reason that other signaling pathways are not affected

directly perhaps is attributed to the fact that both xyloside-primed GAG chains and enzymatically synthesized HS molecules lack core proteins, and this needs to be investigated in future studies.

Further studies will focus on expanding the library of oligosaccharides carrying the rare 3-*O*-sulfation, and also on using different isoforms and different orders of addition of enzymes to generate distinct structures. This study has opened up a new approach towards the understanding of the structure-function relationships of HS by utilizing a library of size- and structure-defined oligosaccharides in studying a wide array of HS biological functions in a systematic manner.

4.2 References

1. Sugaya, N.; Habuchi, H.; Nagai, N.; Ashikari-Hada, S.; Kimata, K., 6-O-Sulfation of Heparan Sulfate Differentially Regulates Various Fibroblast Growth Factor-Dependent Signalings in Culture. *J Biol Chem* **2008**, *283* (16), 10366-76.
2. Merry, C. L.; Bullock, S. L.; Swan, D. C.; Backen, A. C.; Lyon, M.; Beddington, R. S.; Wilson, V. A.; Gallagher, J. T., The Molecular Phenotype of Heparan Sulfate in the Hs2st^{-/-} Mutant Mouse. *J Biol Chem* **2001**, *276* (38), 35429-34.
3. Kamimura, K.; Maeda, N.; Nakato, H., In Vivo Manipulation of Heparan Sulfate Structure and Its Effect on Drosophila Development. *Glycobiology* **2011**, *21* (5), 607-18.
4. Kamimura, K.; Koyama, T.; Habuchi, H.; Ueda, R.; Masu, M.; Kimata, K.; Nakato, H., Specific and Flexible Roles of Heparan Sulfate Modifications in Drosophila Fgf Signaling. *J Cell Biol* **2006**, *174* (6), 773-8.